ENERGY-EFFICIENT I/O INTERFACE DESIGN WITH
ADAPTIVE POWER-SUPPLY REGULATION

A DISSERTATION

SUBMITTED TO THE DEPARTMENT OF

ELECTRICAL ENGINEERING

AND THE COMMITTEE ON GRADUATE STUDIES

OF STANFORD UNIVERSITY

IN PARTIAL FULFILLMENT OF THE REQUIREMENTS

FOR THE DEGREE OF

DOCTOR OF PHILOSOPHY

Gu-Yeon Wei

June 2001

Abstract

The demand for high-bandwidth and low-power I/O interfaces for intra-chip communication motivates this work. Aggressive CMOS scaling has enabled higher performance and integration at the expense of higher power dissipation and design complexity. This work investigates a technique that adaptively regulates the supply voltage to minimize power consumption while enabling a simpler I/O design.

Adaptively regulating the supply voltage offers significant energy savings due to energy's squared dependence on voltage for digital circuits. In order to find the minimum voltage required for proper operation at speed, a digital power-supply regulator relies on an inverter-based model of the worst-case critical path and the model's ability to track the delay of the critical path with respect to process and environmental conditions. A purely digital implementation leads to a robust design that can also benefit from the same power savings technique as in the load. An experimental prototype demonstrates conversion efficiencies greater than 90-% across a wide range of regulated voltage levels.

A high-speed parallel I/O interface driven with an adaptively regulated supply can take advantage of several properties that lead to a simple, low-power solution. In addition to minimizing power consumption, given the tracking ability of the inverter-based model of the critical path, the regulated voltage level contains information about process and operating conditions. This property allows the designer to replace precision analog circuits with simple digital gates and results in a simpler design. Furthermore, it enables a receiver design whose bandwidth tracks the bit rate and a transmitter with automatic slew-rate control. A parallel I/O prototype with adaptive power supply regulation was fabricated in

a 0.35μm CMOS technology. The prototype achieves 0.2-0.8 Gb/s link operation and its power consumption is a function of the bit rate to a power greater than two.

Acknowledgments

Looking back on the nineties at Stanford, I fondly remember many wonderful experiences and friendships. Stanford has a dynamic collection of students, teachers, and staff that encourages one to pursue knowledge in an exciting environment. I will always cherish my time here.

I am indebted to my adviser, Professor Mark Horowitz, who was kind enough to support a clueless undergraduate to do research one summer in 1994. Little did he know that it would last more than six years. I thank Mark for his keen insight, guidance, and patience throughout the course of my research and thesis. I feel incredibly fortunate to have had him as my adviser.

I would also like to thank Professor Bruce Wooley for being my associate adviser, serving on my orals committee, reading this thesis, and continued support throughout the years in CIS. I am grateful to Professor James Harris and Professor Bob Dutton for also having served on my orals examination committee. I also extend thanks to Professor Jim Plummer for being my undergraduate adviser and giving me an opportunity to play in the clean room for a summer. I am also fortunate to have received technical wisdom and guidance from Professor Tom Lee.

This research and thesis could not have been possible without the collaboration, encouragement, and aid of many colleagues. I especially thank Stefanos Sidiropoulos for his generous help and guidance throughout the design and layout of the test chip and for reading this thesis. This work also would not have been possible if it were not for the hard work and dedication of Dean Liu and Jaeha Kim. I am grateful for the discussions and

camaraderie of fellow students, past and present: Dan Weinlader, Birdy Amrutur, Ron Ho, Ken Mai, Ken Yang, Ricardo Gonzalez, John Maneatis, Arvin Shahani, Derek Shaeffer, Bennett Wilburn, Patrick Yue, Tom Soh, Adrian Ong, Joe Ingino, and all of the students in the Wooley, Horowitz and Lee groups.

Outside of school life, I have many people to thank for their continued support and friendship. Dan Kim, Woo-Young Rhee, Stephen Ryu, Jaeson Kim, Jay Kim, James Yao, Charles Watson, K.C. Chang and Eugene Jhong have enriched my graduate school years. Kenny Park, Eddie Ahn, David Kim, Jeehun Hwang, Christian Gehman, Steve Martinez, Dave Atkins, and countless others have made my undergraduate years memorable. I also thank Jin Lee for her friendship and support through the last stretch.

Throughout my life, my parents have always supported me with love and prayer. I dedicate this thesis to them. I am also fortunate to have had three sisters who watched over their little brother. Lastly, I am grateful for my nieces and nephew, who were always so loving and cheerful.

Table of Contents

List of Figures

List of Tables

Chapter 1

Introduction

Aggressive CMOS technology scaling has enabled explosive growth in the integrated circuits (IC) industry with cheaper and higher performance chips. However, these advancements have led to some chips being limited by the chip-to-chip data communication bandwidth. This limitation has motivated research in the area of high-speed links that interconnect chips [21],[37],[47],[52] and has enabled a significant increase in achievable communication bandwidths. Enabling higher I/O speed and more I/O channels further improves bandwidth, but these approaches also increase power consumption that eats into the overall power budget of the chip. In addition, complexity and area become major design constraints when trying to integrate hundreds of links on a single chip. Therefore, there is a need for building high performance I/O interfaces with low power consumption and low design complexity. This thesis explores using a technique that dynamically scales the supply voltage, called adaptive power supply regulation, to achieve these goals. Controlling the on-chip supply voltage so that the delay of an inverter is a fixed fraction of a bit time allows one to replace precision analog circuits with digital CMOS gates and reduce overall power consumption at the same time.

1.1 Low-Power Techniques

Performance of digital systems has been increasing exponentially, driven by higher clock frequencies and higher chip complexity. Unfortunately, power in digital systems has also increased as a result and has become a primary concern. Modern high-performance microprocessors can consume more than 100 W [17],[21] and require special cooling and power supply systems. The recent proliferation of portable devices also emphasizes the

1

need for lowering power dissipation, requiring chips with lower energy consumption to extend battery life.

Power in synchronous CMOS digital systems is dominated by their dynamic power dissipation, which is governed by the following equation:

$$P_{dynamic} = \alpha \, C_{sw} \, V_{DD} \, V_{swing} \, f_{clk,} \qquad (1\text{-}1)$$

where α is the switching activity, C_{sw} is the total switched capacitance, V_{DD} is the supply voltage, V_{swing} is the internal swing magnitude of signals (usually equals Vdd for most CMOS gates), and f_{clk} is the frequency of operation. And since power is the rate of change of energy,

$$E = \alpha \, C_{sw} \, V_{DD} \, V_{swing}. \qquad (1\text{-}2)$$

Technology scaling enables lower power and energy since when a chip transitions to a new scaled technology, both capacitance and voltage decrease for this chip. Scaling technology also means that the gates get faster, so it is possible to run this scaled chip at higher frequencies, while still dissipating less power than before.

Aside from technology scaling, reducing just the supply voltage for a given technology enables significant reduction in power and energy; both are proportional to the supply voltage squared. However, voltage reduction comes at the expense of slower gate speeds. So, there is a trade-off between performance and energy consumption. Recognizing this relationship between supply voltage and circuit performance, dynamically adjusting the supply voltage to the minimum needed to operate at a given frequency enables one to reduce the energy consumption down the minimum required. This technique is referred to as adaptive power supply regulation, and requires a mechanism that tracks the worst case delay path through the digital circuitry with respect to process, temperature and voltage in order to determine the minimum supply voltage required for proper operation.

There have been several examples of this power saving technique applied to general purpose microprocessors [4],[29],[38],[46] and digital signal processing (DSP) chips

[5],[15],[35] for mobile and other applications where minimizing energy consumption is a priority. These systems commonly rely on the bursty nature of their operation to dynamically adjust the speed and supply voltage in order to minimize the energy consumed for the required computational tasks at hand. Furthermore, these systems employ both hardware and software based schemes to monitor the computational needs of the system.

Adaptive power supply regulation can be used for more than optimizing energy consumption based on the varying computational needs of a digital chip in time. It can also be used for varying computational needs of different parts within a chip. An extreme example of this would be to partition large, somewhat autonomous blocks within a digital chip and operate them at their own optimum frequency and voltage. However, the overhead associated with communication between the potentially asynchronous blocks and to efficiently provide separate voltages to each of them is a formidable challenge. A subset of this example would be to identify a block within a digital chip that consumes a significant component of the overall power and could operate at a lower supply voltage. In other words, a block whose critical delay paths are much shorter than the rest of the digital chip such that, as a separate entity, it could operate at a much lower voltage for the same clock rate. We will see throughout this thesis that a high-speed parallel interface for high-bandwidth communication between chips meets these criterion and its function is briefly introduced next.

1.2 CMOS Parallel Links

High-speed links can provide high communication bandwidth between chips and consist of four main components as shown in Figure 1.1. A transmitter converts digital binary data into electrical signals that travel through the channel. This channel is normally modeled as a transmission line and can consist of traces on a printed circuit board (PCB), coaxial cables, shielded or un-shielded twisted pair wires, traces within chip packages, and the connectors that join these various parts together. A receiver then converts the incoming signal back to digital data and requires a timing recovery block to compensate for delay through the channel. A common architecture to enable high bandwidth communication

between two chips integrates several parallel sets of these links for data and relies on a separate synchronous clock link for accurate timing recovery [41],[53]. This architecture assumes that delays through the different parallel channels match well. To reduce the power consumed in this link, this thesis focuses on low power link operation and introduces techniques to minimize power in all of the link's components and to enable minimum signal swings through the channel. Although the line power can be significant, power in the supporting circuitry can dominate the total link power when low signal swing levels are used. A significant fraction of the total link power is consumed by the digital circuitry that prepares signals for transmission and the synchronization circuitry that realigns the received data to the system clock of the receiver chip. Since these are predominantly digital circuits, adaptively regulating the supply voltage to the I/O subsystem can enable energy efficient operation without sacrificing performance.

This thesis describes the necessary components to build an adaptive power supply regulator and describes a parallel I/O transceiver that leverages a dynamically scaled supply environment for a simple and robust interface design.

1.3 Organization

Since this work relies on a technique that dynamically regulates the supply voltage to reduce energy consumption, Chapter 2 presents background information that starts with a review of power and delay in digital CMOS circuits and their dependence on process, temperature and voltage variations. Adaptive power supply regulation relies on being able to dynamically track circuit performance to supply the minimum voltage required, so the chapter continues by investigating using inverters as a flexible mechanism for modeling
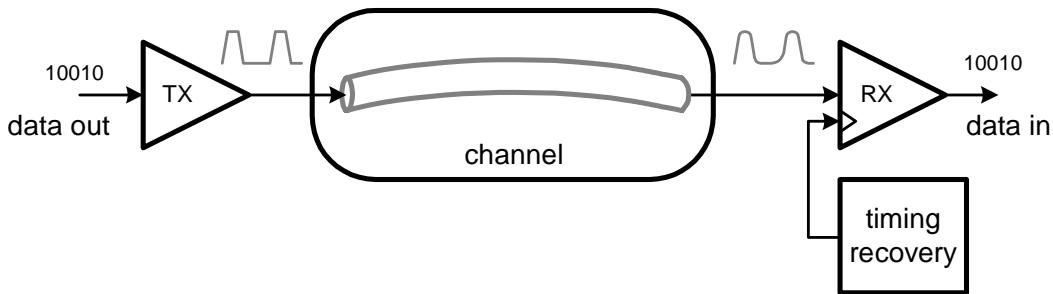
Figure 1.1. Link components

critical path delay. It then reviews the components necessary to build an adaptive power supply regulator by looking at the characteristics of a buck converter that creates a lower regulated voltage, and the resulting feedback control loop architecture. For effective application to digital systems, Chapter 3 describes a digital implementation of an inherently analog power supply control loop.

Chapter 4 describes how applying this power saving technique to an I/O subsystem leads to a simple and low-power design. A core DLL, which is a necessary component for timing recovery in the interface, also serves the dual role of determining the "right" voltage of operation with respect to frequency by tracking the worst case delay path in the I/O subsystem. The chapter then describes issues associated with building transceiver circuit components that can function in a variable voltage environment, and presents the resulting transmitter and receiver designs. Another key component of the link is the timing recovery block, which can also leverage the adaptively regulated voltage environment to yield a simpler, mostly digital implementation. The circuit implementations of the building blocks are described and experimentally measured results from a fabricated test-chip prototype present the power savings offered by adaptively regulating the supply voltage that drives the I/O subsystem.

Chapter 2

Background

This work focuses on a power-saving technique for digital CMOS circuits that dynamically lowers the supply voltage down to the minimum required for proper operation. By tracking the variable process and environmental effects on circuits, the supply voltage can be regulated to operate circuits at their most energy efficient point without special circuit techniques or logic families, and can be applied to standard static CMOS logic gates. The ability to determine the minimum voltage required for operation requires two components: *(i)* a mechanism to track circuit performance (or delay) with respect to process, temperature and voltage, and *(ii)* an efficient power supply regulator to power the digital CMOS circuits. These two issues are the main topics for this chapter.

While simply adjusting the supply voltage to preset levels relative to discrete clock frequencies, set by system performance requirements, enables power reduction, we must also consider the inefficiencies due to overhead voltage margins that are normally imposed on digital circuits. Therefore, before looking at delay tracking mechanisms, Section 2.1 first looks at how process and operating parameters affect circuit performance and power dissipation in digital circuits. Although circuit delay is roughly inversely proportional to supply voltage, process variations and environmental conditions affect device parameters to cause delay and performance variations. By using a unit inverter as being representative of general digital CMOS circuits, we can investigate the energy savings offered with an adaptive power supply regulation scheme that is aware of local process and operating conditions. The assumption that inverters can be used to model the performance of general circuits requires the delay of complex gates track the delay of an inverter across a variety of parameters that affect performance. Section 2.2 investigates the

delay tracking ability of inverters with respect to process, temperature, and voltage variations, and identifies some caveats of simply using inverters as a delay tracking mechanism. An efficient switching power supply regulator design that can enable this power savings is the subject of the rest of this chapter.

2.1 Power and Delay in Digital CMOS Circuits

The delay of digital CMOS circuits depends on three main parameters: *(i)* process, *(ii)* temperature, and *(iii)* supply voltage. Variability in manufacturing results in chips that exhibit a range of performance due to variations in device thresholds, oxide thicknesses, doping profiles, etc. Operating conditions also affect performance. Temperature affects the mobility of holes and electrons, and also the transistor's threshold voltage. Lastly, circuit delay strongly depends on supply voltage. The delay of a static CMOS gate can be approximated by the following equation:

$$delay \propto \frac{C_{load} V_{swing}}{\beta (Vdd - V_{TH})^{\alpha}} \qquad (2\text{-}1)$$

where C_{load} is the load it drives, V_{swing} is the swing magnitude of the output (which is *Vdd* for static CMOS gates), *Vdd* is the supply voltage, and $\beta(Vdd\text{-}V_{TH})^{\alpha}$ models the device current [39]. For low fields, α is around 2, but for modern devices α is as low as 1.25 [20]. Delay variation of a typical fanout-of-4 (FO4) inverter[1] versus supply voltage in an HP0.35µm CMOS process is shown in Figure 2.2 and matches extremely well with the above delay equation for α=1.4. Assuming that the critical path delay of a digital system is a function of some number of inverter delays[2], the normalized frequency of operation versus supply voltage can be found by inverting and normalizing the inverter's delay and is also presented in Figure 2.2. The frequency of operation achievable by a chip is roughly

---

[1] A fanout-of-4 inverter is an inverter that driver another inverter with four times its own input capacitance.

[2] Section 2.2 shows that a string of inverters can be used to model the critical path delay of digital circuits, consisting of a variety of complex gates, and it tracks well over a wide range of process corners and temperatures. Although the delay of complex gates do not track as well over a wide range of voltage, Section 4.1.1 shows that a string of inverters is a good model for the I/O subsystem's critical path.
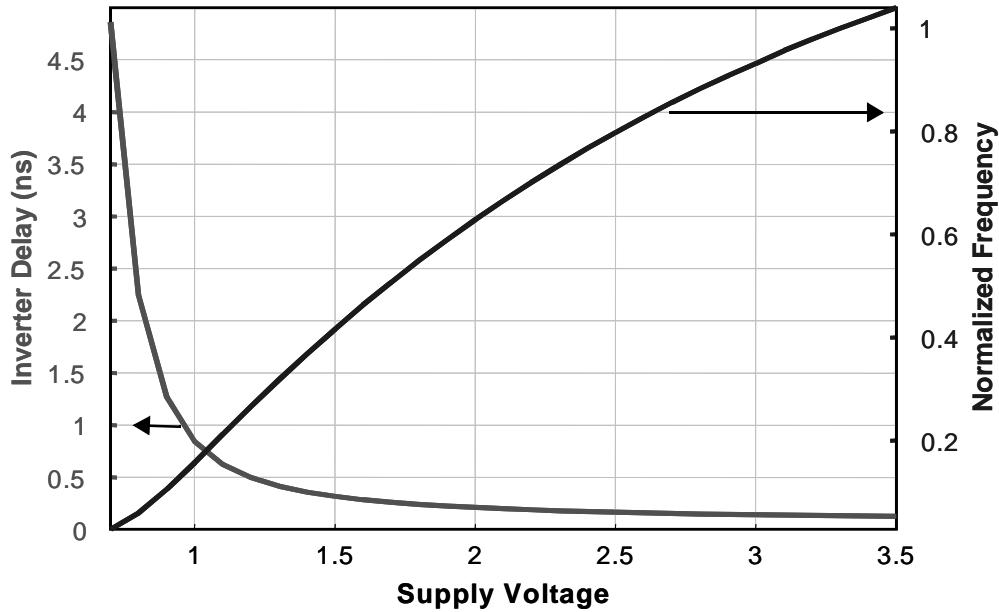
Figure 2.2. Normalized delay and frequency vs. supply voltage

linear with supply voltage. This way of visualizing relative circuit performance versus supply voltage is used extensively throughout this section to analyze the effects of different parameters on performance and power.

To understand what this relationship means for power, the delay data is applied to the dynamic power equation (Equation 2-1) and the resulting normalized power is plotted relative to normalized frequency for two supply voltage configurations in Figure 2.3.
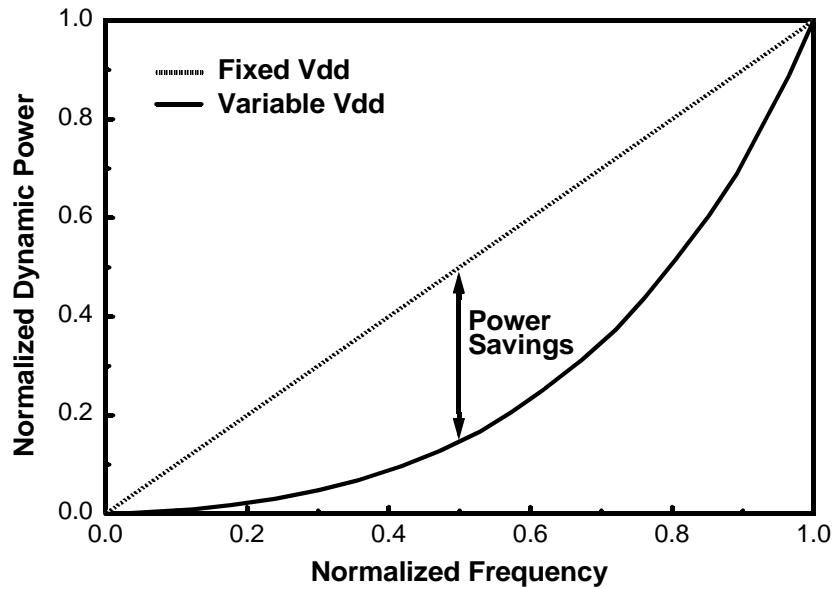
Figure 2.3. Normalized power vs. normalized frequency
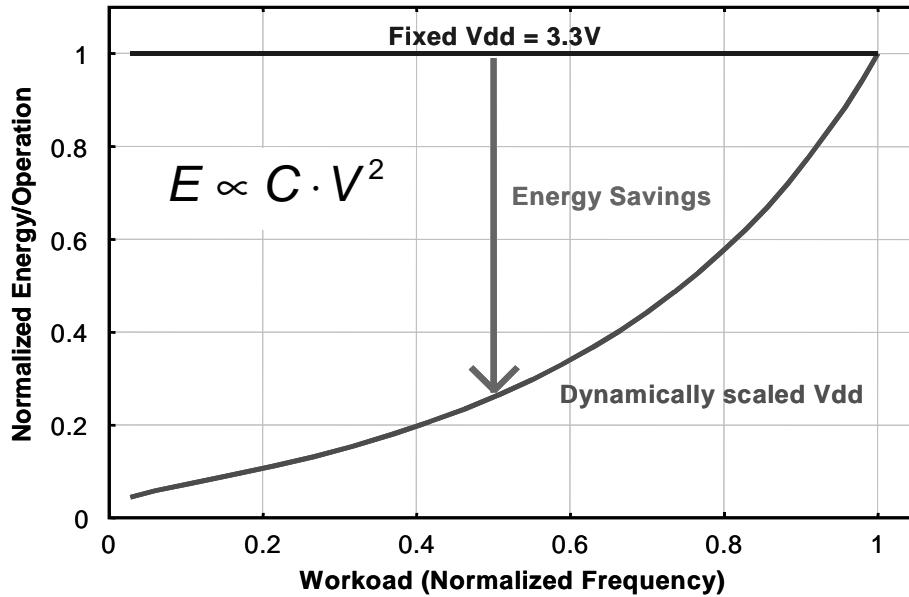
Figure 2.4. Normalized energy vs. normalized frequency

Given a fixed supply voltage, power consumption is proportional to frequency, resulting in a straight line in this figure. Since gate delay can increase if the required operating frequency is reduced, the circuit can operate at lower supply voltages. Therefore, further power savings are possible by reducing the supply voltage to the value indicated by Figure 2.2, for each lower operating frequency. Now, power consumption reduces dramatically for lower frequencies and is proportional to frequency cubed. Another way to analyze this savings is to look at the energy consumed per operation, where an operation is assumed to complete within some fixed number of clock cycles [3]. Figure 2.4 plots the normalized energy consumption per operation versus normalized frequency, again for two voltage conditions. Since the energy consumed is independent of frequency, it is constant regardless of frequency for a fixed supply voltage. However, by appropriately adjusting the supply voltage, there is a quadratic relationship between energy and frequency. Therefore, significant energy savings is possible by operating the chip at lower than peak frequencies.

In addition to the energy savings possible by adaptively regulating the power supply down to lower levels for lower frequencies, there is a potential for saving energy due to inefficiencies found in conventional digital designs that operate off a fixed supply voltage. Variability in circuit performance due to process and temperature variations require
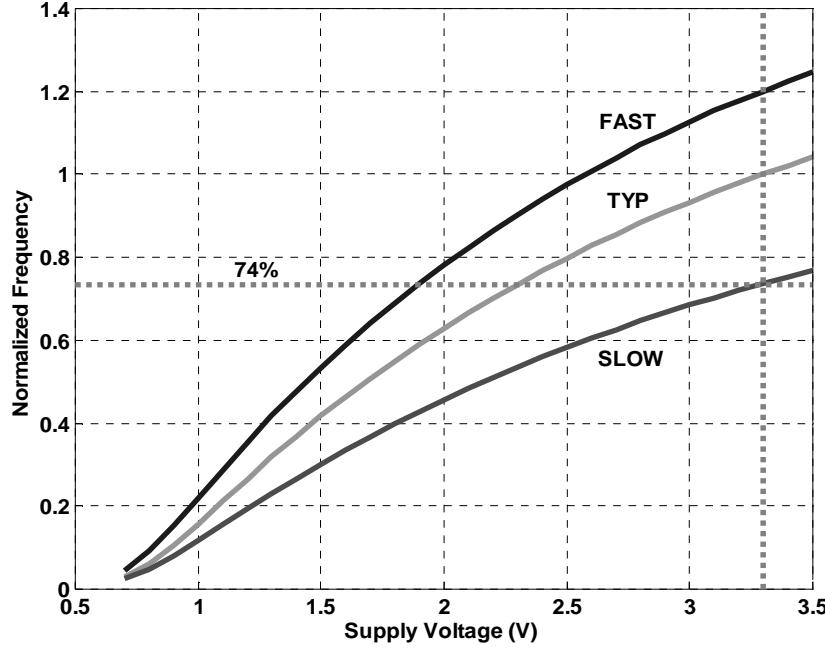
Figure 2.5. Normalized frequency vs. supply voltage vs. corners

conventional designs incorporate overhead voltage margins to guarantee proper operation under worst-case conditions. This is due to the circuit delay's strong dependence on process parameters and temperature as shown by the equations for device transconductance, β, and threshold voltage, V_{TH}, below. [33]

$$\beta \;=\; \mu_{n,p} C_{ox}\frac{W}{L} \tag{2-2}$$

$$_{TH} \;=\; V_{T0} + \gamma(\sqrt{\left|\text{Ð }2\phi_F\text{ Ð }V_{SB}\right|}\;\text{Ð}\;\sqrt{\left|2\phi_F\right|}) \tag{2-3}$$

Device transconductance strongly depends on oxide thickness, C_{ox}, which can vary by 12-% between process runs[1]. Mobility and threshold voltage both have strong dependence on temperature which can significantly degrade circuit speed. Performance dependence on process and temperature can be exemplified by plotting the normalized frequency vs. supply voltage under typical (typical nMOS, typical pMOS, 25-C), fast (fast nMOS, fast pMOS, 0-C), and slow (slow nMOS, slow pMOS, 100-C) corners, shown in Figure 2.5.

---

[1] Oxide thickness variation based on COX parameters for corner case BSIM models for HP0.35μm process.

Although a chip may be able to operate at a peak normalized frequency of 1, under typical conditions and 3.3-V, slow device corners and high temperature degrade circuit performance so that it is unable to function properly at the high target speed. To accommodate this performance variation, chips are normally run at frequencies lower than the normalized peak, identified in the figure at 74-% as an example. Although a slow corner chip can now properly function at this lower frequency, typical and fast corner chips incur large voltage overheads, with a supply fixed at 3.3-V, of 1-V and 1.4-V respectively. This overhead translates into excess power dissipated to allow margins for worst case corners. By taking a look at the energy consumed per operation versus frequency again, as shown in Figure 2.6, since chips under typical and process and temperature conditions can operate at higher speeds with a lower supply voltage and due to energy's quadratic dependence on voltage, not only is energy conserved compared to the fixed supply case, but significant savings is possible at typ and fast corners compared to the slow corner.

A common technique employed by the IC industry to deal with process variability is called speed binning and is common practice for commodity parts such as semiconductor memories and microprocessors. Fabricated chips are categorized into different groups
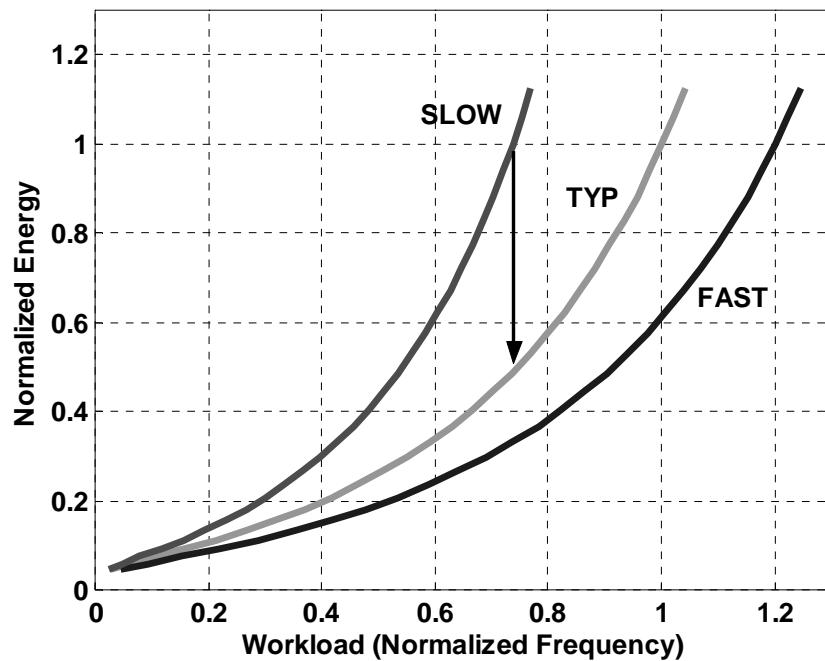
Figure 2.6. Normalized energy vs. normalized frequency vs. corners
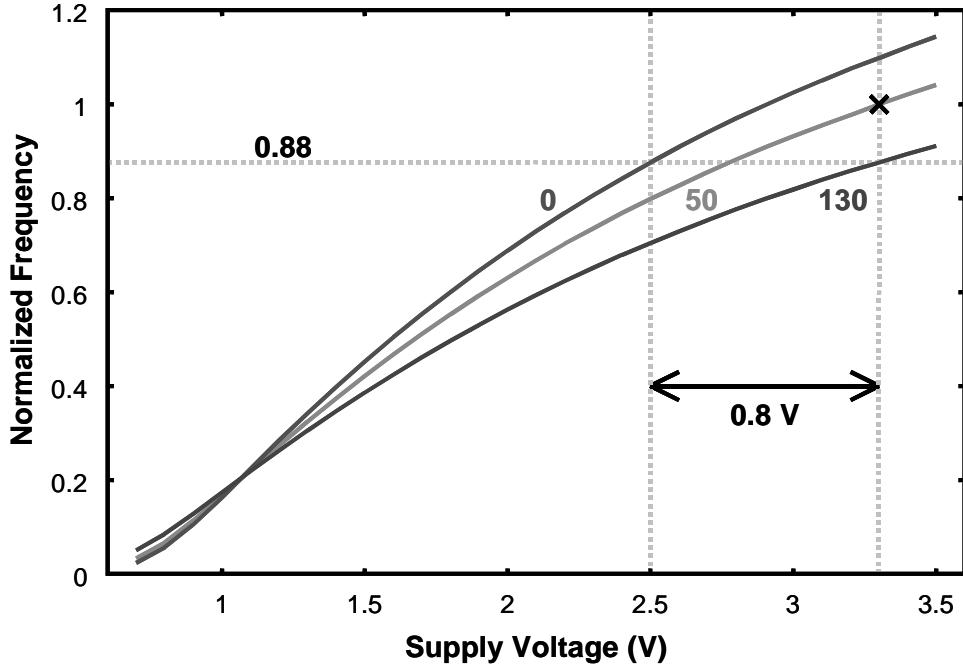
Figure 2.7. Normalized frequency vs. supply voltage vs. temperature

based on the maximum speeds that can be achieved. Although binning allows manufacturers to deal with process variability, operating temperature generally cannot be known *a priori* and therefore chips still need margins to be meet specifications over a wide range of temperatures. Figure 2.7 reveals that chip performance strongly depends on temperature and in order to guarantee operation at the worst case temperature, presented as 130-C, specification at lower speed is inevitable and a potentially large voltage overhead again results for a fixed supply voltage. By actively tracking on-die environmental conditions, namely temperature, dynamic supply voltage regulation accommodates the differences imposed by temperature variations to minimize energy consumption. Furthermore, since temperatures can vary over time, active compensation is necessary to eliminate this time-varying effect on performance, and is not possible with one-time binning after fabrication.

This analysis of how an inverter's speed and power consumption changes relative to process and operating conditions shows there is a potential for considerable power savings due to a large voltage overhead incurred with a fixed supply voltage. While much of the overhead may be reduced, the actual savings that can be achieved depends on how well

the critical path's delay tracks relative to an inverter's delay (or the delay of circuit that models the critical path) versus process, voltage, and temperature (PVT). Mismatches between the two lead to margins required to guarantee proper circuit operation. Therefore, the next section investigates how well the delay of several complex gates track the delay of an inverter across PVT.

2.2 Delay Tracking

The ability to actively track the performance of digital circuits with respect to local process and temperature variations enables the circuits to operate at a more energy efficient point. Since the performance of a digital system is limited by its worst case critical path delay, an exact replica of this delay path is one of the most accurate ways to measure delay variation with respect to different process corners and variations in operating conditions within a single chip. However, in real designs, designers normally balance delay paths within digital blocks as much as possible. Therefore, identifying a single path to replicate may be difficult. Furthermore, critical paths may differ depending on process corner and operating environment. Instead, we will consider using a series chain of inverters to model the critical path delay. This approach relies on a basic assumption that the delay of complex gates that make-up the critical path track the delay of an inverter. Section 2.2.1 investigates how well the delay of several static and dynamic gates track an inverter's delay. Mismatches measured across voltage variations set the margins necessary for an adaptively supply regulation scheme that use inverters to model the critical path. In addition to matching pure gate delays, the ability to track the delay of wires is also important in modern VLSI systems. Section 2.2.2 this and other non-ideal effects on inverter delay tracking.

2.2.1 Inverter-based tracking

A static CMOS inverter is the simplest unit logic gate and can account for a significant portion of the total gate count in digital IC's. It is the primary gate used for clock distribution and the most efficient mechanism for ramping up drive strength to drive large capacitive loads. Chapter 1 mentioned that an inverter's delay variation versus process,
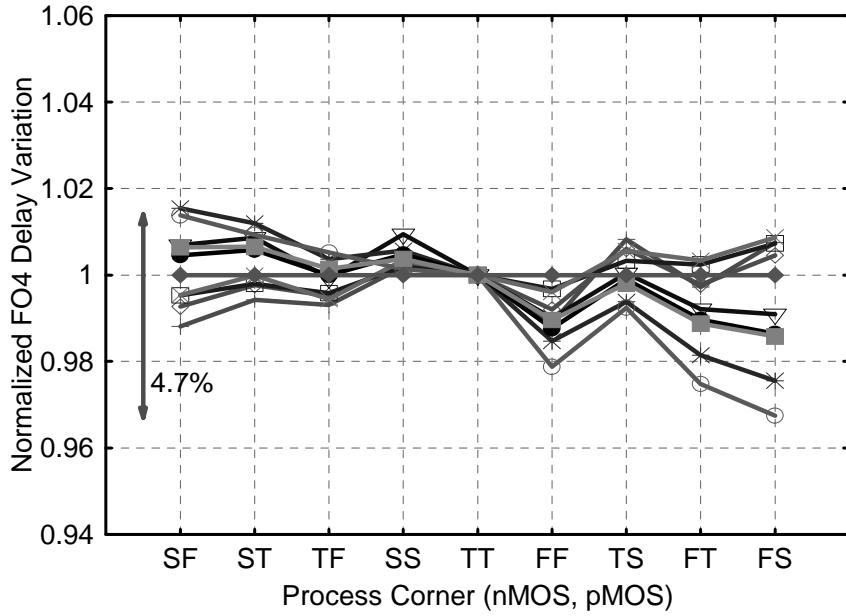
Figure 2.8. Normalized delay tracking of various complex
static and dynamic gate vs. process corner

temperature and voltage can be used to predict general circuit performance trends. In this
subsection, we look at how valid that assumption is by measuring the delay of various
static and dynamic complex gates (nand2, nand3, nor2, nor3, transmission gate,
dynamic-nand2, -nand3, -nor2, and -nor3) relative to an inverter delay, across a wide
range of process corners, temperatures and voltages. Results are presented in terms of its
tracking variation with respect to the variable on the x-axis, by taking the normalized
delay of the gates with respect to a FO4 inverter and then calculating how much it varies
relative to a fixed point on the x-axis value. Delay tracking variations versus process
corner are presented first, in Figure 2.8, where FS denotes the fast nMOS, slow pMOS
process corner. The lines are all relatively flat which is an indication that delay of these
gates track well with the delay of an inverter across different process corners. The same
holds true for tracking with respect to temperature as shown in Figure 2.9, where
temperature ranges from 0-C to 130-C. Unfortunately, tracking is not as good across a
wide range of supply voltages, presented in Figure 2.10. Variations in normalized delay
can be attributed to velocity saturation which affects short-channel devices more than
longer-channel devices. If we take a NAND3 for example, there is a series stack of three
nMOS devices which must all be conducting to pull the output low. This stack of three
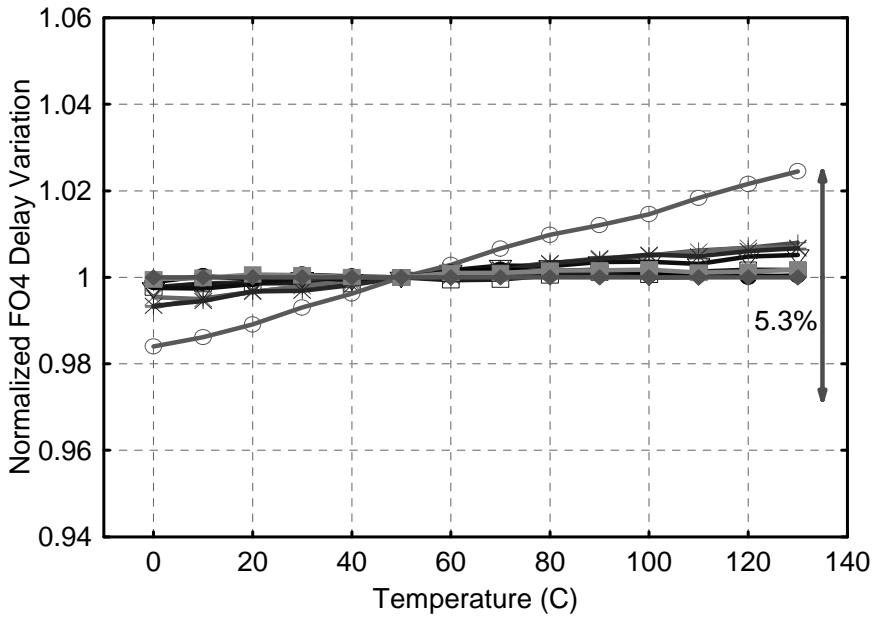
Figure 2.9. Normalized delay tracking of various complex
static and dynamic gates vs. temperature

minimum channel length devices can be modeled as a single device with an effective channel length that is three times longer. An inverter, on the other hand, consists of a single minimum channel length nMOS device. Higher lateral electrical fields saturate the velocity of carriers in shorter channels lengths more than in longer channels. This
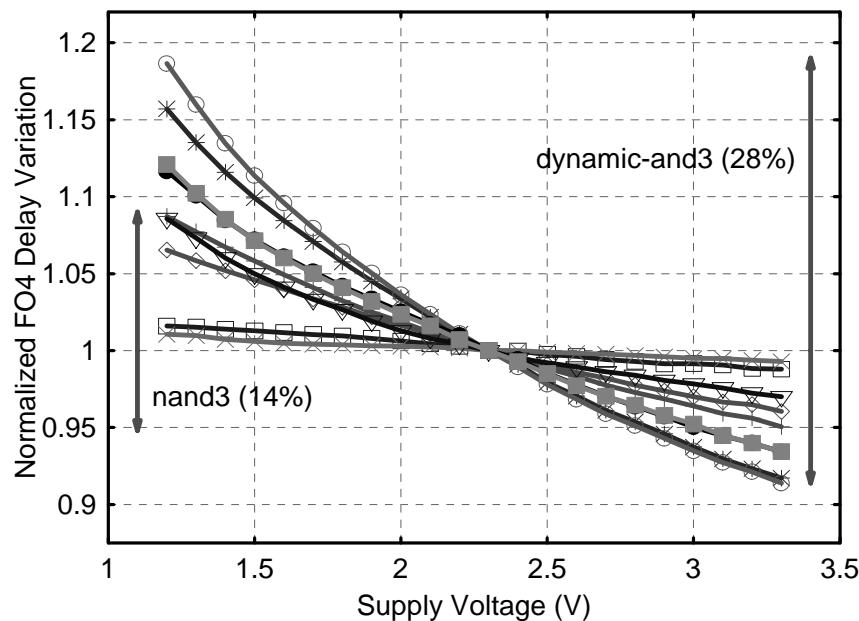
Figure 2.10. Delay tracking of various static and complex gates
normalized to L_{min} FO4 inverter vs. supply voltage
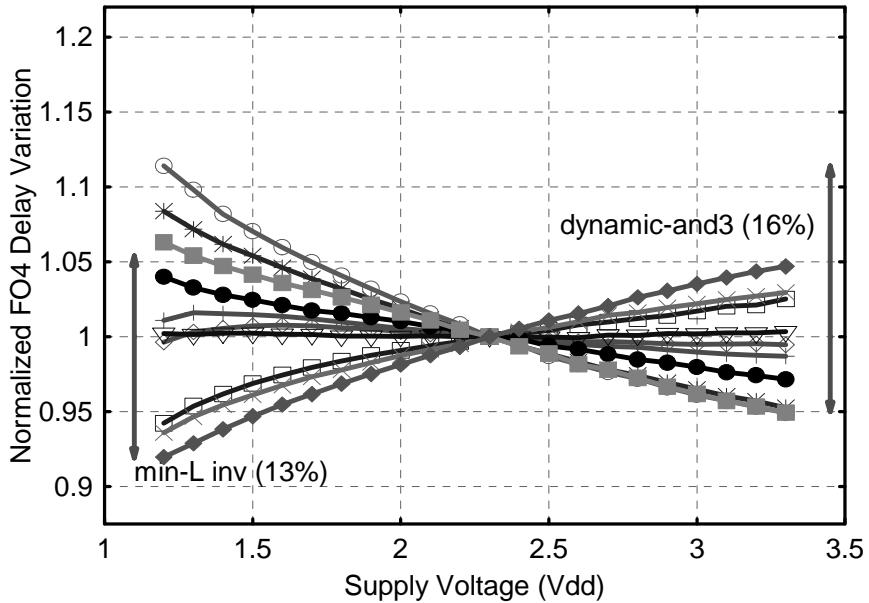
Figure 2.11. Delay tracking of various static and complex gates
normalized to 1.5*L$_{min}$ FO4 inverter vs. supply voltage

saturation makes the current in an inverter less sensitive to Vdd, and thus the delay of a
NAND3 increases faster than an inverter as the supply voltage decreases. As a result, the
lines slope downward as supply voltage increases to varying degrees depending on the
gate. The worst case critical path delay occurs at the lowest supply voltage. This
unfortunately means that the extra voltage margins required for lower voltages leads to
excess power consumption at higher speeds and voltages when the chip consumes more
power.

One way to mitigate this velocity saturation effect is to change the reference circuit to
instead use inverters with longer channel lengths. Figure 2.11 reveals that worst case
variation is reduced from 28-% to 17-%, when using an inverter with lengths 1.5 times the
minimum channel length as the reference. However, notice that now several curves slope
upward where the steepest is for a minimum channel length inverter. This mix of upward
and downward delay tracking trends relative to supply voltage makes finding the worst
case conditions for the critical path challenging since it varies with the types of gates used.

Depending on the gates that constitute the critical path, the choice of channel length
for inverters in the delay-line varies. Furthermore, delay margins must be added to

guarantee operation across all voltage conditions. As an example, let us choose 2.3-V to be the nominal voltage condition for design and we have a choice between two channel lengths: L_{min} and $1.5*L_{min}$. If the critical path consists mostly of dynamic-and3 gates, extra delay margin is necessary to guarantee proper operation under low frequency and low supply conditions. But utilizing longer channel length inverters to model its delay reduces the margin from 18-% to 12-%. On the other hand, if the critical path consists mostly of minimum channel length inverters, using 1.5*Lmin inverters to model its critical path requires an additional 5-% delay margin to guarantee operation under high speed and voltage conditions. Instead, using minimum channel length inverters in the delay line would be best. In fact, matching the delay-line elements with the gates that dominate the critical path would yield the best matching. Chapter 4 shows that an inverter chain is a good match for an I/O subsystem because the worst case delay path is in the clock distribution network which predominantly consists of inverters.

2.2.2 Other non-ideal effects

In addition to gate delays, critical paths consist of wires that interconnect different gates and functional blocks together. The delay through these wires are not governed by the same physical principles as in MOS gates. Therefore, it is important to consider how tracking varies when appreciable wire loading is present. In large digital systems, the delay associated with driving long busses across a chip can be large and often require repeater buffers to cut down the quadratic dependence on length to a linear one [1],[16]. This analysis utilizes a simple test-bench circuit consisting of inverters interconnected with a distributed π-model for a wire of variable lengths, as shown in Figure 2.12. Relatively large device sizes and wire lengths are used in order for wire resistance to be non-negligible. By modeling the inverter with an output resistance (R_{gate}), this test bench reduces to a simple RC model for delay given by the following equation:

$$T_{delay} = R_{gate} \cdot (C_{gate} + C_{wire}) + R_{wire} \cdot \left(C_{gate} + \frac{C_{wire}}{2}\right). \qquad (2\text{-}4)$$

The simulated delays of an inverter with wires (of different lengths ranging from 500-μm to 3000-μm and 1-μm wide) normalized to an inverter delay without wires, but with the
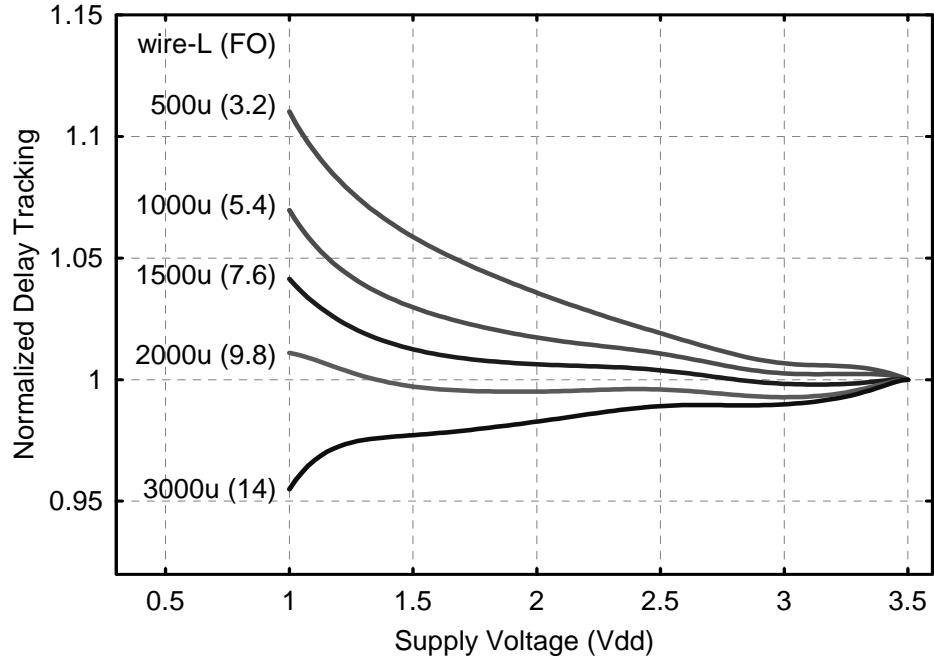
Figure 2.13. Wire delay tracking vs. supply voltage

same effective fanout at 3.3-V, versus supply voltage are presented in Figure 2.13. Wire lengths and effective fanouts with the wire loading are labeled on the graph. Across this wide range of lengths, delay tracking varies less than 12-% across a wide supply voltage range. As supply voltage decreases, inverter drive strength reduces and R_{gate} increases. As
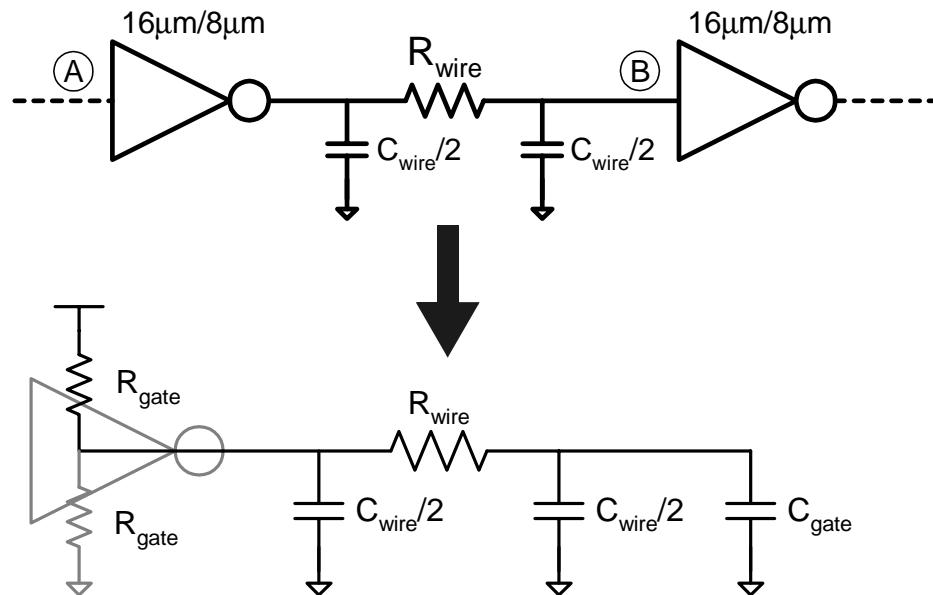
Figure 2.12. Wire delay test bench and RC model
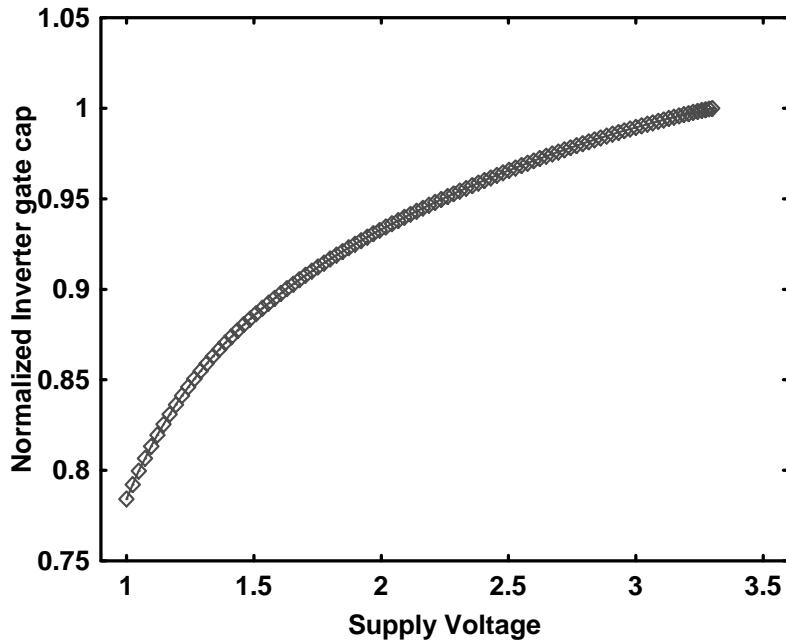
Figure 2.14. Normalized effective inverter gate capacitance vs. supply voltage

a result, one would expect the contribution of wire delay to become less significant and result in an upward slope in the delay vs. voltage plot. However, the opposite is observed for wire lengths less than 2000-μm. This can be attributed to a reduction in the effective gate capacitance on inverters as supply voltage decreases, as shown in Figure 2.14. Once the load is almost entirely dominated by the wire, the expected upward trend is observed, which is for wire lengths greater than 2000-μm in this example. In the case of long wires that use repeaters to linearize delay with respect to distance (versus a quadratic relationship for non-repeated wires), since optimal fanout is on the order of 4, additional delay margins of up to 8-% will be necessary to meet the worst-case delay conditions occurring at low supply voltages.

Apart from variations due to velocity saturation effects and wires, the inverter model of the critical path must also consider other non-ideal effects that can adversely affect tracking. Although a chain of inverters may be able to model how different process and environmental conditions generally affect individual chips, intra-die variations can lead to delay mismatches which are more difficult to track. For example, hot spots in a chip can arise from differing circuit activity in different parts of the chip to cause temperature gradients within in chip. Since the silicon substrate is an imperfect thermal conductor, if

the delay tracking inverter-chain model is located far from the critical path that happens to be in or near the hot spot, the model may be incorrectly optimistic. Higher activity also means larger currents and so larger resulting IR drops on the supply lines may exacerbate the mismatch. Intra-die process variations are generally less than the variations between individual chips, but it can also cause delay mismatches. All of these non-ideal effects stress the importance of location and strategic placement of the inverter chain that models delay to accurately monitor local conditions. As mentioned before, since the critical path may vary and exist in different parts of the chip during normal operation, multiple inverter chains may be required to monitor the variations within a chip and capture the worst case. However, circuit layout may not allow easy integration of these inverter blocks close to the critical path in the core logic. Therefore, the model may require additional margins to account for these variations. Careful characterization of potential intra-die process, temperature, and current differences can find the minimum margins necessary. An ability to tune the inverter chain model to actively find and set the minimum margin may also prove useful.

2.2.3 Delay Tracking Summary

This section has investigated the potential delay tracking mismatches between an inverter model of the critical path and actual gates and wire that make up delay paths in an actual digital system. Although there is a large potential for optimizing energy consumption by adaptively adjusting the supply voltage to the minimum required to meet timing, additional margins to compensate for tracking mismatches are necessary and reduce some of the energy savings that may be possible in a perfect environment. While the worst case corner for conventional digital circuits are in the slow corner, we have seen that the delay of complex static and dynamic gates can speed up or slow down relative to an inverter delay for different conditions. Tracking is extremely good with respect to process and temperature, but it can vary by 28-% across voltage. Therefore, a designer must adjust the delay elements used in the delay-line with respect to the types of gates in the critical path and use the tracking relationships shown in Figures 2.10-12 to reduce the delay margins needed.

Now that we know how to deal with some of the caveats of designing circuits in a regulated supply voltage environment, we need a power-supply regulator that can dynamically scale the voltage with respect to the desired frequency of operation, process and operating conditions. Issues associated with designing such a regulator is the topic of the next section.

2.3 Adaptive power supply regulation

Given a model of the critical path, adaptive power supply regulation needs to generate the minimum supply voltage required for proper operation at the desired frequency and efficiently distribute it to the synchronous digital system. This task requires two components: *(i)* a power supply regulator and *(ii)* a control mechanism to generate the correct voltage. Although a linear regulator can be used to supply power as demonstrated in [29], the power that the regulator itself consumes can be substantial and therefore counteracts the power savings of this approach. Instead, a switching regulator that has much higher conversion efficiency is preferred and is described in the following section. Driving the output of this regulator to the desired voltage with respect to operating frequency requires a feedback control loop that utilizes a ring oscillator to measure and monitor circuit performance, and Section 2.3.2 covers this design in more detail.

2.3.1 Buck Converter

In order to dynamically generate a lower supply voltage from a fixed high voltage set by the system, a DC-DC step-down converter is used. The buck converter, shown in Figure 2.15, is a switching regulator that can efficiently deliver power to a load. Its operation is straight forward and relies on an inductor and capacitor that act as a low-pass filter. Although there have been significant developments to build inductors and capacitors on-chip [54], current CMOS technology still cannot provide reactive elements that store sufficient energy to efficiently convert power, and therefore this design requires off-chip reactive elements. As long as the switching frequency of the input pulse-width modulated (PWM) rectangular-waves is at least an order of magnitude greater than the cut-off
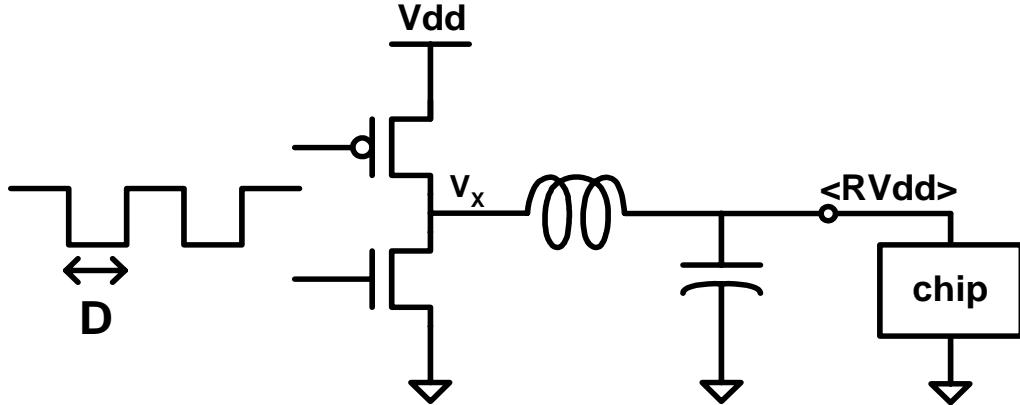
Figure 2.15. Buck converter

frequency of the low-pass filter, the output voltage of the filter is an average value where its magnitude is set by the duty-cycle of the incoming rectangular-wave. Low pass filtering through the inductor and capacitor therefore reduces the AC component of the incoming rectangular wave to an acceptable ripple and its magnitude is set by the ratio of the switching frequency to the filter cut-off frequency. Since the LC filter is a second-order filter, high-frequency AC attenuation is 40-dB/dec. The pMOS and nMOS transistors are large on-chip devices that chop the input high voltage Vdd to generate a rectangular-wave at node V_X with an average voltage that is equal to the desired output voltage with the following equation:

$$\langle RVdd \rangle = D \cdot Vdd \tag{2-5}$$

Therefore, modulating the duty-cycle, *D*, of the input rectangular wave modulates the regulated output voltage, *RVdd*. These devices also support the average current delivered to the load.

The conversion efficiency of this type of converter approaches 100-% as all its components become ideal. However, due to several loss mechanisms, efficiency degrades, but values greater than 90-% are still attainable [6],[24],[32]. Using off-chip reactive components can provide very high quality reactive elements with quality factors (Q) greater than 100 and are not the dominant source of loss. Instead, loss is dominated by the resistive losses through the on-chip switching transistors and the power required to switch them. The "on" resistance of these devices is inversely proportional to the gate width (W).

The resistive loss, denoted as P_{IR}, also strongly depends on the current magnitudes that flow through these devices and is set by Equation 2-6. Wider devices clearly yield lower resistive losses. However, the switching power required to drive these devices constrains the size of these devices since its power is governed by Equation 2-7, where C' is the effective capacitance per micron of gate width (including capacitance of the buffer chain that drives it), Vdd is the supply voltage, and F_s is the frequency at which the converter is switched. Equation 2-8 represents the optimal gate sizing for these devices found by solving for gate width, W, that yields the minimum total power for a given load current, $i_{ld\text{-}rms}$.

$$IR = \frac{i_{ld\text{-}rms}^2 R_{ON}}{W} \tag{2-6}$$

$$P_{gate} = C' \cdot W \cdot Vdd^2 \cdot F_s \tag{2-7}$$

$$W_{opt} = \sqrt{\frac{i_{ld\text{-}rms}^2 R_{ON}}{C'Vdd^2 F_s}} \tag{2-8}$$

Figure 2.16 illustrates the normalized sum of the losses in the switching transistors versus gate width and load current and reveals an optimum gate width.

In Equation 2-8, notice two variables, load current and switching frequency, also affect the optimal gate size. Therefore, a designer must consider the power consumption specifications of the load to accurately determine the optimum gate width, which is set by the maximum power requirements. However, for performance driven voltage regulation, power consumption dramatically reduces at lower frequencies due to power's quadratic dependence on voltage. Under lower power conditions, the resistive losses also quickly reduce, but gate switching power remains constant for fixed switching transistor sizes. Appropriately adjusting the widths to be closer to optimal sizing under performance driven load conditions therefore reduces the losses associated with the converter. The optimum gate width varies with load current and Section 3.2 describes a technique that
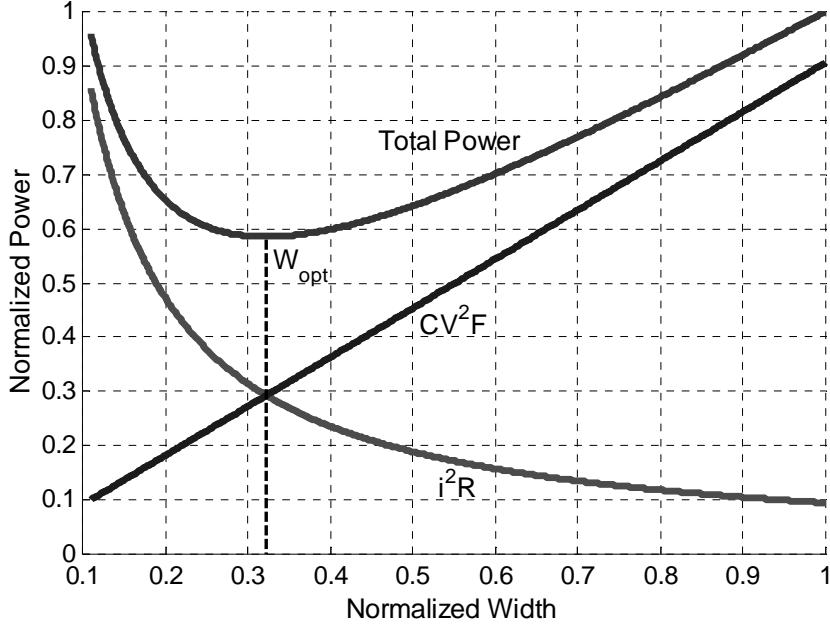
Figure 2.16. Buck converter switching transistor power loss vs. width

leverages this property to achieve higher conversion efficiencies. Switching frequency also affects optimal sizing, but is a nominally fixed parameter constrained by several other factors. Higher switching frequency allows a higher LC filter cut-off frequency, which requires smaller inductor and capacitor sizes. This is desirable for portable applications where form factor is a primary concern. However, magnetic saturation of the magnetic core, introduced to increase inductance without affecting the series resistive losses, limits the maximum frequency [6].

Given that the switching frequency is at least an order of magnitude higher than the LC cut-off frequency, a frequency-domain transfer function of the buck converter can be approximated by the following equation:

$$H_{LC}(s) = \frac{1/LC}{s^2 + \left(\dfrac{R_S}{L} + \dfrac{1}{R_L C}\right)s + \dfrac{1}{LC}\left(1 + \dfrac{R_S}{R_L}\right)}, \tag{2-9}$$

where the L and C are the inductor and capacitor values, R_S is the series "on" resistance of the switching transistors, and R_L is the resistance of the load chip and dielectric loss of the capacitor at the output. Given the availability of high-quality off-chip inductors and

capacitors, there is a resonance at the cut-off frequency due to the complex pole pair of the LC filter. Although high Q's are desirable for efficient power conversion, it can complicate the enclosing control loop design.

Given this mechanism for efficiently delivering power to the load, this adaptive power supply regulation technique needs a way of setting the duty-cycle of the input rectangular wave to regulate the buck converter's output to the desired voltage with respect to some desired frequency of operation. This is the topic of the next subsection.

2.3.2 PID Control Loop

Adaptively setting the duty-cycle of the PWM rectangular to regulate the output voltage with respect to some desired frequency of operation requires a control loop, as shown in Figure 2.17. It consists of a voltage-controlled oscillator (VCO) that converts the regulated voltage output of the buck converter into a clock signal that oscillates at a voltage-dependent frequency, F_{OSC}. This VCO consists of an odd number of inverters in a ring, which oscillates due to positive feedback, and acts to monitor variations in circuit performance relative to process and operating conditions. Taking the difference between the input reference, F_{REF}, and F_{OSC} generates an error that feeds into the loop control block. Through negative feedback, the loop locks the output voltage such that the two frequencies match. Therefore, the output voltage tracks with the input frequency reference, where the relationship between the two is dictated by the performance monitoring VCO.
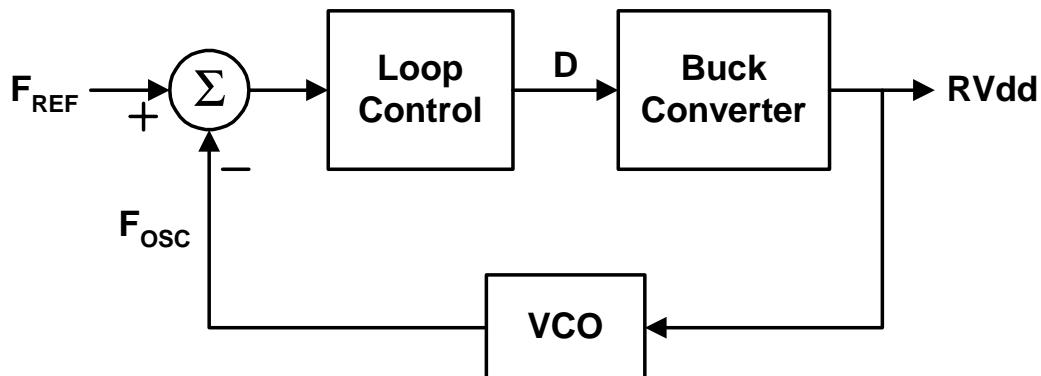
Figure 2.17. Control-loop block diagram
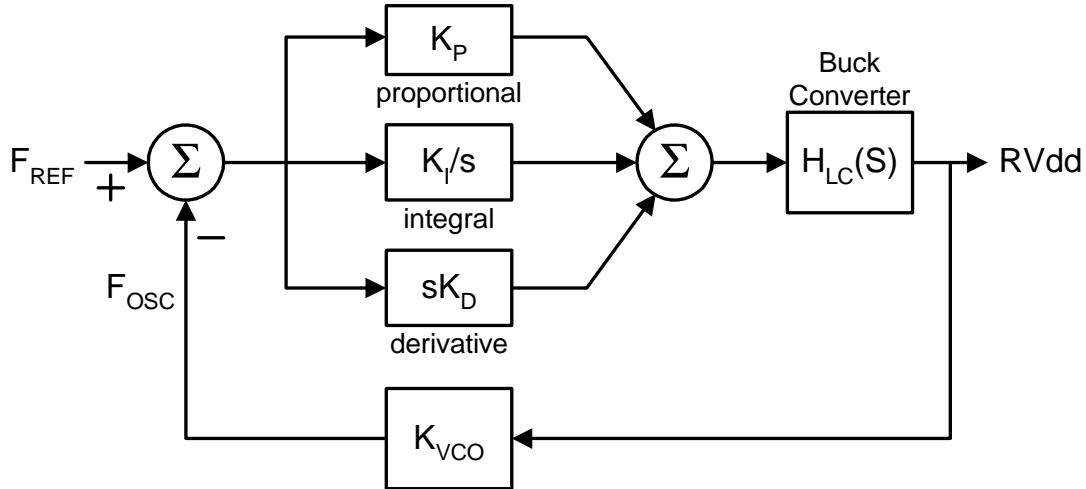
Figure 2.18. PID control-loop frequency-domain model

To achieve good transient response characteristics and stability without sacrificing bandwidth, the loop uses proportional, integral, and derivative (PID) control. A frequency-domain model of this PID loop is presented in Figure 2.18. The resulting open-loop transfer function (loop gain) is as follows:

$$\text{Loop Gain} = H_{LC}K_{VCO}\left(K_P + \frac{K_I}{s} + sK_D\right)e^{-sT} \tag{2-10}$$

K_P, K_I, and K_D set the pole and zero locations of the proportional, integral, and derivative control block. K_{VCO} represents the oscillator gain (Hz/V). Due to the time required to perform the PID control calculations, its delay (*T*) through the loop causes additional negative phase shift accounted for by the exponential term in the equation.

One difficulty associated with designing this type of controller arises from the resonant peak in the frequency response of the buck converter. For simple integral control, which consists of an integrator followed by the buck converter, there is a potential for instability. An open-loop frequency analysis for this type of loop shows that if the magnitude of the resonant peak crosses above the unity-gain magnitude, negative phase shift due the integrator pole and a pair of poles from the LC filter eliminates phase margin. Therefore, the integrator's gain must be sufficiently low as to guarantee that the buck converter's resonant peak never crosses unity gain. Unfortunately, such a configuration
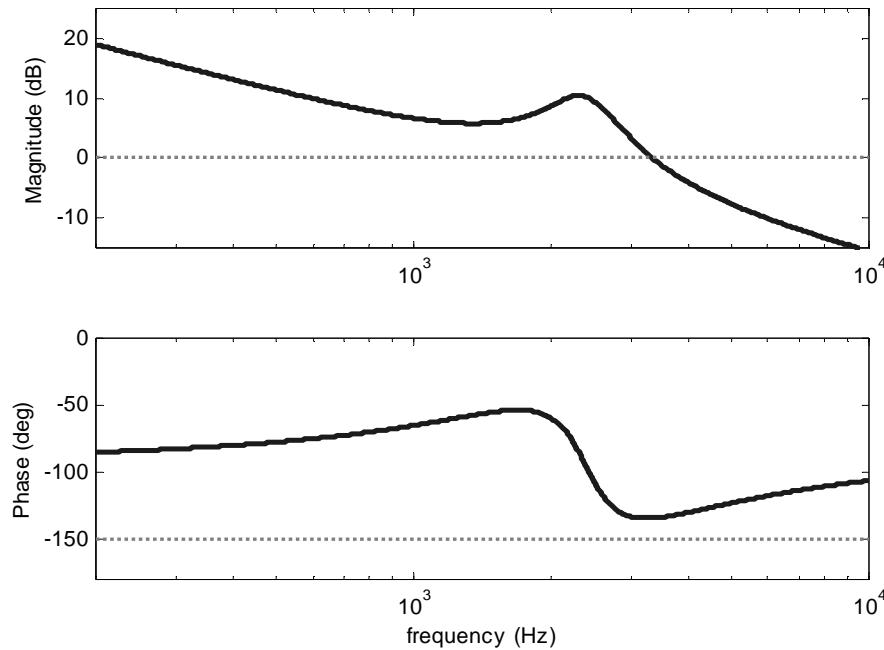
Figure 2.19. PID control open-loop frequency response

leads to low loop bandwidth and slow closed-loop transient response characteristics. To combat this effect, adding a pair of zeros, utilizing proportional and derivative blocks, can stabilize the loop without sacrificing bandwidth. Introducing the zeros at frequencies below the cut-off frequency of the LC filter pushes unity gain crossing of the open-loop response beyond the resonant peak and roles off at -20dB/dec. Furthermore, positive phase shift from the zeros provides sufficient phase margin for a stable loop, as the magnitude and phase response of the simulated open-loop transfer function in Figure 2.19 demonstrates. The bandwidth of the loop extends beyond what was achievable with integral control alone and the resonant peak of the regulator LC is no longer a limiting factor since it occurs below the unity gain frequency. In addition, because the bandwidth exceeds the LC filter's cut-off frequency, the loop can quickly respond to sudden load transients that would otherwise perturb the output voltage. This fast response also prevents other noise sources, such as sudden transients in the supply voltage to the buck converter, from propagating to the output.

Implementation of the controller in Figure 2.17 relies on the ability to generate a PWM rectangular wave, where the duty-cycle (D) is the value dictated by the output of a PID control block. One possible approach would be to use a frequency detector that compares
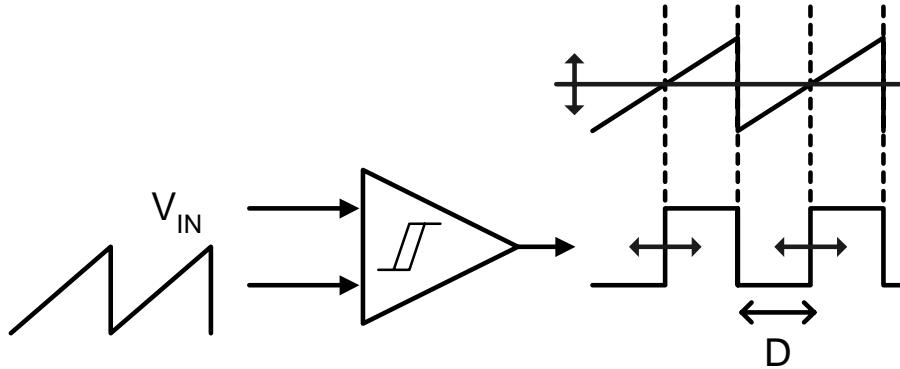
Figure 2.20. PWM rectangular wave generation

the incoming reference clock with the output of the oscillator and generate an analog voltage that corresponds to the frequency difference (or error). This error then drives the PID control implemented with a set of amplifiers to generate an analog voltage that corresponds to the desired output voltage. Translating this voltage to the appropriate duty-cycle then relies on a comparator that compares a linear ramp wave that has a period equal to the switching frequency of the buck converter to the PID control output. Figure 2.20 illustrates its operation. While the PID output is less than the ramp input, the output of the comparator is low and goes high once the ramp exceeds the PID output. As a result, changing the PID output proportionally changes the duty-cycle of the rectangular wave. The enclosing feedback loop compensates for any offsets and non-linearities that may exist in the translation.

Although this is a straight forward approach for implementing the PID control, it requires several analog components that can be sensitive to supply and substrates noise that exists in the targeted digital system. Also notice that the update rate of the buck converter is set by its switching frequency. Therefore, the update of the control blocks can occur at a rate much lower than the reference clock frequency. In addition, there is an inherent analog-to-digital (A/D) conversion that occurs in the ring oscillator, which takes an analog input voltage and generates a digital clock signal. Therefore, there is a potential to build this controller consisting entirely of digital gates, and can be embedded along with the rest of the digital system to which power is delivered. The issues and design of a digital control loop are the topics of the next chapter.

2.4 Summary

Power consumption in digital systems has been increasing at an accelerated rate and one of the most effective ways to reduce unnecessary power consumption is to minimize the overhead voltage normally required in fixed voltage designs by dynamically adjusting the voltage to the minimum required for operation at a desired frequency. Given the quadratic dependence on voltage, significant reduction in power consumption is possible and this technique can enable more energy efficient operation for synchronous digital circuits.

The minimum supply voltage required with respect to frequency can be found by using a ring oscillator that models the critical delay path in a synchronous digital system and use negative feedback control to servo the output of an efficient switching regulator [18]. Given the difficulty associated with generating an exact replica of the critical path, a more flexible approach to modeling delay based on inverters is possible. This approach, however, still requires some overhead margins to account for imperfect matching over a wide range of supply voltages stemming from velocity saturation effects. The tracking performance of the power supply regulator is set by the bandwidth of the control loop, which can be improved with a PID control that guarantees stability without sacrificing bandwidth. A PID loop has the added advantage that its bandwidth extends beyond the cut-off frequency of the LC filter so that the loop can quickly respond to noise injected at the output due to load transients. Although there are several approaches to designing this adaptive supply voltage regulator, the following chapter describes a fully digital implementation that fits well within a larger digital system.

Chapter 3

Digital Power-Supply Controller

This chapter describes a fully-digital implementation of the analog power supply controller described in Chapter 2, which avoids static currents necessary in analog circuits and sensitivity to digital supply noise when embedded within a larger digital system. Since the power consumed by the controller contributes to the overhead power consumed by the regulator, a controller that consumes very little power or one whose power tracks the power delivered to the load is desirable for enabling high conversion efficiency over a wide range of load power and chip operating frequencies. This is especially true for performance driven adaptive voltage regulation schemes, since power consumption has a cubed dependence on frequency. In this chapter, several techniques are introduced to achieve this goal of reducing controller power whenever possible by building a digital IIR filter to implement the PID control. This requires three main components: (i) A/D conversion, (ii) digital PID control, and (iii) D/A conversion, along with the buck converter, as shown in Figure 3.1.

The chapter starts with a section that describes two techniques for A/D conversion
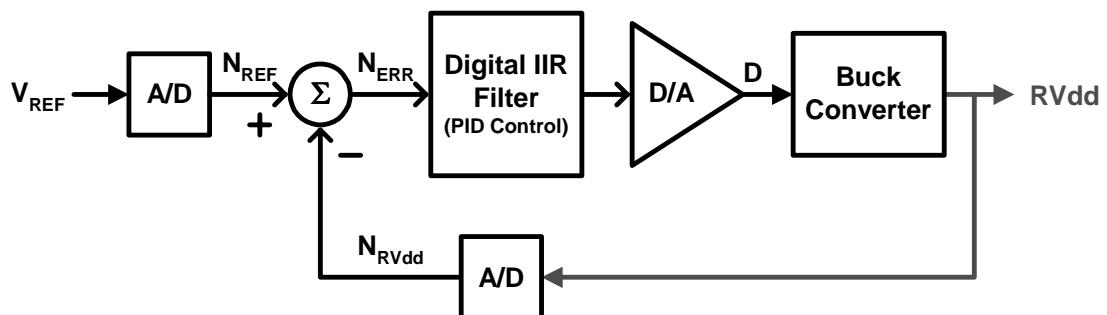
Figure 3.1. Digital controller block diagram

based on the inherent A/D property of a ring oscillator and then presents a discrete-time sampled data implementation of the analog PID control blocks. The chapter continues with a description of a variable-frequency controller which allows the digital controller to operate with adaptive power supply regulation. Then, Section 3.3 presents a simpler and lower power digital controller that operates at a fixed frequency, which has been implemented to drive a low-power parallel link described in Chapter 4. An additional advantage of building a fully-digital controller is the ease with which non-linear techniques can be implemented to improve power conversion efficiency. These techniques are described in Section 3.4.

3.1 A/D Conversion

A digital controller first requires the analog inputs and outputs of the system be converted into digital signals in order to process them with digital functional units. As described in Chapter 2, this adaptive supply-voltage regulation scheme uses the delay of inverters (T_{INV}) to model the critical path in the digital system and monitor how it reacts to process, temperature, and voltage variations. A ring oscillator, consisting of an odd number of inverters in a ring (n_{stages}), performs a voltage-to-frequency conversion, where the oscillation period is $2 \cdot n_{stages} \cdot T_{INV}$, since an edge traverses through the inverters in the ring twice within a period. As illustrated in Figure 3.2, tapping out at a single point in the ring and counting the digital clock signal over a fixed period of time performs a simple A/D conversion. The binary output is a quantized representation of the voltage (V_{IN}) that depends on the counting interval (T_{count}), with the following equation:

$$N = \frac{T_{count}}{2 \cdot n_{stages} \cdot T_{INV}}. \tag{3-1}$$
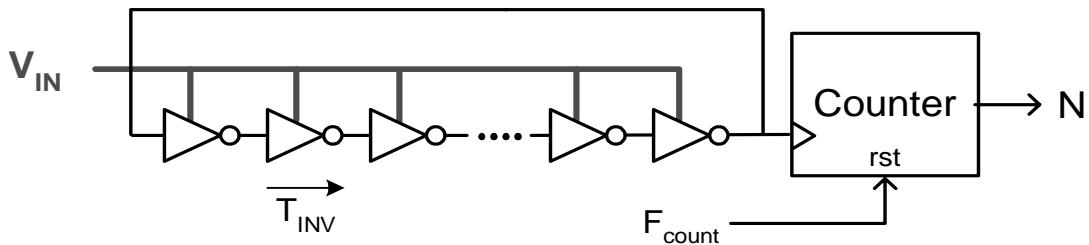
Figure 3.2. Ring oscillator and counter based A/D converter

At the end of each interval, N is stored and the counter resets to zero for the subsequent count. F_{count} (= $1/T_{count}$) is set by the buck converter's switching frequency. Since N depends on T_{count} and n_{stages}, longer counting intervals and less inverter stages enable higher resolution of the output. However, there is a $n_{stages} \geq 3$ limit and T_{count} affects the overall loop dynamics. It is important to count over the full period to obtain an average magnitude of the power supply due to a small voltage ripple at the output of the buck converter.

Since the performance of the counter can be measured as a function of inverter delays, as long as its critical path is less than double the number of inverters in the ring, the counter can also operate at the same voltage as the oscillator. In the case of a simple ripple counter, only the first stage, implemented as a toggle flip-flop, sets the critical path since subsequent stages operate at lower rates. Figure 3.3 illustrates the ring oscillator, ripple counter, and finite state machine (FSM) used to implement this simple A/D converter [48]. The finite state machine not only resets the counter, but also allocates additional time at the end of the counting interval, before the latching the output, to accommodate for the worst-case ripple path through the counter. Assuming the clk-to-Q delay of a flip-flop is on the order of 2-3 inverter delays, the worst-case ripple delay is set by the number of bits
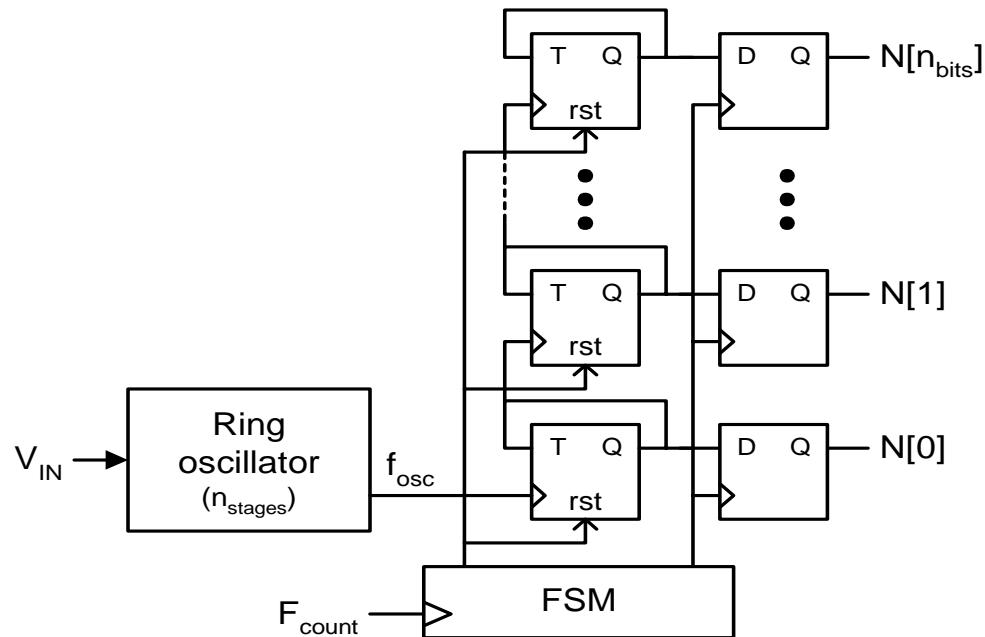
Figure 3.3. A/D converter detailed schematic

in the counter (n_{bits}) and the following equation:

$$\text{Worst-case ripple path} \ = \ 3n_{bits} \cdot T_{INV}. \tag{3-2}$$

Hence, for the following inequality,

$$\Delta_{delay} \ = \ 3n_{bits} \cdot T_{INV} \text{Ð} 2n_{stages} \cdot T_{INV} > 0, \tag{3-3}$$

the FSM must allow an additional Δ_{delay} of time before latching the counter outputs. Since the FSM enables the counter to operate at the same frequency and voltage as the ring oscillator, the A/D converter's power consumption tracks with the ring oscillator and ultimately with the rest of the digital system to which power is supplied.

This simple approach to building an A/D converter can be improved by using phase information to increase digital resolution of the analog voltage without a power penalty. High switching frequency (for the buck converter) and high resolution are desirable for building a digitally controlled regulator with good performance. Higher switching frequencies enable higher bandwidths for the control loop and higher resolution minimizes quantization error that results from a digital implementation of an inherently analog loop. Given a target switching frequency of 1-MHz and 10 bits of resolution, a simple ring oscillator and counter used for A/D conversion must run at an extremely high rate. Since the least significant bit (LSB) corresponds to a single oscillator cycle, to convert the maximum voltage to the maximum digital output of the counter, the counter must run at 1-GHz. This leads to significant power consumption in the A/D conversion block which increases overhead power and degrades the converter efficiency. Instead, reducing the LSB to a fraction of the oscillation period is preferable.

To lower the A/D converter's power consumption, an improved version based on a technique that relies on a delay-line instead of a ring oscillator [8] is presented in Figure 3.4. In this implementation, the ring oscillator and counter structure is retained for hardware reuse and to avoid the geometrically increasing number of delay stages with each additional bit of resolution. The counter output now only accounts for the five higher order bits, N[9:5], of the digital output. Similar to the original approach, the counter counts pulses out of the ring oscillator over the switching period of the buck converter, but

generates a course grain representation of the input voltage. The lower order bits of resolution are extracted from the delay line. Instead of a just implementing a delay line consisting of inverters, each delay element consists of a static pass transistor latch that captures the internal state of the ring at the end of the counting period. A synthesized encoder takes the output of each of the 32 delay stages and determines how far an edge has traversed through the ring to generate the lower order bits, N[4:0], of the binary representation of the input voltage. NAND gates reset the ring in order to have it restart from a known initial state. This approach reduces the LSB of the A/D converter from an entire oscillation period to a single delay stage and reduces the counter's power consumption. So, while the previous design would require a 1-GHz oscillator for 10 bits of resolution at a switching period of 1-MHz, the oscillator in the new implementation only needs to oscillate at 32-MHz for the same resolution and switching frequency. It is important to point out here that this approach does not reduce the ring oscillator's power since it is set the by total switched capacitance and inverter delay, and not the oscillation frequency. Since the additional cost of the encoder block is small, this implementation enables low-power solution.

The A/D conversion techniques described thus far have been used to convert the output of the buck converter into a frequency and then into an equivalent digital representation of the voltage and frequency. Comparing this value to a reference determines whether the buck converter output voltage corresponds to the value required for the digital system to operate at the desired frequency of operation. If the reference is a
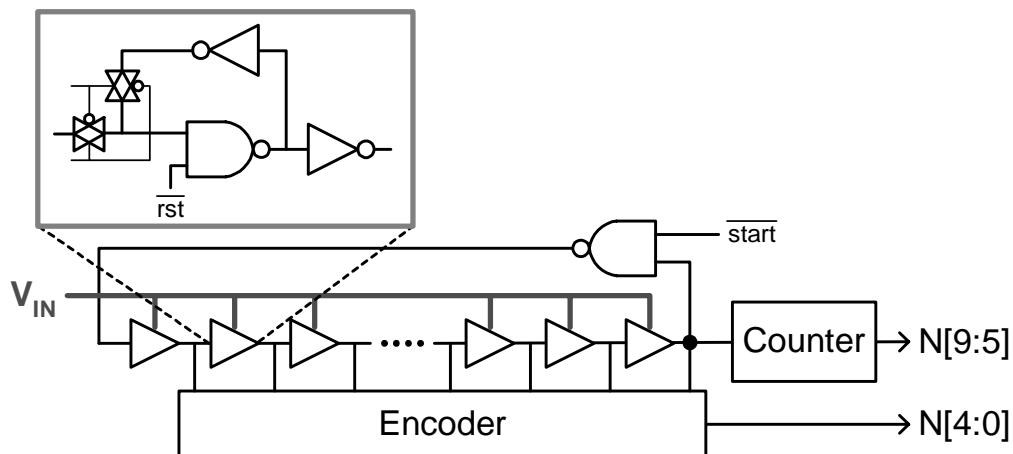
Figure 3.4. Low-power A/D converter

voltage, the difference between the outputs of two A/D blocks with the same counting interval generates a binary equivalent of the voltage difference. Good matching between the two oscillators ensures the regulated voltage matches the reference voltage. Given a frequency-locked loop, as described in Chapter 2, which assumes the reference is a clock frequency, the reference clock would feed straight into the counter and bypass the ring oscillator in the reference A/D path. In this case, the oscillator in the feedback path of the regulator must accurately model the critical path of the digital system to which power is delivered.

Given a digital representation of the difference between the regulated voltage and the reference, this error must then drive PID control blocks to servo the duty-cycle of the PWM rectangular wave to the buck converter, and drive the error to zero through negative feedback. A digital circuit equivalent of the PID control that operates on the error is covered next.

3.2 Digital PID Control

This section describes the digital implementation of the PID controller [49] that operates on the error generated by the A/D converters described above. Separate digital blocks implement the discrete-time equivalents of the proportional, integral and derivative functions of the controller. The output sum, y_{PID}, is a binary representation of the duty-cycle of the PWM rectangular wave that drives the buck converter. These digital blocks implement the following discrete-time functions:

$$y_P(n) = k_P \cdot x(n) \tag{3-4}$$

$$y_I(n) = y_I(n-1) + \frac{1}{k_I} x(n) \tag{3-5}$$

$$y_D(n) = k_D[x(n) - x(n-1)] \tag{3-6}$$

$$y_{PID}(n) = y_P(n) + y_I + y_D(n) \quad . \tag{3-7}$$

x(n) represents the feedback error between the regulated output voltage and the reference at each discrete-time n. Each discrete interval n is equivalent to the switching period of the
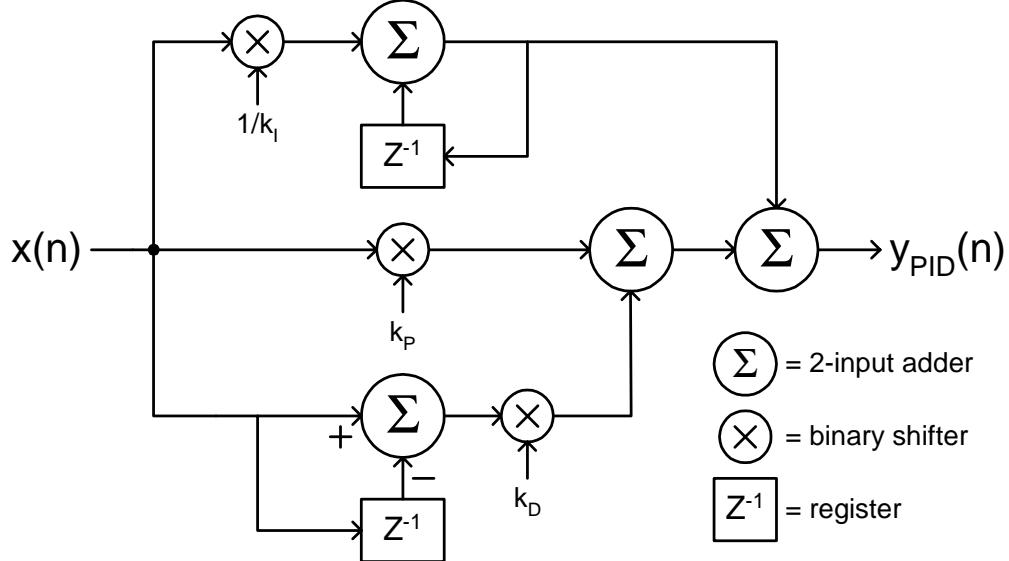
Figure 3.5. Circuit implementation of PID control blocks

buck converter and control signals are pipelined through the digital blocks at this rate. The resulting discrete-time equivalents of the PID control blocks closely mimic the continuous-time transfer function, described in Chapter 2.

Detailed block diagrams of the three control blocks are presented in Figure 3.5. Since the update rate of the digital control is significantly lower than the rest of the digital system to which power is regulated, it has low performance requirements. Therefore, discrete-time control blocks utilize simple ripple-carry adders for addition and subtraction. Binary shifters implement multiplication and division, but limits multiplication and division to powers of 2, as follows:

$$k = 2^{N_{shift}},$$
(3-8)

where N_{shift} corresponds to the binary shift amount with negative values corresponding to division by shifting right (e.g. $2^{-2} = 1/4$). Proportional control is a simple multiplication by k_D. Integral control is equivalent to accumulation in the digital domain and requires a register to store the output from the previous cycle (n-1) and add a fraction of the error, set by constant k_I, in the current cycle. In order to avoid quantization effects that can result from shifting, all lower order bits are preserved for the calculations. Lastly, the derivative function takes a difference between the current and previous cycle's error values, and

multiplies it by a constant k_D. An output sum of these blocks result in the desired PID control and corresponds to a binary equivalent of the required duty-cycle D input to the buck converter.

Minimum device sizes reduce controller energy consumption at the expense of slower operation. This slow performance is acceptable in this case because of its relatively low update rate. Furthermore, its low performance requirements allow all the PID control logic to operate off of the regulated supply voltage. Therefore, both A/D converter blocks and the PID control, described so far, also benefit from the power savings provided by adaptive power-supply regulation and their power consumption tracks with the load. If the rest of the controller, namely the D/A converter and buck converter, can also operate off of the regulated voltage, the controller's total power can always be a fixed percentage of the power delivered and maintain high conversion efficiency across a wide range of regulated voltage levels. Unfortunately, this may not always be possible and power consumed in the D/A converter and buffers required to drive the buck converter can limit converter efficiency.

Inefficiencies in the overall regulator stem from three main sources of overhead power. While losses due to switching transistor resistance tracks with load current, the ramp-up buffer chain to drive these large switches consumes a relatively fixed amount of power to drive a fixed capacitive load. Lastly, the D/A converter consumes overhead power and can vary depending on its implementation. Efficiency is measured as a ratio of the power delivered to the load versus the total power consumed by the regulator, defined by the following equation:

$$\text{Converter Efficiency} = \frac{P_{load}}{P_{load} + P_{driver} + P_{buck} + P_{controller}}. \tag{3-9}$$

P_{load} varies depending on the requirements of the system being driven and affects conversion efficiency. For high load power requirements, power consumed by the controller can be a small fraction such that efficiency is dominated by the buck converter and load. However, for low power conditions, the controller's power can be significant and the dominant factor that limits conversion efficiency.

The loop's update rate (or switching frequency), designated as F_{loop}, clocks the digital controller and sets the time base for the overall regulator system. A sampled average of the buck converter output voltage and input reference are found during a single F_{loop} cycle as well as the PID calculations. A subsequent D/A block operating over the same period translates the digital PID control output to a PWM rectangular wave. Given that the error sampling and update occur at the loop frequency, the PID control time constants are proportional to F_{loop}. The cut-off frequency of the LC filter in the buck converter, however, is fixed and independent of F_{loop}. In order to maintain a stable control loop over a dynamic range of regulated voltage levels, a fixed loop frequency is necessary to guarantee a fixed relationship between the loop parameters of the PID control and buck converter. The most obvious approach is to use a fixed-frequency controller. Unfortunately, such an implementation can result in considerable overhead power consumed by the D/A block that doesn't track with the regulated voltage and power delivered to the load. A breakdown of the power consumed by an initial implementation of a fixed-frequency controller briefly described in the following subsection motivates a variable-frequency controller design that is described next.

3.3 Variable-Frequency Control

Whether the loop is a fixed- or variable-frequency controller is determined by the implementation of the D/A conversion. Figure 3.6 presents a block diagram of the overall
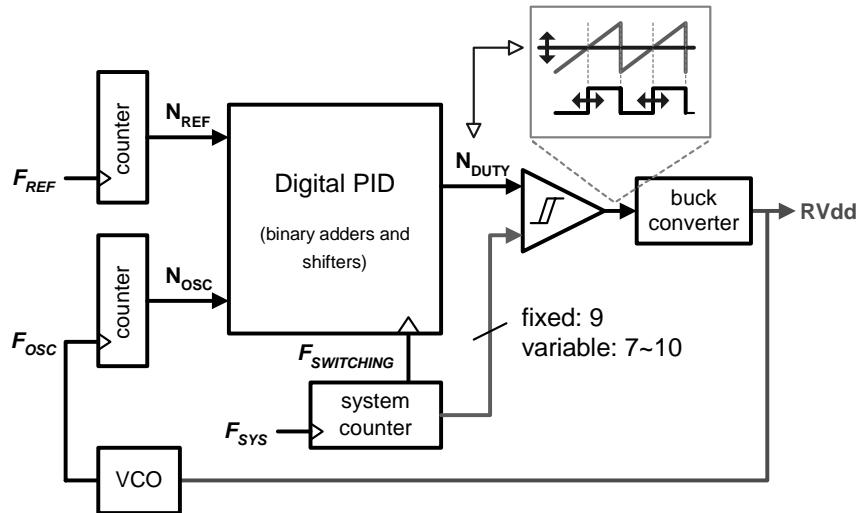
Figure 3.6. Digital PID control loop

power-supply regulator loop. D/A conversion is achieved by taking the output of the digital PID controller and comparing it to a binary ramp wave generated by a free-running synchronous counter. This is a digital equivalent of the analog PWM rectangular wave generator described in Chapter 2. The monotonically increasing binary ramp repeats at a rate set by the input clock, F_{sys}, and the number of bits in the counter, N_{ramp}. This rate corresponds to the update rate of the controller and set by the following equation:

$$F_{loop} = \frac{F_{sys}}{max(N_{ramp})}. \tag{3-10}$$

Waveforms in the inset box in Figure 3.6 illustrates the generation of the variable duty-cycle rectangular wave that drives the buck converter. The conversion is governed by the a linear relationship between y_{PID} and the duty cycle as follows:

$$\text{Duty cycle} = \frac{y_{PID}}{max(N_{ramp})}, \tag{3-11}$$

where N_{max} corresponds to the maximum count value of the synchronous counter and has the same number of bits as y_{PID}. The ramp wave's period sets the period of the rectangular waveform. A binary comparator, implemented with only the carry portion of a subtractor, takes the difference between the PID output and the binary ramp, and looks at the carry output of the highest order bit. At the beginning of the comparison, the binary ramp starts lower than the PID output and the carry out is low. Once the binary ramp exceeds the PID output, the highest order carry bit flips high and this transition corresponds to the appropriate pulse-width set by the PID control. The overall feedback loop constantly updates the PID output to proportionally modulate the duty-cycle of the rectangular wave input to the buck converter.

In a fixed-frequency implementation, F_{sys} is a fixed-frequency clock and generates a fixed update rate, F_{loop}, for the controller. This constraint requires the counter for the D/A conversion to be operated at a fixed rate and a fixed voltage, and as a result, is the dominant source of overhead power dissipation. To highlight the inefficiencies stemming from this overhead, Figure 3.7 presents a distribution of the measured power consumed by a power supply regulator, fabricated in a MOSIS 1.2μm CMOS technology [48], at three different voltages regulated down from 5-V. The bar graph presents the percentage of the
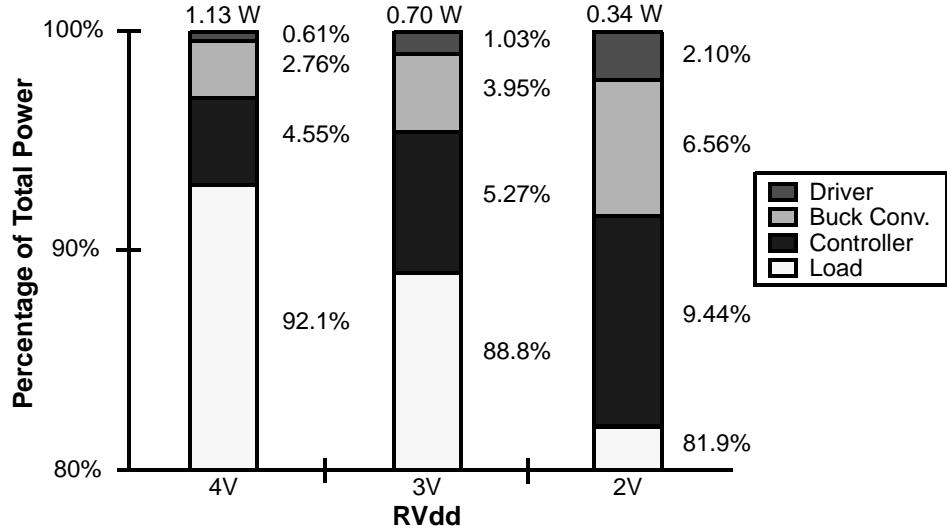
Figure 3.7. Normalized power breakdown

power consumed by different parts of the regulator and the power delivered to a resistor load relative to the total identified on the top of each bar. The controller's power, dominated by the D/A converter, increases as a percentage of the total to degrade converter efficiency as voltage reduces. To make matters worse, dynamic power of typical digital circuits is proportional to V^3, while a resistor's power is proportional to V^2. Therefore, application to an actual digital load would result in even lower conversion efficiencies.

The key to improving conversion efficiency while maintaining loop stability is to allow the internal frequency and voltage of the controller to change while keeping the controller's loop parameters relatively constant [49]. Since these parameters are proportional to the update rate (or loop frequency) of the controller, F_{loop} must remain relatively constant (within a factor of two). In the previous design, the buck converter's switching frequency corresponds to the frequency of the binary ramp wave generated by the synchronous counter, which was clocked by an external fixed-frequency system clock. In a variable loop-frequency scheme, this system counter is clocked by the ring oscillator driven by the regulated voltage or the reference, and the number of counter bits varies depending on its region of operation. To accomplish this, a frequency detection circuit is required. A new system counter has a maximum count ($max(N_{ramp})$) ranging from 128 to 1024 (7 to 10 bits), determined by a frequency-detect circuit and a variable-frequency
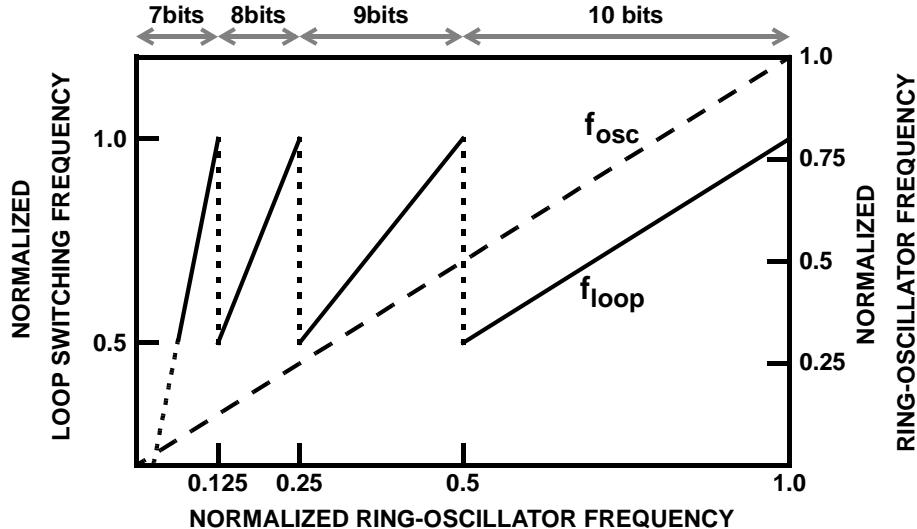
Figure 3.8. Normalized frequency shifting

clock. Figure 3.8 plots the normalized loop frequency that results from changing the maximum counter bits across a normalized range of input frequency to graphically illustrate frequency shifting that limits loop frequency range. The controller monitors the system counter's input clock frequency and determines the number of bits up to which the counter needs to count in order to maintain a switching frequency that varies by no more than a factor of 2. For example, when the reference or oscillator frequency falls to less than half the maximum rate, the counter only counts up to 9 bits instead of 10. This effectively doubles the loop switching frequency and keeps it from falling below half the peak. In order to keep the loop from dithering between two loop frequencies at the frequency shifting boundaries, hysteresis is built into the frequency detection circuit.

Since the PID control's time constants are proportional to this loop frequency, the PID coefficients are also dynamically adjusted to further limit the loop parameters' excursions with respect to frequency. By incorporating these two methods into the controller, a stable loop configuration results and is verified by the open-loop frequency response simulation shown in Figure 3.9. The two curves represent the two extremes of loop frequency which both exhibit sufficient phase margin for stable operation. Figure 3.10 presents the resulting behavioral-model simulation of the closed-loop transient response to changes in the reference. By clocking the system counter at a variable clock rate set by the regulated voltage, as long as the worst case critical path delay in the digital controller is less than the
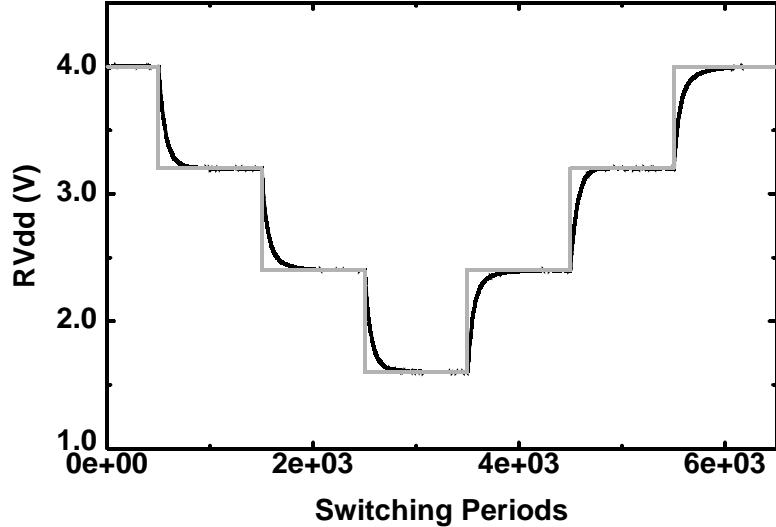
Figure 3.10. Simulated voltage-transient response

delay modeled by the ring oscillator, both the system counter and comparator can operate off the lower regulated voltage. Hence, it is possible to keep the controller's power-consumption overhead at a fixed fraction of the total power consumed.

To verify the power saving improvements, this variable-frequency controller was designed and fabricated in a MOSIS 0.8-μm technology [49]. Figure 3.11 presents a photo micrograph of the test-chip prototype. The controller consists of a 15-stage ring oscillator
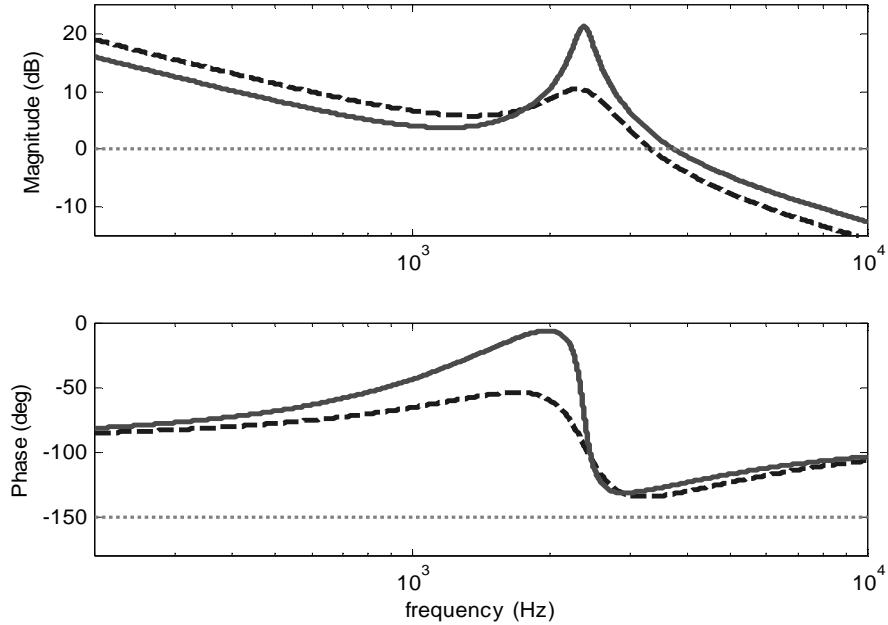
Figure 3.9. Simulated open-loop response at high and low loop-frequency limits
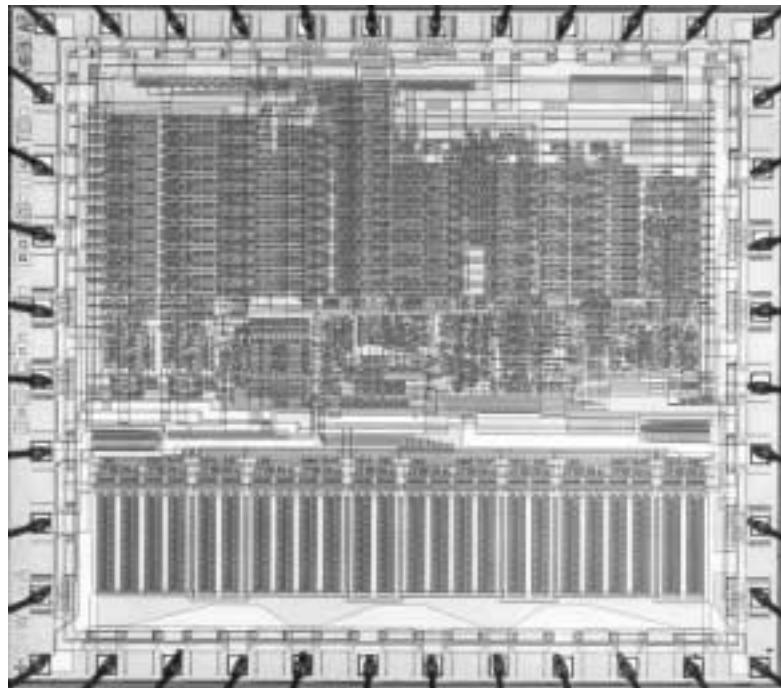
Figure 3.11. Test-chip micrograph

that oscillates at a peak frequency of 116-MHz at 5-V and the loop frequency ranges from 57-114 kHz. The switching transistors for the buck converter are shown on-chip. The converter's external LC filter components are 70-µH and 70-µF and regulate down from a 5-V external supply. Figure 3.12 plots the measured power for the digital controller and buffers that drive the large on-chip switching transistors across a wide range of regulated
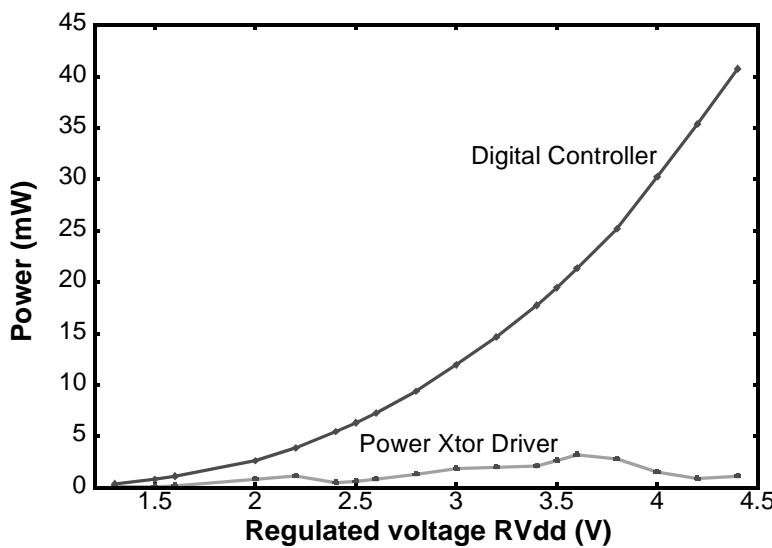
Figure 3.12. Overhead power vs. regulated voltage
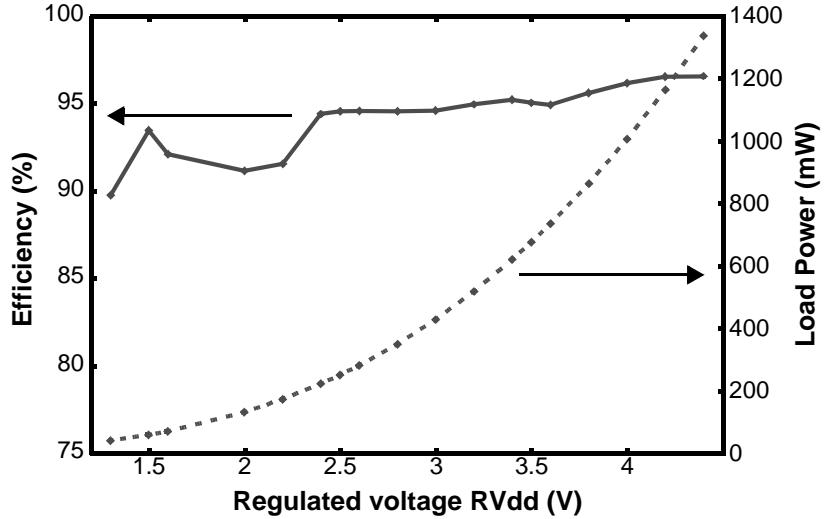
Figure 3.13. Conversion efficiency vs. regulated voltage

voltages. Since the digital controller powers off the regulated supply, its power consumption exhibits the same cubed dependence on voltage as the dynamic power of synchronous digital circuits that load the regulator. Buffers that drive the buck converter switches, however, must operate off a fixed supply and so its power doesn't track with regulated voltage. Instead, variations in this power is governed by the variable loop frequency and other non-linear low-power techniques described in Section 3.5. Now that the controller is no longer a dominant source of overhead power at lower voltages, conversion efficiency significantly improves for lower supply voltages as demonstrated by the measured converter efficiency versus regulated voltage plotted in Figure 3.13. The regulator targets a synchronous digital logic chip that consumes 1-W at 4-V, and its dynamic power is proportional to V^3 as shown by the dotted line with its corresponding magnitudes specified on the right axis.

While conversion efficiency is an important measure of regulator performance, good transient response characteristics are also desirable. There are two aspects of the regulator's transient response that must be evaluated. An important characteristic for all power supply regulators is its response to sudden changes in the load. As described in Section 2.2, PID control extends the loop bandwidth to exceed the LC cutoff frequency of the filter. Since load variation perturbs the regulator output voltage at a time constant set by the resonant frequency of the filter, the higher bandwidth allows the loop to quickly
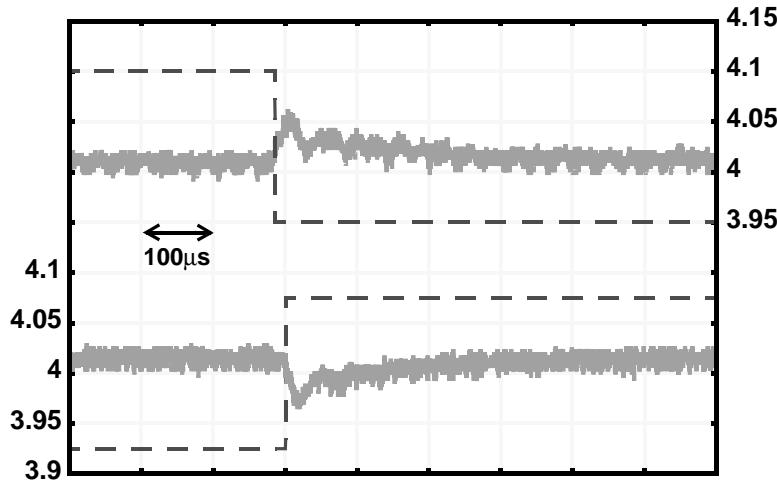
Figure 3.14. Measured load transient response

correct for load variations. Figure 3.14 plots data extracted from a digital sampling oscilloscope to demonstrate the loop's ability respond to both increasing and decreasing step changes in load current; where the dotted lines delineate step changes in load current between 0-mA and 100-mA at 4-V. The output varies by less than 2-% of the regulated voltage level and settles within 200-µs. In order to enable a digital system that can adapt its operating frequency depending on performance needs, this regulator must also quickly adapt its voltage to the needs of different frequencies. The rate at which this power supply regulator can change its voltage is set by the bandwidth of the loop. Figure 3.15 presents the loop's output voltage-transient response which tracks rising and falling step changes in the reference. Due to a loop frequency shifting boundary that exists halfway through the
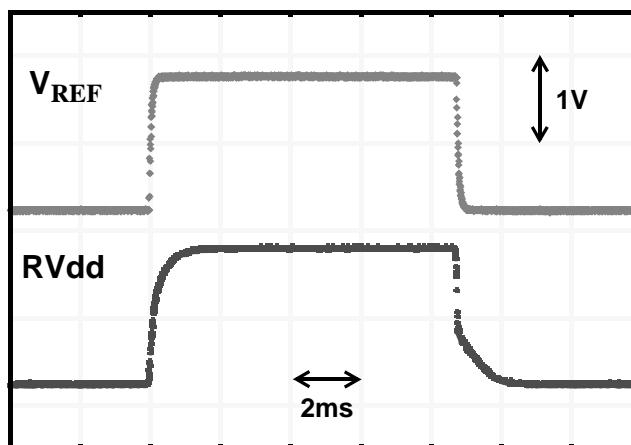
Figure 3.15. Measured voltage transient response

voltage transient, the loop's bandwidth also changes halfway through the falling transition and therefore results in slightly different bandwidths for the rising and falling transitions.

Enabling variable frequency operation results in a controller whose power tracks with the variable frequency and regulated voltage such that its power consumption is a fixed fraction of the CV^2f power consumed in the load. However, this approach still suffers from high power consumption at high frequencies and voltages, limiting its efficiency for low-power loads. A digital controller requires blocks that digitize voltage and time into discrete increments. The two iterations described so far rely on a ring oscillator and counter for digitizing operations. And digitalization that relies on a ring oscillator results in the least significant bit (LSB) equivalent to an oscillation period. Therefore, in order to achieve high resolution and high buck converter switching frequencies, the ring oscillator and counter must run at a high rate. A 1-MHz switching frequency and 9-bit resolution requires a maximum rate on the order of 500-MHz. Higher resolution requires even higher oscillation frequencies. The ring oscillator does not have to exactly match the critical path since some gain factor can be used in the loop to account for the differences, but the higher frequency stresses the performance of the counter and leads to higher power consumption. However, an implementation that relies on a delay line, rather than a ring oscillator, can leverage more timing information that is available within the delay line for higher resolution. A technique that builds on this ability to obtain higher resolution can lower the overall power consumption of the controller, eliminate the complexity required for variable frequency operation, and is described next.

3.4 Low-Power Control

A digital controller design that utilizes a tapped delay-line to implement an effective D/A conversion with low overhead was demonstrated in [6]. In this implementation, the total delay through the delay-line matches the switching period and a digital number taps out the fractional delay that corresponds to the desired pulse width. So, it reduces power consumption by obviating the need for a highly active system counter and comparator operating at high frequencies. To address the high power consumption in the digital controller that limits conversion efficiency, a low-power implementation that utilizes a

low-power A/D converter, described in Section 3.1, and a subsequent D/A block that also leverages a delay line is described. It relaxes the need for higher frequency operation in the D/A block and reduces its LSB to a few gate delays.

This lower power controller relies on a D/A that taps out at discrete points along a delay line and uses this additional timing information to reduce the LSB to a fraction of the oscillation period. A detailed block diagram of the improved D/A blocks, presented in Figure 3.16, generates a fixed frequency PWM rectangular wave whose pulse width is set by the digital output of the PID block denoted as D[9:0]. A ring oscillator consisting of several delay stages operates off of a fixed voltage to generate fixed frequency pulses to a counter. However, a single period is no longer the LSB and therefore allows much slower oscillation periods to reduce the frequency of operation for the counter. At the beginning of the switching cycle, the counter is reset to zero and a comparator waits until the counter output matches the five higher order bits of D[9:4]. Once there is match, it triggers the control to latch an edge of out the multiplexor. The multiplexor chooses a point along the ring which has a delay that corresponds to the number of buffer stages set by the four lower order bits of D[3:0]. Therefore, the LSB is reduced to the delay of a single buffer stage as opposed to a complete oscillation period. This implementation retains the ring oscillator and counter structure to reuse hardware and avoid a large delay line that can result in order to implement a large number of bits for high resolution. The counter
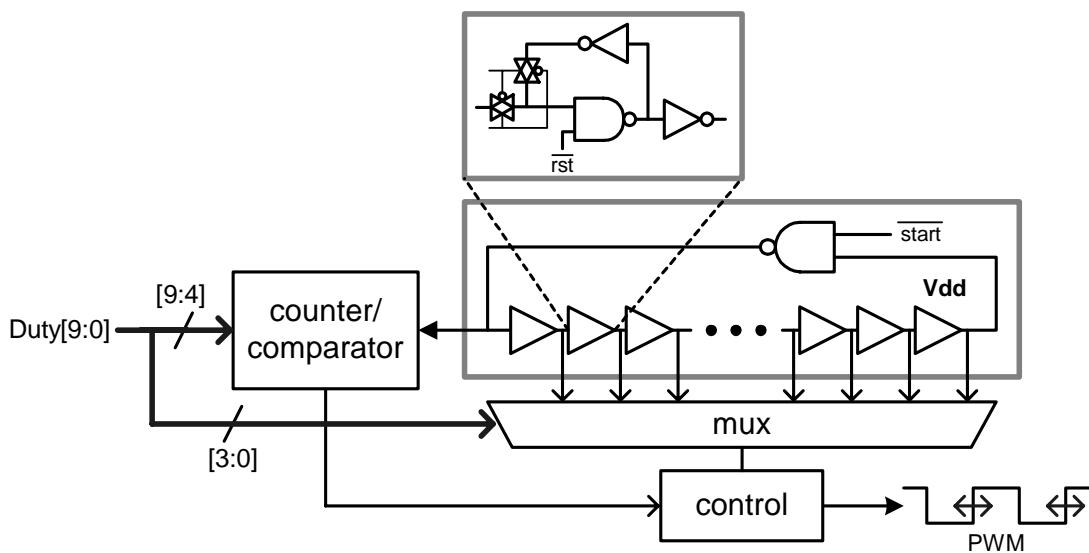
Figure 3.16. Low-power D/A block diagram
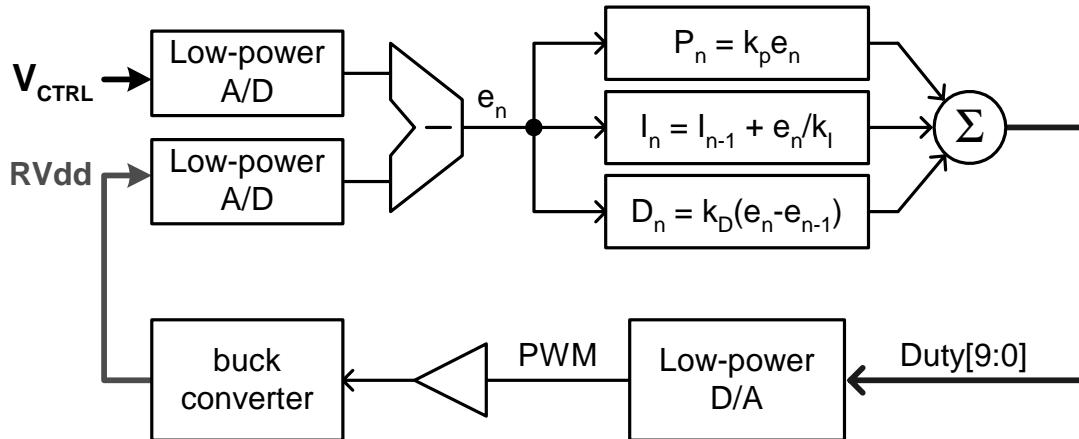
Figure 3.17. Low-power controller block diagram

continues to count pulses out of the oscillator until the counter reaches its maximum count which denotes the end of the switching period.

The ring-oscillator frequency and counter set the switching period (or F_{loop}). Given a 5-bit counter, there are 32 ring-oscillator cycles in the switching period and thus requires the ring to oscillate at 32-MHz for a 1-MHz PWM rectangular wave. The ring consists of 16 delay stages to generate the finer delay granularity set by the four lower order bits. Each delay stage consists of a NAND gate, as shown in the inset box in Figure 3.16, in order to restart the ring at the beginning of each switching period from a known state. Since this ring must operate at a fixed frequency, it operates off of a fixed supply voltage. The external high supply of the buck converter is used and the delay of each stage is designed to be approximately 1ns for an oscillation frequency of 32-MHz. Since the performance requirements of the counter is now much lower, the other components of the D/A conversion block operates off the regulated supply so that it dissipates less power.

Figure 3.17 presents the overall block diagram of this improved digital controller for adaptive supply regulation. Low-power A/D blocks that consist of tapped ring oscillators convert the reference and regulated voltages to binary equivalents to generate a feedback error. A discrete-time digital implementation of the PID control operate on the error to generate a binary equivalent of the duty-cycle for the buck converter. The low-power D/A block which also consists of a tapped ring oscillator converts the binary PID output into a PWM rectangular wave. This block also generates the 1-MHz update rate for the PID

control blocks and counting interval of the A/D converter blocks. Except for the fixed-frequency ring oscillator in the D/A block and the buck converter, all digital components in this controller operate off a lower regulated supply in order to reduce power consumption. A simple low-to-high swing converter, shown in Figure 3.18, is used to interface the lower voltage blocks to the high voltage buffers that drive the buck converter.

This digital power supply controller was implemented within a high-speed I/O interface chip in order to offer the power savings possible with adaptive supply voltage regulation. A DLL in the I/O interface generates the reference voltage, which sets the desired regulator voltage output. A zoomed-in photo micrograph of the power supply prototype fabricated in a HP0.35-μm CMOS technology [50] is presented in Figure 3.19. On-chip switching transistors for the buck converter operate off a 3.3-V external supply and have maximum widths of 7-mm and 3.5-mm for the pMOS and nMOS devices, respectively. These sizes are optimized to drive 250-mW of peak load with a switching frequency of 1-MHz. nMOS gate capacitors fill empty die space to reduce power supply noise that can result from large current switching transients. The external filter inductor and capacitor are 10-μH and 10-μF, respectively. The digital controller's overhead power is 1.5-mW while regulating 2.7-V, and converter efficiency is greater than 90-% while delivering 200-mW. This overhead, considerably less than that achieved in previous
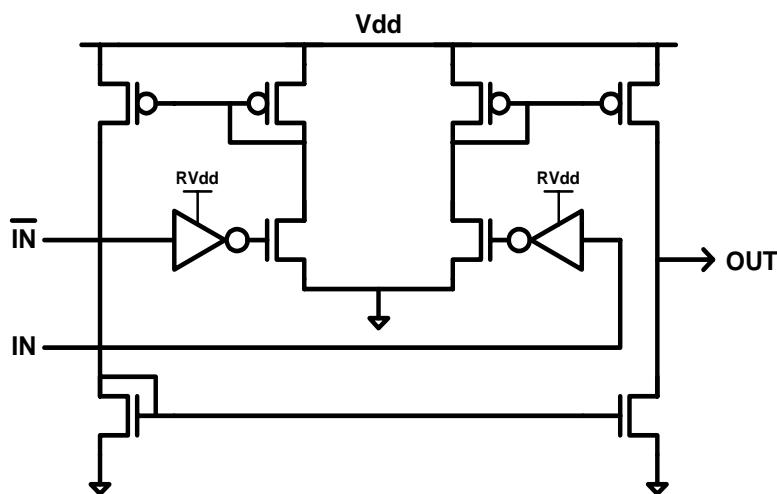
Figure 3.18. Low-to-high voltage converter
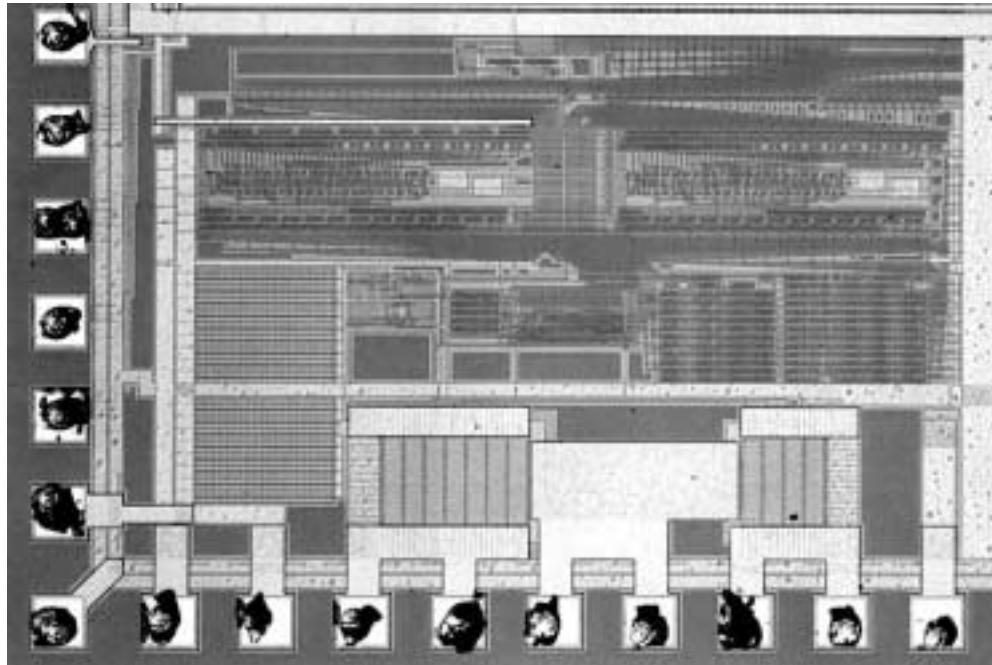
Figure 3.19. Power-supply controller block photo micrograph (zoom)

implementations, is possible through the low-power A/D and D/A blocks. The measured

regulator voltage range is limited by a lower range limit in the I/O implementation and is

1.3-3.2 V. Converter efficiencies greater than 80-% is achieved for this range with

delivered load power ranging from 50-mW to 300-mW.

3.5 Non-Linear Power Reduction Techniques

One of the advantages of a completely digital, discrete-time implementation of the power

supply controller is the ability to easily incorporate non-linear techniques in efforts to

improve converter efficiency [6],[45],[48]. The previous sections described various

techniques to reduce power consumption in the digital implementation of a linear PID

control. This section describes techniques to reduce two dominant components of loss in

the buck converter: *(i)* resistive loss through the transistor switches and *(ii)* switching loss

needed to drive the switching transistors. An equation to optimally size the switching

transistor that trade-off these two loss components is a function of load power. Over a

wide operating range, however, this optimum changes due to the load power's strong

dependence on its operating frequency. Therefore, dynamically reducing transistor sizes

close to the optimum under lower load conditions leads to higher conversion efficiencies
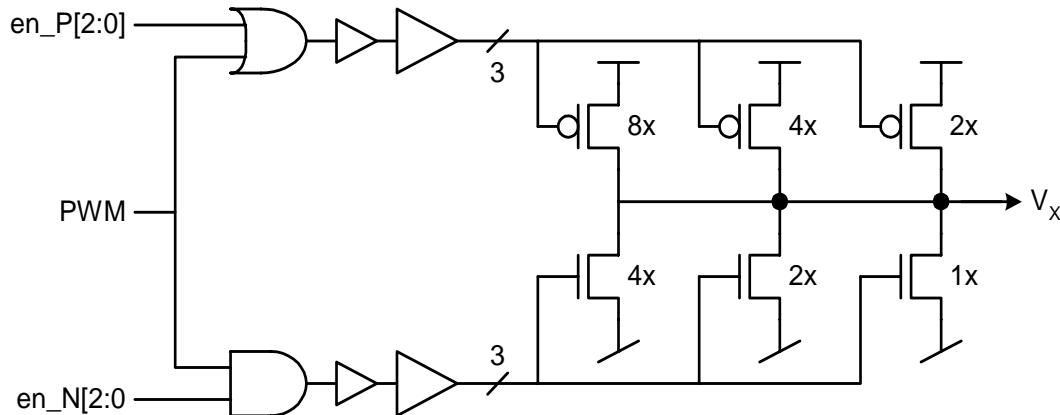
Figure 3.20. Segmented buck converter switching transistors

[34]. In addition to transistor sizing, for ultra low-power load conditions, very little current is drawn from the filter capacitor. Therefore, under normal buck converter operation, only a small fraction of the charge from the external supply supplies the load's current consumption and the rest recirculates back through the switching transistors which leads to wasted power dissipated through the nMOS switch. By recognizing these low-load conditions, the regulator can enter a discontinuous mode of operation that turns off the converter and periodically replenishes charge to the filter capacitor.

The ability to dynamically vary switching transistor size requires parallel transistor segments that can be individually enabled or disabled. Since extremely wide devices are used to reduce resistive loss in these devices under high load current conditions, layout of wide devices are implemented by folding the gates into parallel segments in order to consume a compact area with a manageable aspect ratio. Therefore, adjustable sizing is possible by grouping these segments into blocks and driving them separately as shown in Figure 3.20. Three blocks of binary weighted parallel transistor segments enable 8 possible sizes, including a width of zero. Inverter buffer chains drive these four blocks and enable signals gate the beginning of the chain to eliminate dynamic power dissipation in the buffer chain for segments that are disabled. Since the buffers that drive the switching transistors also consist of a parallel set of smaller buffers, four separate buffer chains can be implemented without additional overhead.

Although implementing adjustable switching transistor sizes is straight forward, effectively using them is more complicated. It requires a measure of load power to

appropriately size them. The power supply regulator can leverage the dynamic power equation, which has a cubed dependence on voltage. The regulated output voltage can be determined by looking at the output of the PID control and used to set the appropriate width. This simple approach assumes the activity of the load is a nominally fixed value. Unfortunately, power saving techniques, such as clock gating, can cause significant fluctuations in circuit activity for the same voltage. Additional information provided by the system is therefore required to compensate for these differences in power requirements of the load. Alternatively, a current sensor that monitors the average current delivered to the load may provide the necessary information to set optimal transistor widths.

While there is a strong correlation between voltage and power consumption, dynamic power can also vary with respect to switching activity. Therefore, a condition may arise that requires a high voltage to enable fast operation for a small segment of a chip, while the rest of the system is inactive. This can result in a condition where the buck converter dissipates power through recirculating current, because the average current delivered to the load is less than half the ripple current amplitude. Recirculating current can be avoided by sensing when recirculating current occurs and then disabling subsequent pulses to the buck converter until the output falls below a preset threshold. Once a voltage droop is detected, the controller sends discrete packets of charge until the output magnitude is restored. This discontinuous operation still requires the front-end of the controller to remain active to sense the voltage error, but, it reduces the buck converter switching losses by reducing switching activity and removing recirculating currents. The mechanism for detecting when recirculating current occurs uses a voltage detector illustrated in Figure 3.21. At the end of the switching period, both pMOS and nMOS devices are briefly turned off and the drain voltage is sampled. In the case of recirculating current, the current magnitude through the inductor is negative and therefore charges up the drain capacitor. A fast precharged inverter senses whether the drain voltage rises above a threshold voltage and drives a series of meta-stability hardened flip-flops. Detecting when there is recirculating enables the controller to operate in a discontinuous mode that periodically send packets of charge to supply the low currents consumed by the load and otherwise minimizes resistive losses through the buck converter.
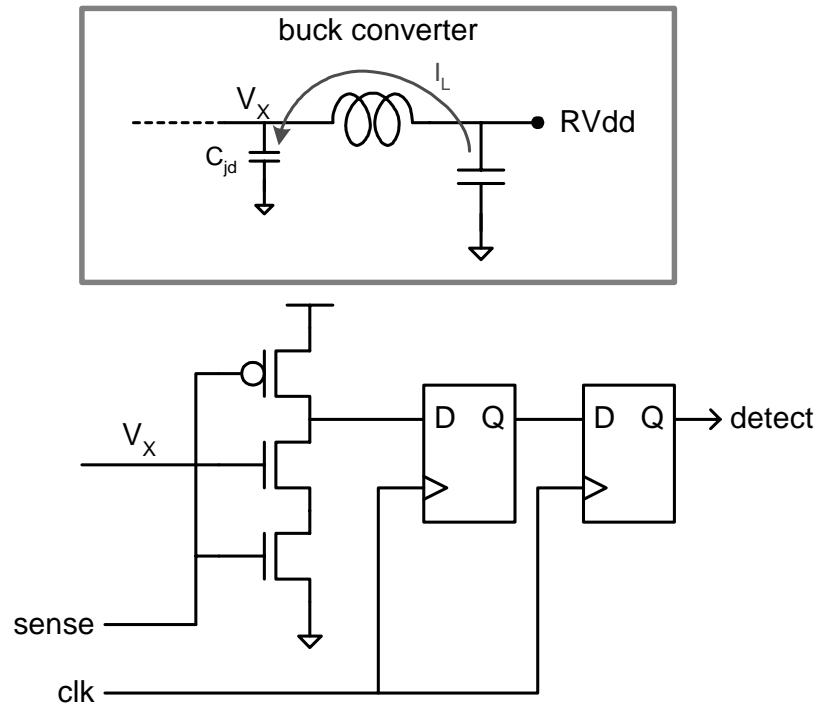
Figure 3.21. Recirculating current detector

3.6 Summary

Implementing the power supply controller entirely out of digital gates offers several advantages. Since this adaptive power supply regulation scheme targets large digital systems to optimize its energy consumption, a digital implementation can be embedded within the same die and does not require the special attention normally required for mix-signal designs. It results in a simpler and robust design that may be synthesized and is portable. Furthermore, a digital implementation can leverage the same power saving technique enabled by the regulator such that its power consumption tracks with the frequency of operation. Lastly, a digital implementation allows non-linear techniques that can reduce losses and improve converter efficiency.

This chapter described three iterations of the digital controller, where each iteration reduces the overhead power consumption of the controller to improve power conversion efficiency. An approach that relies on a simple ring oscillator and counter for A/D and D/A conversion is effective, but high switching activity and operation off of a fixed high

supply voltage results in significant overhead power dissipation and low converter efficiency. A variable-frequency controller improves the design and enables the controller power to track with the load, but high switching activity in the D/A block still limits its use for low-power loads. A new approach that removes the high switching activity without sacrificing resolution yields a much more viable solution for low load-power applications. Another digital controller that utilizes a non-linear sliding window control scheme also has been developed to further improve converter efficiency for low-power digital applications [25].

The low-power controller described in this chapter has been implemented along with an I/O subsystem to adaptively regulate the voltage to a low-power parallel interface. By using feedback to lock the regulated voltage with respect to an input reference, the regulated voltage contains information about the process and environmental conditions. This information can be leveraged by the circuits in the I/O subsystem to replace precision analog circuits with simple digital gates that now have precise delays with respect to frequency. Chapter 4 describes how an adaptively regulated power supply environment enables a simple and robust I/O interface and the power savings it offers.

Chapter 4

I/O Interface Design

High performance point-to-point parallel interfaces have become increasingly important. They are used in driving flat panel displays [13], communication between microprocessors in parallel machines [37], processor to memories [55], graphics subsystems and peripherals [21], and for enabling high bandwidth communication in high-speed network devices [14]. This chapter describes how adaptive power supply regulation can be applied to a high-speed parallel I/O interface implementation to reduce its power consumption. Furthermore, dynamically scaling supply voltage with respect to operating frequency also offers several advantages the link designer can leverage to build a simple and yet robust interface.

Building a supply adjusted parallel I/O interface requires the same set of components found in conventional parallel links, with the addition of an adaptive power supply regulator. Section 4.1 begins with an overview of a parallel data interface, presents the critical path that limits the peak clock rates achievable, discusses signal integrity issues that affect high performance links, and highlights potential advantages of operating off of an adaptively regulated power supply. One of these potential advantages is the ability to maximize energy efficient operation, which requires that the critical path delay in the I/O subsystem must be known in order to optimally regulate the supply voltage. Section 4.2 describes a core DLL design that generates the "right" (optimal) voltage of operation relative to the critical path in the I/O subsystem in addition to providing multiple equally spaced clock phases to the timing recovery block. Section 4.3 then presents a current-mode transmitter and describes how adaptively regulating the supply voltage affects its operation and performance. The subsequent section then describes a receiver

that can leverage a dynamically scaled voltage environment to yield a simple and robust design. I/O performance also critically relies on a timing recovery block to align its internal clock signals relative to the incoming I/O clock. Section 4.5 describes a digital peripheral loop, utilizing clock edges driven from the core DLL, to perform accurate timing recovery. Experimental results from the I/O test-chip prototype fabricated in a HP0.35μm technology follows in Section 4.6.

4.1 Overview of parallel links

High-speed links can provide high communication bandwidths between chips and consist of four major components as shown in Figure 4.1. A serializer converts parallel data bits into a serial bit stream that sequentially feeds a transmitter. The transmitter then converts the digital binary data into low-swing electrical signals that travel through the channel. This channel is normally modeled as a transmission line and can consist of traces on a printed circuit board (PCB), coaxial cables, shielded or un-shielded twisted pairs of wires, traces within chip packages, and the connectors that join these various parts together. A receiver then converts the incoming electrical signal back into digital data and requires a timing recovery block to compensate for delay through the channel and accurately receive the data. A de-serializer block converts the received serial bit stream into parallel data and re-times the data to the clock domain of the rest of the digital system that consumes it. A common architecture to enable high bandwidth communication between two chips integrates several parallel sets of data links whose delays through the channels match [44].
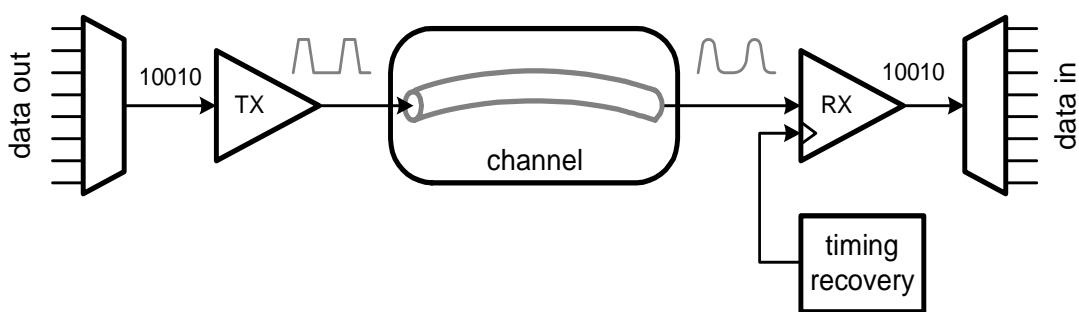
Figure 4.1. Link components
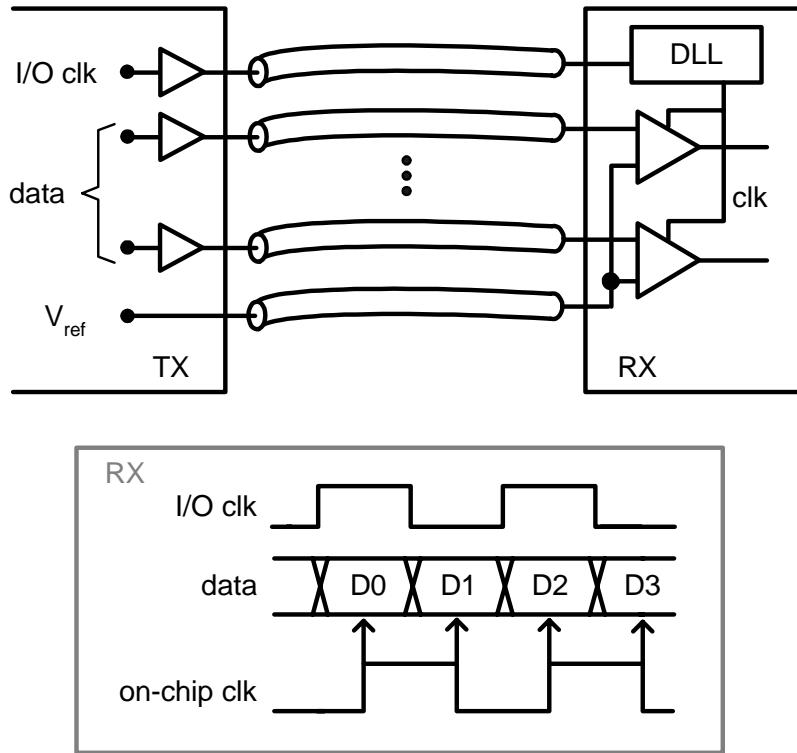
Figure 4.2. Source synchronous parallel interface

This type of interface relies on a separate clock signal for accurate timing recovery. A system-level block diagram of this type of parallel link interface is presented in Figure 4.2. In its implementation in the test-chip prototype, a DLL locks the on-chip clocks relative to the incoming synchronous clock and samples the incoming data in the middle of the data eye.

The following two subsections address two important aspects of high-speed parallel link design that determine the peak performance achievable -- clock speed and signal integrity. In order to maximize bandwidth, high clock frequencies are desirable, which are limited by the process technology, operating conditions, and worst-case delay paths through the circuits in the interface. The second subsection then looks at the signal integrity of an electrical signal that travels through the channel that interconnects the transmitter and receiver. Since this channel is not an ideal transmission line, these non-idealities affect the performance of links and impose some restrictions on transmitter and receiver design. A review of these restrictions reveals some of the potential ways adaptive supply regulation can enable a simplify interface design.

4.1.1 Critical-path delay

The I/O interface is not a stand alone unit, but is a component of a larger digital system that functions to transmit and receive data to and from multiple digital chips. One of the advantages of separately regulating the supply voltage to the I/O subsystem comes from the fact that its performance requirement is generally less than the performance of the rest of the digital system that it serves. In other words, its critical path delay is less than the critical path delay normally found in the core digital logic where most of the computation is performed. For example, the cycle time in a high-performance microprocessor can be on the order of 20 FO4 inverter delays in order to execute complex computations. On the other hand, the computational requirements of the I/O interface is much lower. It only consists of latches to hold data, the transceiver to drive bits on and off the chip. Propagation through the off-chip link does not lie in the critical path since the timing recovery block compensates for its delay.

In order to identify the worst case critical path delay in a high-speed interface, this subsection reviews the critical paths associated with each of the blocks that comprise the link interface. The blocks that connect the link to the rest of the digital system on both the transmitter and receiver side are the serializer and deserializer. Looking first at the serializer, it consists of a parallel set of latches that hold data and a multiplexor that converts the parallel data into serial bits that drive into the transmitter. The ratio between the data transmission bit rate and the digital system's clock rate determines the width of the multiplexor. High-speed transceivers commonly transmit data on multiple phases of the clock and require multiplexors to stagger the transmitted data in time relative to a timing reference. The test-chip prototype transmits data on two phases of the clock and only requires a 2:1 multiplexor. Delay through the latches and delay through the multiplexor are on the order of 2 FO4 inverter delays each, assuming a simple static latch and transmission gate based multiplexor.

The block that follows the serializer is the transmitter that drives the channel. Although there is latency through the transmitter, it is not bounded by a timing reference period and therefore does not impose a delay limit to the link interface. The receiver also
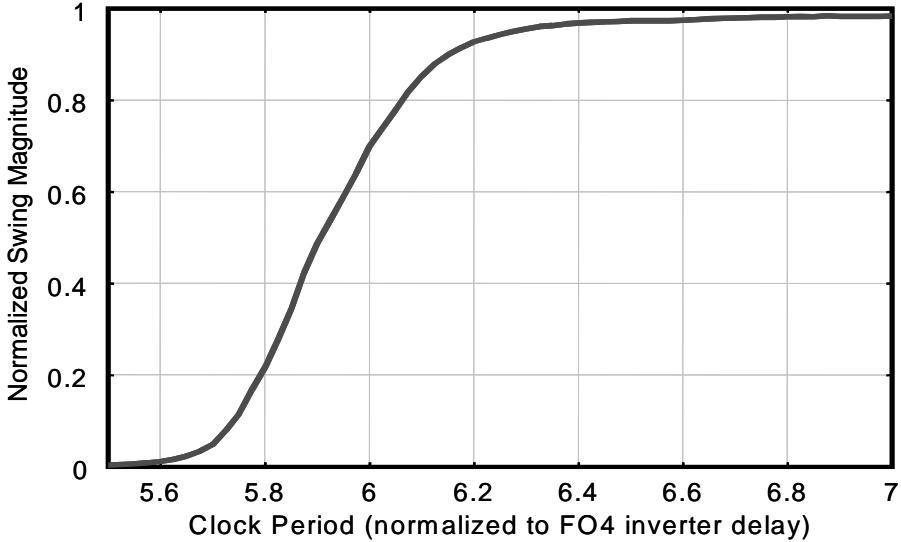
Figure 4.3. Clock swing magnitude vs. clock period

has latency, but it does not impose a limitation to the speed of the link. This latency is absorbed in the timing recovery block that generates the clock signal to the receiver. However, what limits the speed of the receiver is the time it takes to resolve a low-swing input signal to full-swing binary data. The receiver in the test-chip prototype consists of a preamplifier that provides a fixed signal swing to a regenerative latch, and does not limit link speed. The regeneration time-constant of the latch is typically fast and on the order of a couple of FO4 inverter delays. Therefore, delays in the transmitter and receiver do not present the worst case critical path.

As mentioned above, the receiver relies on a timing recovery block to accurately sample the incoming data. This block is normally a phase- or delay-locked loop that aligns the on-chip clock signal to the incoming data stream. The test-chip prototype relies on the peripheral timing loop of a dual-loop delay-locked loop (DLL) architecture that locks to the synchronously transmitted clock [43]. The components of this loop are described in detail in Section 4.5, and will show that it also does not represent the worst case critical path. Instead, the critical path in the I/O subsystem is set by the delay requirements of the clock distribution network which is limited by the minimum cycle time required to sustain a full-swing signal through a inverter buffer chain required for clock distribution [51]. Simulated data, plotted in Figure 4.3, presents the normalized signal magnitude of a clock signal at the output of a 6-stage inverter fan-up chain versus the clock period normalized

to an inverter delay. As the clock period decreases below six inverter delays, the output suffers significant attenuation because the inverters in the chain cannot switch fast enough to generate full-swing signals. Therefore, the clock period is limited to no less than six inverter delays and values closer to eight are often used to offer some safety margins.

4.1.2 Signal Integrity

Besides raw silicon speed, signal integrity is another aspect of high-speed link design that dictates the peak performance achievable and the energy required. Although an ideal channel, modeled as a lossless transmission line, may allow arbitrarily high bandwidths, several non-idealities limit the data rates that can be achieved. For high-speed data transmission across long distances, frequency dependent attenuation due to dielectric and conduction loss can significantly distort a transmitted signal causing inter-symbol interference (ISI) which makes it difficult to decipher the data from the signal received at the end of the line. As a result, equalization and relatively high transmit power are needed to compensate for the attenuation and low-pass filtering characteristics of the channel, and are important issues for serial links [12],[7]. However, parallel links over relatively short distances between chips on a board rely on parallelism and simplicity to achieve high aggregate bandwidths and these losses are not as significant for Gb/pin transmission rates. Lower transmit power without significant ISI or signal degradation is possible. However, other non-idealities associated with the channel, such as inductive and capacitive coupling of signals through bond wires and package leads that connect the silicon chip to the external channel, can significantly degrade the peak performance achievable.

Noise due to the package parasitics depend on the frequency content of the signals that are incident upon them. For Gb/s data rates, the parasitic inductors and capacitors normally have a resonant frequency higher than the transmitted data rate. However, the frequency content of transmitted signals not only depends on the data rate, but also their edge rates. As edge rate increases, more energy exist at higher frequencies and can excite the parasitic LC elements to cause more timing and voltage uncertainty in the signal. Therefore, it is important to reduce edge rates of transmitted signals to reduce energy at frequencies higher than the clock or bit rate. Although a sinusoidal signal best constrains

signal energy to exist only at the data rate, it may be difficult to generate random sinusoidal NRZ data. Instead, a good compromise is to transmit trapezoidal signals, where the first and third harmonics contain most of the signal energy.

In addition to restricting the frequency content of the transmitted signal energy, limiting the bandwidth of the signal into the sampling circuit of the receiver can improve link performance. This is because high-frequency energy can couple into the received signal from nearby signals on and off the chip. The frequency can be constrained with a low-pass filter, with its bandwidth set slightly above the data bit rate. An integrating receiver, proposed by Sidiropoulos in 1997, is a good example of a technique that achieves this type of filtering [40]. Alternative receiver architectures that implement a pre-amplifier that precede the sampling circuit are also possible and utilized in the test-chip prototype described in this chapter.

Efforts to constrain the frequency content of transmitted and received signals require feedback mechanisms to set the bandwidths (or slew rates) of circuits in the transceiver relative to the bit rate, independent of process and environmental conditions. Although this can be achieved with precision analog circuits that employ local feedback schemes, a fully digital implementation may also be possible given an adaptively regulated power supply voltage which contains the necessary feedback information. The next section describes how this adaptive supply voltage is determined.

4.2 Finding the "right" voltage

The critical delay path, identified in the preceding section to be a string of inverters that comprise the buffers in a clock distribution network for the parallel I/O interface, can be leveraged to optimize the energy consumed by all the digital circuitry in the presence of process and environmental variability. To do so a feedback loop is required to regulate the optimum voltage that guarantees the I/O interface can meeting timing. Since the critical path consists of clock buffers, a delay line consisting of inverters can be enclosed in a feedback loop that regulates its supply voltage so that delay through the inverters equals some percentage of the operating clock period (or bit time). This loop resembles a

conventional DLL design and the implementation of and issues associated with each of blocks in the DLL are described throughout the rest of this section.

A block diagram of the loop is presented in Figure 4.4. The delay line consists of 6 inverters whose delay is controlled via the supply voltage. A phase detector compares the 0 and 180 degree clock edges and drives UP and DN signals to the loop filter charge-pump and generates the control voltage, V_{CTRL}, for the delay-line. Through negative feedback, the loop locks the delay through the six stage delay line to one-half the input clock period. This clock sets the timing reference for data transmission and reception. And by design, the delay of each inverter in the delay line is a fixed fraction of the clock cycle. It is precisely this property that enables precise delay (and frequency) control of signals in the transceiver datapath without precision analog circuits. Instead, digital gates that operate off of an adaptively regulated supply can be used with delays that track with the inverter delays and hence are also a fixed fraction of the clock period.

The basic structure of this DLL resembles standard DLL designs, but supply-controlled inverters as delay elements require the delay line control signal supply the current required by the inverters [42]. Other delay elements such as current starved inverters [22] and differential delay buffers [27],[31] found in conventional designs have high impedance control nodes and can be directly controlled by the loop filter output. So,
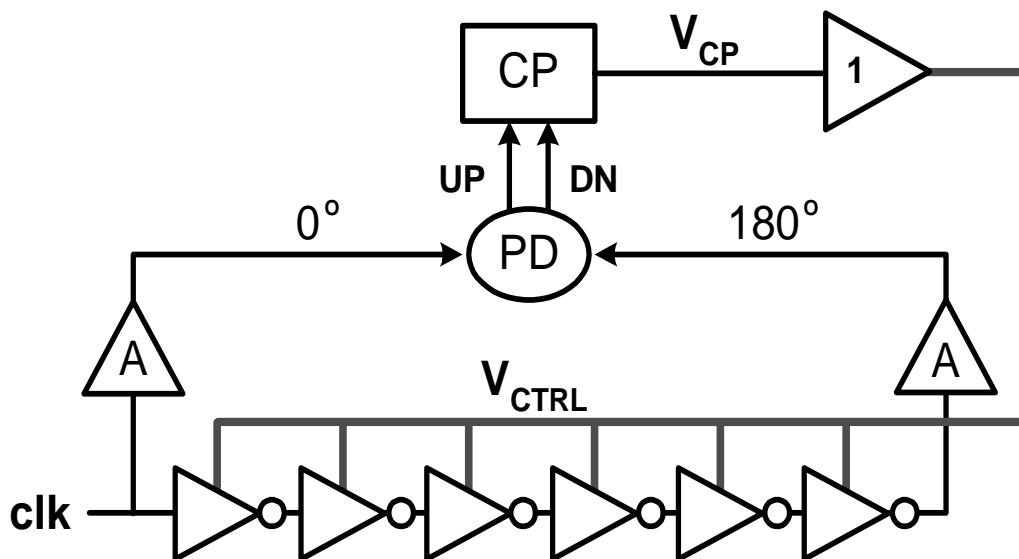
Figure 4.4. Delay-locked loop block diagram

this design requires a buffer to isolate the control voltage to the inverters from the loop filter output. Implementation of the regulator that drives the inverters is described first.

RegulatorDesign

The regulator that drives the inverters has two constraints that influence its design. Its bandwidth must be higher than the bandwidth of the enclosing feedback loop as to not compromise loop stability and its power consumption should be kept to a minimum. Since power for the supply-controlled inverters is proportional to V^2f and is provided by this regulator, it is desirable to have the regulator's total power consumption track with the delivered power. If its power tracks the load, its overhead will be a small, fixed percentage of the total power. Implementing a regulator whose bandwidth and power consumption both track with operating frequency can accomplished by carefully biasing a two stage current-mirror based regulating amplifier design illustrated in Figure 4.5. Most of the amplification is achieved through the differential pair in the first stage and the second stage current mirror provides current drive to the loads.

A stable unity-gain configuration can be achieved for the amplifier without the need for stabilizing compensation by using a small inter-stage mirroring ratio, labeled M_R in Figure 4.5. Thus, the amplifier is virtually a single pole system which can achieve high bandwidths and is easy to analyze. The transconductance of the two-stage amplifier is set
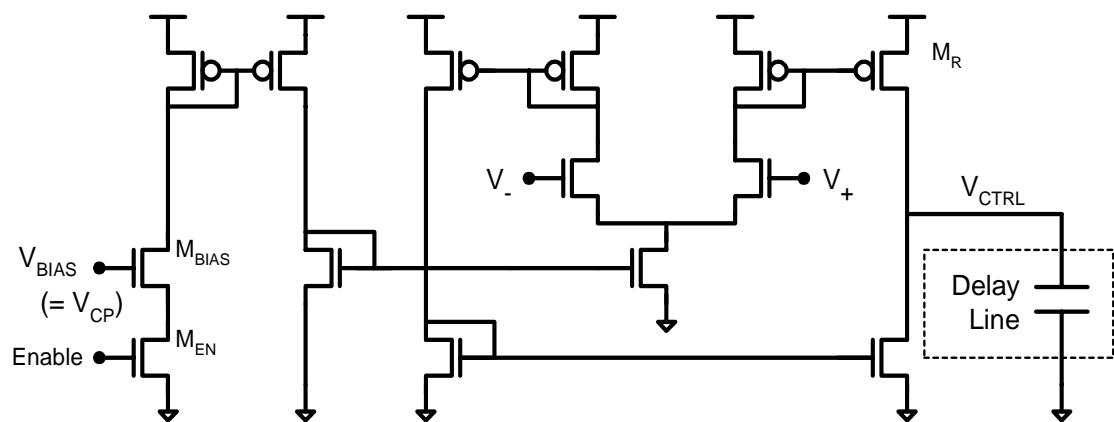
Figure 4.5. Regulating amplifier loaded with delay-line

by the following relationship

$$g_{mAMP} = g_{mIN} \cdot M_R \tag{4-1}$$

where g_{mIN} is the transconductance of the differential pair and M_R is the inter-stage mirroring ratio. The resulting bandwidth of the two-stage amplifier is then,

$$f_{BW} = g_{mAMP} / C_{DL} \tag{4-2}$$

where C_{DL} is the total capacitive load presented by the delay line at the output of the regulating amplifier. C_{DL} includes a decoupling nMOS capacitor added to mitigate capacitance variations due to the switching of the inverters in the delay line. Simulated AC analysis of the amplifier verifies that the amplifier's magnitude response roles off with a single pole at unity gain for $M_R = 4$ and is shown in Figure 4.6. Higher ratios require explicit compensation for stability.

The bias current for the differential pair in the regulating amplifier is set by a current mirror driven by the charge pump output, V_{CP}. Once the loop is locked, this stabilized control voltage contains information regarding the loop's frequency of operation, and process and environmental conditions of the silicon. As a result, current through the
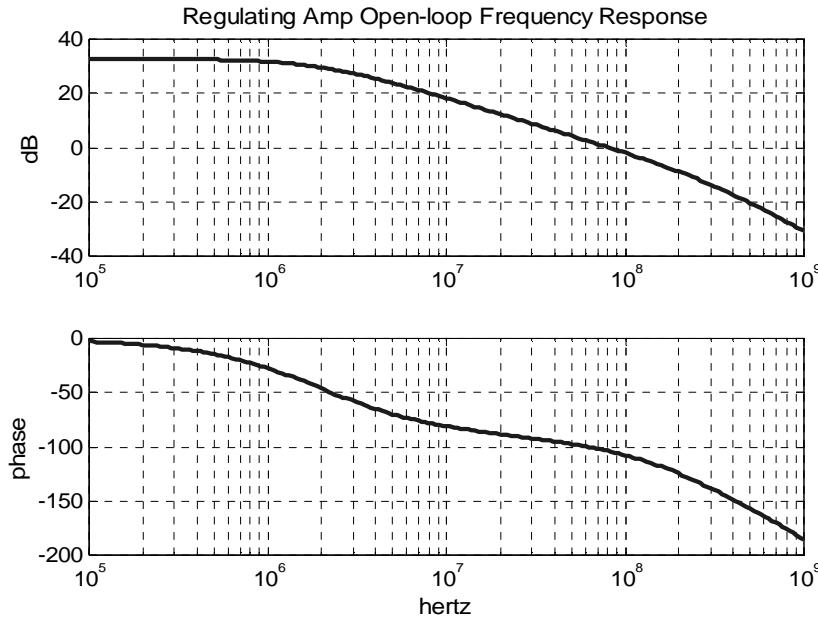
Figure 4.6. Open-loop frequency response ($V_{CTRL} = 2.6$-V)

differential pair tracks with the frequency of operation, and since this current also sets g_{mIN}, the bandwidth of the regulating loop also tracks with operating frequency. Given this tracking, the amplifier does not compromise the enclosing DLL stability even with variations in process and operating environment. In addition to a tracking bandwidth, the operating current of the amplifier also scales with operating frequency. By using a long channel device for M_{BIAS} (L=1μm), the bias current ought to observe a square-law relationship [39] to the bias voltage. Unfortunately, M_{EN}, added to enable and disable the amplifier, acts as a small degeneration resistor and reduces the bias current's squared relationship to the bias voltage. As a result, since the amplifier was designed to guarantee operation at higher control voltages, current reduction at lower voltages is compromised. Furtherer, since the amplifier operates off of a fixed supply voltage, power is super-linear with voltage, illustrated by the simulation results Figure 4.7.[1] Hence, low-frequency operation yields lower power consumption, but power does not track with the loads. Experimental results in Section 4.5 reaffirm this effect.

The maximum operating frequency of the voltage-controlled delay line (VCDL)
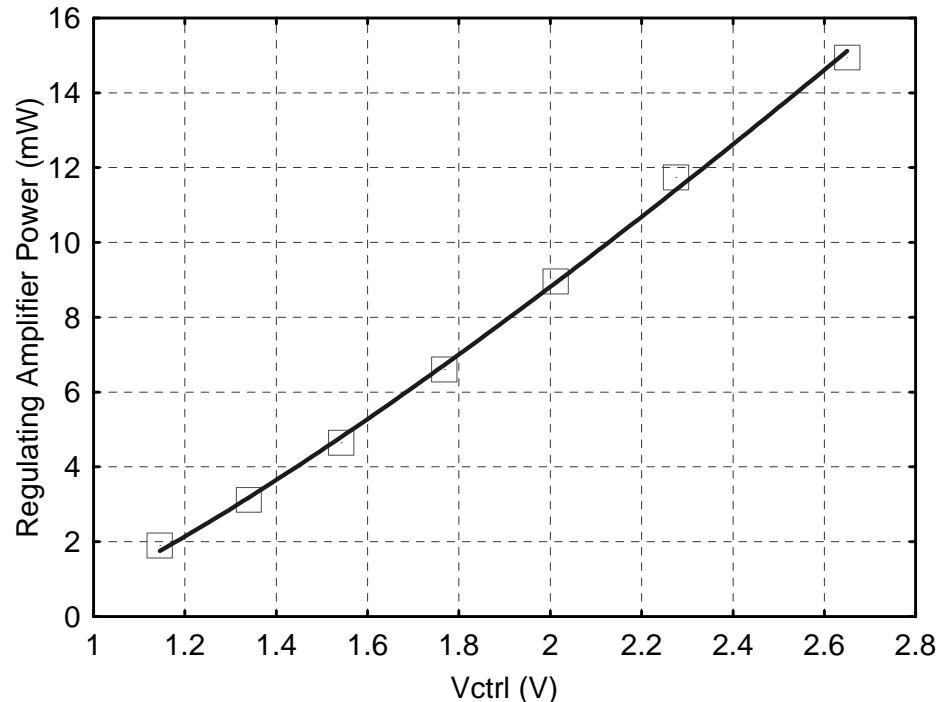
Figure 4.7. Simulated amplifier power vs. Vctrl

---

[1] Curve fits data points with a power of 1.3.
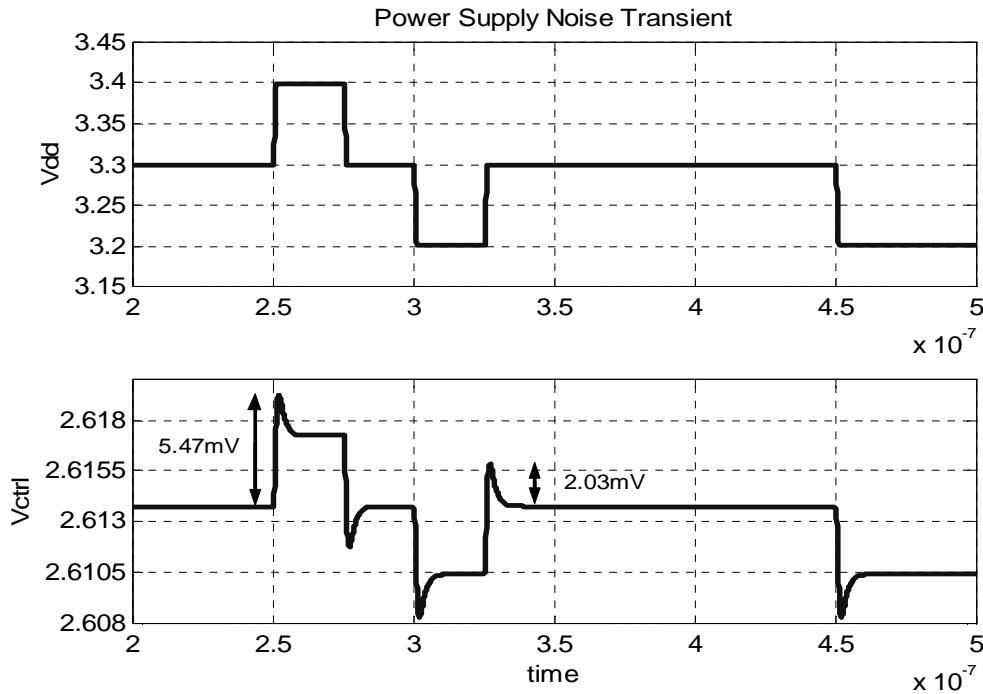
Figure 4.8. Power supply rejection transient response

depends on several factors. The maximum control voltage determines the minimum delay of each buffer and is limited by the voltage headroom required to keep M_R in saturation, which is V_{dsat}. The fanout of each inverter stage and the total number of buffer stages set the overall magnitude of the delay through the delay-line. Therefore, there is flexibility in designing the VCDL for the desired maximum operating frequency. In the test-chip implementation, six FO2 inverter stages result in an overall delay equal to 5 FO4 inverters, which is greater than an initial target of 4 FO4 inverters, due to wire loading and parasitic capacitance from cross coupled inverters that are required for the peripheral timing recovery loop described in Section 4.6.

As long as the amplifier's output pMOS (M_R) remains saturated, the static supply rejection of the design is dictated by the regulating amplifier's open-loop gain, while the dynamic supply rejection is determined by the low-pass filter formed by the output impedance of M_R and the total capacitance on the output node, V_{CTRL}. The regulating loop attenuates supply steps by more than a factor of 18 and is demonstrated by the transient simulation in Figure 4.8. This results in supply sensitivity less than 0.06 %-delay/%-supply. Given the high output impedance possible with M_1 in staturation,

there is a trade-off between the size of the capacitor at the output and its effect on the bandwidth. As mentioned earlier, a sufficiently high bandwidth is needed to keep it from compromising the stability of the enclosing loop. Bandwidth ratio between the two loops on the order of 10x is desirable. Given the good noise rejecting properties of this regulating amplifier, a low-jitter delay line consisting of supply-controlled inverters can be obtained. Its operation is in some ways similar to replica-biased differential delay elements [31]. While replica biasing in the differential buffers dynamically adjusts its current to compensate for power supply fluctuations, the regulating amplifier rejects power supply noise to the control voltage itself. Filtering the control voltage through the regulating amplifier also provides good dynamic noise immunity.[1]

To maintain high saturation margins in the amplifier while delivering power to the delay line, the amplifier current is set to be larger than the current consumed by the VCDL delay elements. There is a factor of three to four between the delivered current through the second stage and current delivered. Small offsets that may result due to imbalance in the amplifier do not affect operation since its compensated by negative feedback in the enclosing delay-locked loop.

Frequency-Tracking Differential Charge-Pump

One of the advantages of using delay lines with supply-controlled inverters is that their delay range is very broad. However, this broad range comes at the expense of a non-linearly varying delay-line gain over the operating frequency range. Transfer function of a conventional charge-pump DLL modeled with a single dominant pole:

$$H(s) = \frac{1}{1 + s/\omega_P},$$ (4-3)

where ω_p represents the dominant pole frequency (also equivalent to the loop bandwidth). Ideally, we want ω_p to track with F_{REF} so that the loop bandwidth is always 10 - 20x lower than the operating frequency. Then, the fixed delay around the loop only causes a small

---

[1] Unfortunately, regulating the supply voltage does not make the cells immune to substrate noise, but the larger V_{gs} values make these elements less sensitive to substrate noise.

phase excess phase shift. ω_p is:

$$\omega_P = \frac{I_{CP} \cdot K_{DL} \cdot F_{REF}}{C_{CP}}, \qquad (4\text{-}4)$$

where C_{CP} is the charge-pump capacitance, K_{DL} is the delay-line gain, and F_{REF} is the input frequency. ω_p would track F_{REF} if K_{DL}, I_{CP}, and C_{CP} were constant and sized to guarantee a stable configuration.

Unfortunately, for a delay line consisting of supply-controlled inverters, its delay versus V_{CTRL} is governed by the following equation:

$$T_{DELAY} = \frac{N \cdot C_{LD} \cdot V_{CTRL}}{\beta(V_{CTRL} Ð V_{TH})^{\alpha}} \qquad (4\text{-}5)$$

where β represents device transconductance, N represents the number of inverters in the delay line, and α corresponds to the exponent in the alpha power model approximation of the saturation current of an inverter, which accounts for velocity saturation effects. A numerical fit of the simulated delays of an inverter in a HP0.35µm CMOS process with the above equation and $\alpha=1.3$ is presented in Figure 4.9 and shows good agreement. K_{DL}
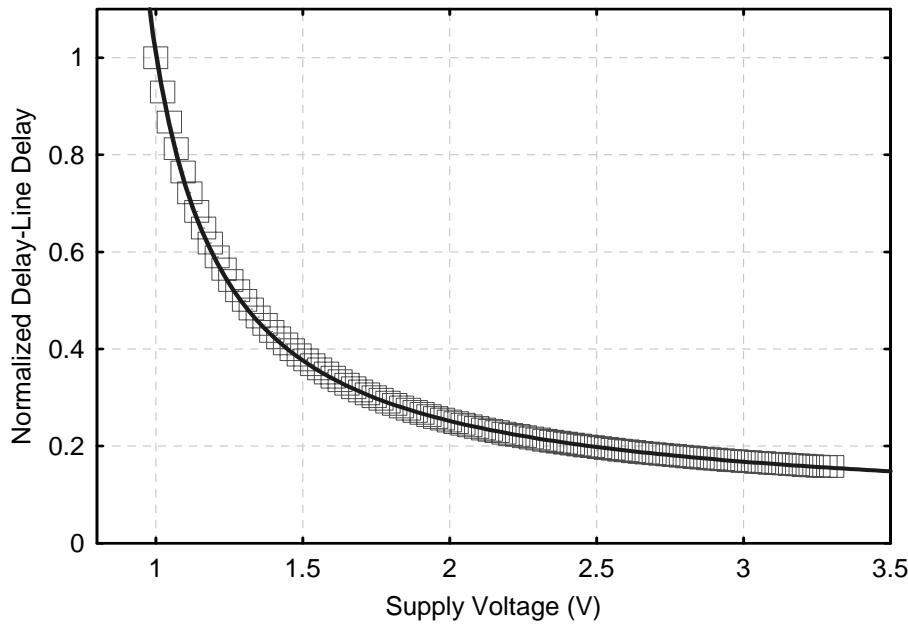
Figure 4.9. Normalized delay-line delay vs. supply voltage
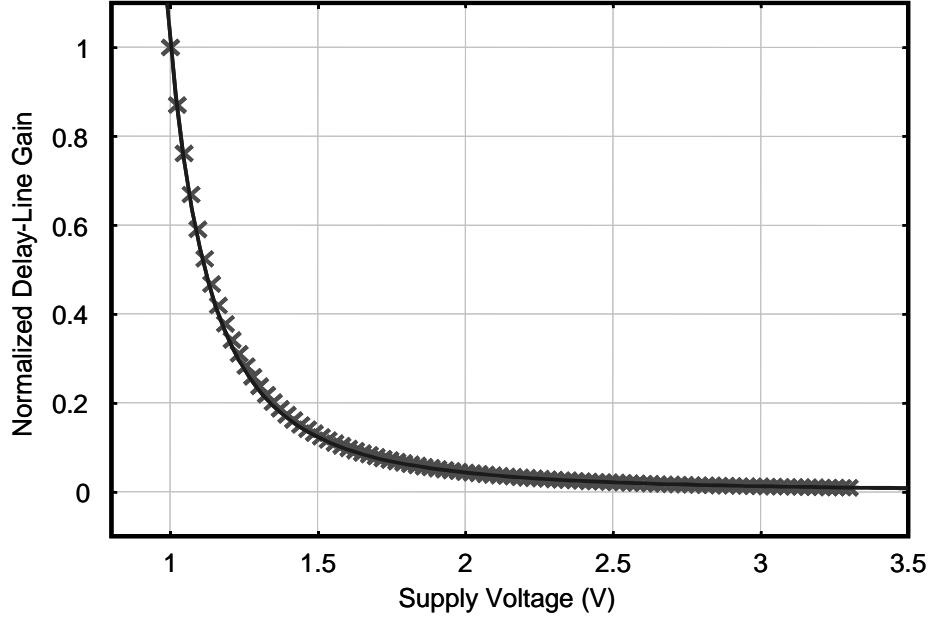
Figure 4.10. Normalized K_{DL} vs. frequency

is proportional to the derivative of an inverter's delay with respect to V_{CTRL}, which takes the following form:

$$\frac{\partial T_{DELAY}}{\partial V_{CTRL}} = K_{DL} \propto \frac{C_{LD} \cdot V_{TH}}{\beta(V_{CTRL} Đ V_{TH})^{\alpha+1}} \qquad (4\text{-}6)$$

A derivative of simulated inverter delay data with respect to the control voltage is presented in Figure 4.10. Notice that K_{DL} is not constant, nor does it vary linearly with V_{CTRL}. It increases as the supply voltage decreases, which means as frequency decreases, the loop bandwidth approaches the reference frequency and compromises stability. This bandwidth limitation can be avoided if I_{CP} can compensate for variations in K_{DL} with respect to the reference frequency such that the product of the charge-pump current and delay-line gain is constant.

A self-biased differential charge pump design proposed in [30] addresses this variable delay-line gain issue, where its charge-pump current magnitude is a function of its output control voltage. A design implemented with pMOS differential pairs is presented in Figure 4.11. Similar to the biasing scheme seen in the regulating amplifier, the current for the pMOS differential pairs are set through current mirror bias controlled by its output
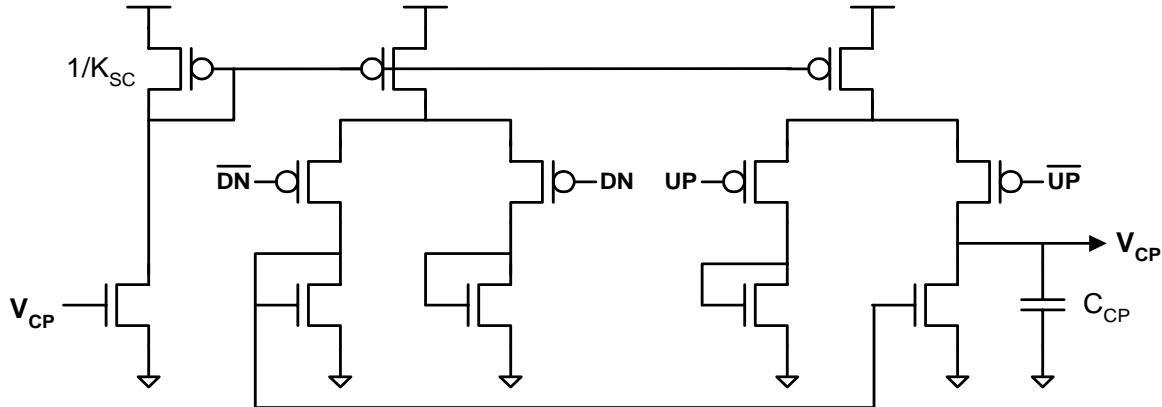
Figure 4.11. Differential charge pump

voltage, V_{CP}. It results in a charge-pump current magnitude that is a function of the output

voltage, as follows:

$$I_{CP} = K_{SC} \cdot \beta (V_{CTRL} Ð V_{TH})^{\alpha_{CP}} \qquad (4\text{-}7)$$

where K_{SC} is a scaling factor through the bias current mirror and V_{CTRL} tracks V_{CP}

through the unity-gain regulating amplifier. And by using long channel devices in the

current sources and bias stack, α approaches 2. Like the regulating amplifier, this biasing

scheme generates a charge-pump current that scales with the control voltage and reference

frequency. Therefore, low-power operation is possible at low operating frequencies.

Replacing Equation 4-7 for I_{CP} and Equation 4-6 for K_{DL} in Equation 4-4 results in the

following expression for the loop's dominant pole frequency (ω_P) with respect to F_{REF}.[1]

$$\frac{\omega_P}{f_{REF}} \propto \frac{K_{SC} \cdot C_{LD}(V_{CTRL} Ð V_{TH})^{\alpha_{CP}}}{C_{CP}(V_{CTRL} Ð V_{TH})^{\alpha_{DL} + 1}} \;. \qquad (4\text{--}8)$$

By plugging in 2 and 2.2 for α_{CP} and $\alpha_{DL}+1$, respectively, the above expression reduces

---

[1] Differences in channel lengths for devices in the charge pump and delay line result in different V_{TH}'s
for the numerator and denominator. These secondary effects have been ignored in this analysis.

to the following expression:

$$\frac{\omega_P}{f_{REF}} \propto \frac{K_{SC} \cdot C_{LD}}{C_{CP}(V_{CTRL} Ð V_{TH})^{0.2}} \tag{4–9}$$

There is only a weak dependence on V_{CTRL} and results in a relatively constant ratio between the loop's bandwidth and operating frequency. This ratio is only a function of a well controlled scaling factor K_{SC} and the ratio of two capacitors. A large nMOS device implements the loop filter capacitor, C_{LF}. Therefore, C_{LF} and C_{LD}, consisting primarily of gate capacitance, track well over process, temperature, and voltage, and result in predictable loop characteristics.

Although this self-biased charge-pump design offers good bandwidth characteristics across a wide range of frequencies, it limits the frequency lock range for the DLL. The charge-pump output's upper range is constrained by the voltage required to keep the current source and differential pair in saturation ($Vdd - 2V_{dsat}$). The lower range is set by the diode connected nMOS loads (V_{THn}). A design that implements a pMOS differential pair with wide current source and differential pair devices was chosen since it enables a higher upper range compared to a design that utilizes nMOS differential pairs with pMOS loads. Furthermore, pMOS inputs can directly interface to lower common-mode voltage swings from the phase detector. Unfortunately, the phase detector was initially designed with an nMOS differential in mind and therefore utilize low-to-high swing converters and do not take advantage of this property. Detailed descriptions of both the phase detector and low-to-high swing converters follow next.

Phase Detector

The charge pump is driven by a phase detector (PD) that compares the 0 and 180 degree clock edge outputs of the delay line and generates *UP* and *DN* whose relative pulse widths represent the mismatch between the two clock edges. A wider *UP* pulse signifies that the 180 degree clock edge lags behind the 0 degree clock edge, telling the charge pump to raise the control voltage and reduce delay through the delay line. A wider *DN* pulse signifies that the 180 degree clock edge leads the 0 degree clock. When the two edges are

aligned together, matched *UP* and *DN* pulses drive into the charge pump resulting in a zero net change at its output. Minimum, non-zero pulse widths are desirable in order to avoid a deadband, which can result from pulses that are too narrow and cannot propagate through the charge pump.

A linear phase detector consisting of precharged gates has been implemented and a detailed schematic is illustrated in Figure 4.12. It is based on a phase-only-detector introduced in [36] and outputs equal overlapping up and down pulses when the input phase error approaches zero, similar to a state-machine based Phase-Frequency-Detector. But, the absence of extra states eliminates loop start-up problems. The phase detector only operates on rising input clock edges,[1] making it immune to duty-cycle variations. Two extra inverter delays added between the master and slave stages, which are highlighted in the schematic, eliminate the potential for deadband in the original design. Clock waveforms illustrate the operation of this phase detector in Figure 4.13. Given some phase
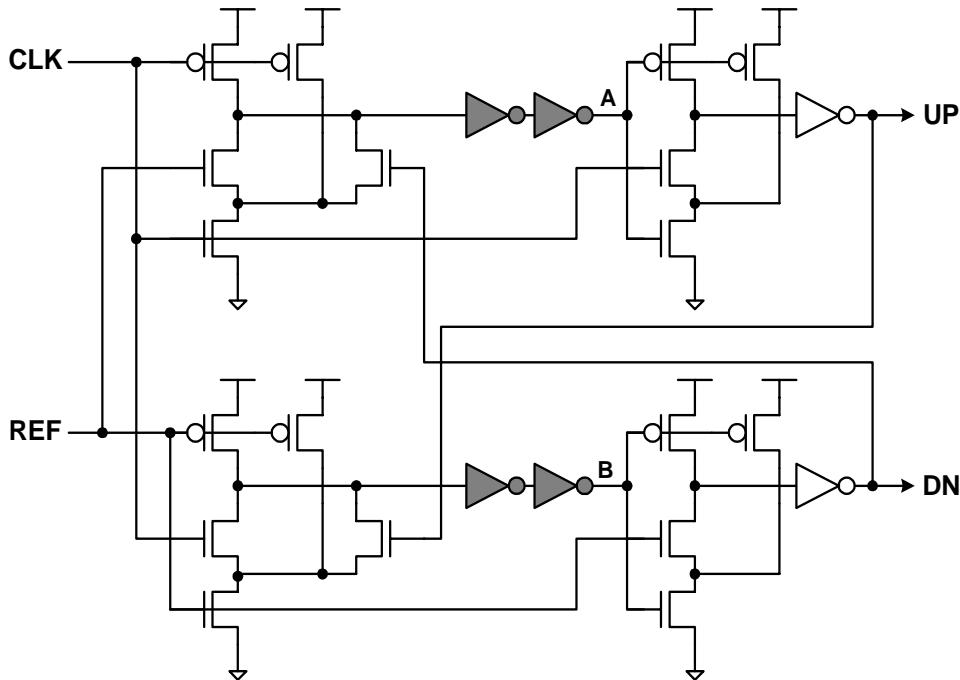
Figure 4.12. Phase-only detector

---

[1] A pair of rising edges through an even number of inverters, while locking to 180 degrees, is possible with a parallel set of delay line driven by complementary clocks. This scheme was chosen due to the requirements of the peripheral loop described in Section 4.5. Otherwise, for a single delay line, an odd number of inverters must be used.
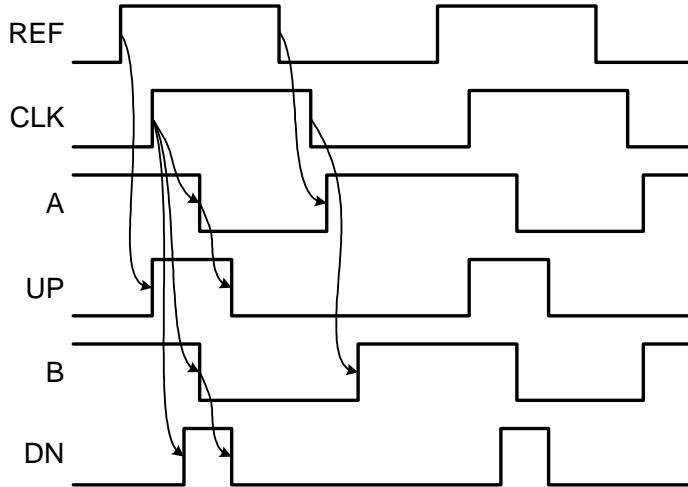
Figure 4.13. Phase detector transient waveforms

offset, where the 180 degree clock out of the delay-line is late, the early clock edge triggers *UP* to transition high. The rising edge of the late clock triggers *DN* to go high and both internal nodes *A* and *B* to fall, which in turn precharges the second stage and both outputs reset to zero. The difference between the generated pulse widths is linear with the phase difference between the two inputs. The two additional inverters delay the internal nodes (A and B) from prematurely resetting the output and the phase detector generates a minimum pulse even when the two input phases are aligned. This eliminates the deadband that can occur due to extremely narrow pulses that cannot propagate through to the charge pump when the phases are nearly matched. The subsequent falling edge of the clocks precharge the first stage, but do not affect the output pulses. Lastly, since a phase-only-detector receives no information about frequency, a sub-harmonic lock condition can potentially occur, where the delay-line locks to N+1/2 periods. The DLL avoids this condition by resetting the delay line to have minimum delay at system start-up.

A simple low-to-high swing converter, presented in Figure 4.14, takes the low voltage swings from the delay line and converts them into full-swing digital signals that drive the phase detector, which operates off of the high supply voltage. The converter takes a differential input voltage and the second stage generates a single-ended full-swing signal through current mirrors that actively drive the output both high and low. The inputs to the differential pair are driven with low fanout inverters to reduce the effect of device
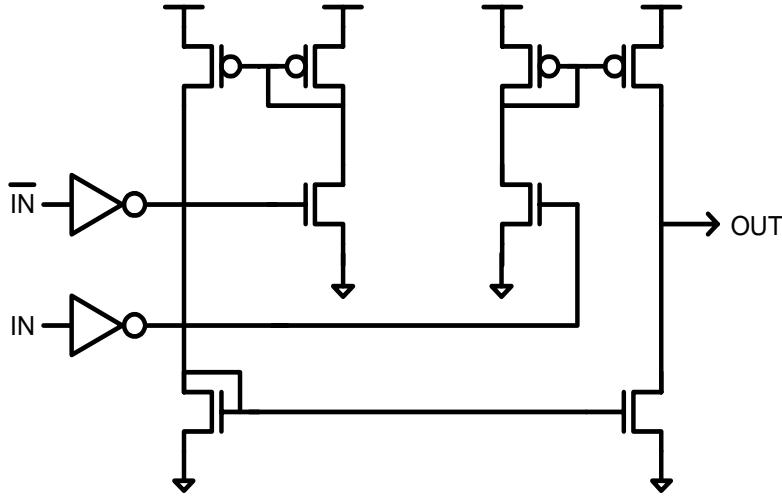
Figure 4.14. Low-to-high swing converter

mismatches and result in low static phase error. This converter can operate with very low input voltages, less than 1-V, since its operation relies on current differences and high gains are achievable with high-g_m input devices.

Although good performance is possible with this low-to-high swing converter, it is actually not needed. The phase detector, running at the full clock rate, consists of dynamic gates which can operate off of the regulated supply where its delay tracks with the delay-line inverters. Furthermore, the differential charge pump can operate with low-swing inputs since a pMOS differential pair is a good fit for the low common mode of signals generated by the lower regulated supply voltage. However, since this observation was made after the chip was fabricated, the DLL in the test-chip prototype consumes more power than is ideal.

4.2.1 Summary

In this section, a core DLL that uses supply-controlled inverters, which models the critical path, as delay elements locks to an input reference clock and determines the "right" voltage of operation for the rest of the I/O subsystem. By implementing this loop in the same die as the rest of the I/O subsystem, the delays of all other digital gates that operate off of the local supply voltage set by the DLL tracks with the inverters in the delay line. Hence, these delays are a fixed percentage of the reference clock period across process

and environmental variations. This property offers an interesting potential for building the I/O transceiver blocks with several desirable characteristics.

4.3 Transmitter Design

The next block in the link interface is the transmitter that converts binary data into electrical signals that propagate through an impedance-controlled channel (or transmission line) to a receiver at the opposite end. This must be done with accurate signal levels and timing for high-speed communication links.

Given two chips that communicate with each other with dynamically regulated voltages, their voltages can differ greatly due to their individual process and temperature conditions. Many conventional high-speed interfaces use current-mode transmitters with an ECL type interface, where transmitted and received signals swing relative to the upper rail. However, this configuration poses a potential problem when operating off of a regulated supply. Besides the transmit and receive sides each having potentially different supply voltages, they are each within larger chips, which can also contain other supply voltage levels. For NWELL technologies, the common reference for all the chips must be ground. Otherwise, if all the different voltages share a common high rail, resulting threshold voltage shifts due to back bias effects significantly reduces the performance for lower voltage blocks. Therefore, ground is chosen to be the common voltage reference for communication. An advantage of having ground as the common reference is that it enables compatibility with different CMOS technologies for the transmitter and receiver chips [2]. A pMOS current source based high-impedance driver that operates off of the same regulated voltage as the rest of the system was implemented in the test-chip prototype and properties associated with its operation in an adaptively regulated supply voltage environment are described in this section.

Section 4.3.1 begins with a description of the transmitter design which has options for both single-ended and differential modes of operation. As discussed in Section 4.1, controlling the slew rate of transmitted signals is desirable for reducing noise and improve link performance. So, Section 4.3.2 then describes how a dynamically scaled supply
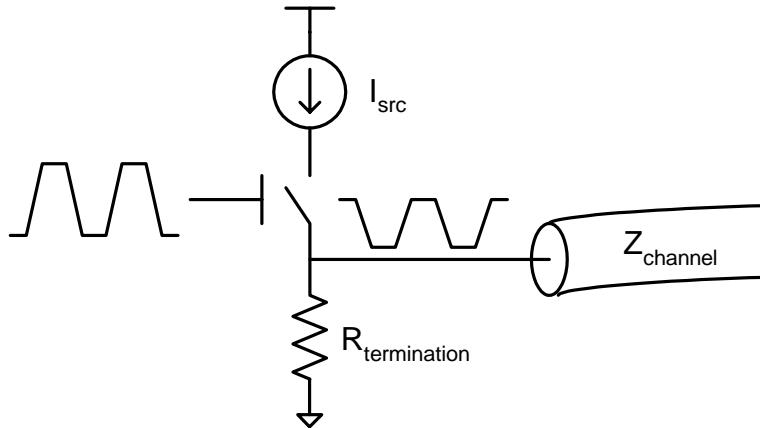
Figure 4.15. Ideal high-impedance driver

voltage environment offers automatic slew-rate control without the need for additional hardware.

4.3.1 High-Impedance Drivers

High-speed links commonly rely on high-impedance drivers to efficiently convert binary data bits into electrical signals that propagate through the channel [19]. These signals are generated via a current source that turns on and off depending on the polarity of the transmitted data. Figure 4.15 presents a schematic of a driver that utilizes a current source that actively pulls up the output to generate signals in the channel that swing relative to ground. The voltage swing seen at the receiver depends on the magnitude of the current and the termination scheme used. There are multiple options for termination. Placing a single termination resistor on the transmitter side yields an impedance-matched driver and is used in the test-chip prototype. Current pulled through the current source launches a voltage waveform through the channel, with a swing magnitude set by the current magnitude times the parallel combination of the termination resistor and channel impedance.

$$swing = I_{src} \cdot (R_{termination} \parallel Z_{channel}) \tag{4-10}$$

The receiver input capacitance presents a high-impedance load so that the waveform reflects off of the open termination of the receiver, doubling the swing magnitude at the
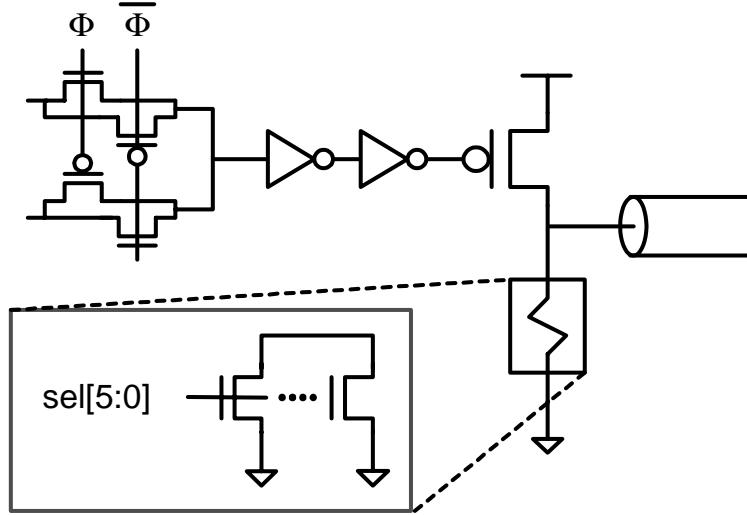
Figure 4.16. Single-ended transmitter

receiver, and traverses back to the source. Given a termination resistor at the source (transmitter) that matches the characteristic impedance of the channel, the energy from the reflected wave is completely absorbed in the resistor. One can see that this scheme requires good matching between the termination and channel impedance. Otherwise, mismatches result in energy sloshing back and forth between the transmitter and receiver and increase the effective noise on the signal. Therefore, in addition to a fixed termination resistance, it is important for the current source to remain in saturation throughout its output swing so that potential variations in its output impedance, which lies in parallel with the termination resistor, do not significantly affect the termination resistance seen by the reflected wave.

In the test-chip prototype, the current source for the high-impedance driver utilizes a pMOS current source with a termination resistor to ground, implemented with nMOS devices, and is shown in Figure 4.16. A 2:1 multiplexor enabled by a pair of complementary clocks generates data bits on every clock phase and a set of predriver inverters drive the input of the pMOS current source. As long as the output swings with a magnitude less than $Vdd-V_{dsat}$, the pMOS current source remains in saturation throughout its swing. Besides the termination devices, all components of the transmitter block operate off of the regulated supply voltage. Operation across a wide operating frequency and subsequently wide regulated voltage range is achievable, since V_{dsat} reduces with the

voltage swing magnitude at the input of the current source. Along with the high-impedance of the current source, parallel on-chip termination, implemented with nMOS devices operating in the linear region, provides a nominally fixed resistance. To ensure that the nMOS devices operate in the linear region throughout the output swing of the transmitter, the select signals are supplied off of the high supply voltage (3.3V). Potential process and environmental variations require resistor tuning, and is made possible with a parallel set of binary weighted devices that can be turned on and off through a configuration register.[1] This digital tuning capability comes at expense of higher capacitive loading at the transmitter, caused by the parasitic drain and overlap capacitance of the off transistors. Fortunately, the added capacitance was small enough not to affect link speed.

One major source of noise in most single-ended transmitters results from the switching current in the supply lines. Since the current is sent out the output line, the return current must flow in through the power supply pins. Parasitic inductance and resistance in the this return path results in noise being generated on the chip supplies. With parallel links, the aggregate current magnitude can be large and result in large voltage noise magnitudes. A differential output eliminates this noise since the supply current for each output pair is constant. Therefore, in order to investigate the difference between single-ended and differential signalling, the test chip also implements an option to utilize a pair of transmitters that transmit differential data, as shown in Figure 4.17. A drawback of differential signaling stems from the need for an additional pin per I/O and potentially doubling the power consumption since there are double the number of transmitters that switch. However, reduction in transmitter noise possible through differential signalling may enable lower signaling levels to reduce the overall power consumed, relative to single-ended signalling. Differential signalling also eliminates an additional source of noise in single-ended transmitters. In order to decipher the polarity of a single-ended signal, a receiver needs a reference voltage that lies in the middle of the signal swing for

---

[1] Production parts typically implement a slow feedback loop to tune this resistance with respect to process and environmental variations. In this test-chip prototype, tuning is performed manually through configuration registers that are set externally.
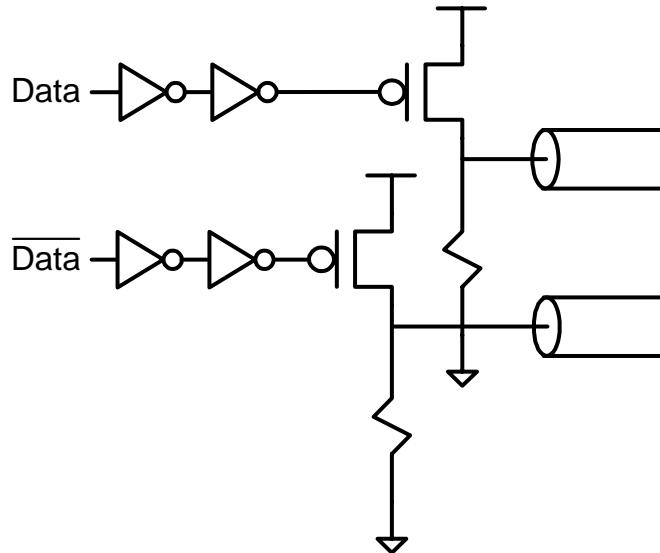
Figure 4.17. Differential signaling

comparison. This is easily achieved with a transmitter that constantly sources half the current required for a full signal swing and transmitting it in parallel with the data. In order to save pin resources, a single reference is typically shared by multiple receivers. However, this makes the reference susceptible to noise coupling in from several transceivers which affects all the parallel links. Experimental results are described in Section 4.6.

4.3.2 Impedance, Current and Slew-Rate Control

In order to achieve robust, high-speed operation, the transmitter must accurately control its output swing magnitude and slew rate. This task is challenging since both parameters can depend on process, temperature, and voltage. Although process variation is fixed for a single chip, on-die temperature can vary with time and therefore requires an active mechanism to compensate for its changes. As shown in Figure 4.18, transmitter designs commonly utilize a set of binary weighted current source legs driven by NAND gates that are driven by a common data signal and individually driven by control bits that set the number of current sources enabled. A servo-A/D based control loop is often used to set the appropriate sizing in response to process and temperature conditions [26]. An adaptively regulated supply voltage has the advantage of offering this process and temperature tracking automatically. Since the regulated supply voltage is set based on the speed of a

chain of inverters, the saturation current of the output driver tracks to first order the saturation current that sets the delay of an inverter. Therefore, adaptive supply voltage regulation plays the role of the servo-A/D based control loop described above. For a desired frequency of operation, sizing the transmitter current source fixes both current magnitude and output voltage swing relative to the data rate. Therefore, the output swing, to first order, is independent of process and temperature. However, adjustable current drive is still required to accommodate a wide range of data rates. As the regulated supply voltage decreases for lower rates, the overdrive voltage on the current sources reduces more quickly due to the a fixed threshold voltage. Thus, a simple table that maps the necessary current source width to data rate can be utilized to generate the necessary swing across different data rates.

In addition to adjusting signal swing magnitudes, slew-rate control is important for reducing cross talk (coupling) and reflection noise in high-speed links. Cross talk occurs due to imperfect isolation of individual signal lines through explicit signal return paths and results in image currents that flow through other signal lines. It is exacerbated in packages that do not employ explicit ground planes. This noise is physically manifest through coupling capacitance and mutual inductance between wires. Because coupling is through frequency dependent reactances (ωL and $1/\omega C$), its proportionality constant depends on the bandwidth of the signals. Therefore, reducing the signal bandwidth helps to reduce coupling, which is why interfaces slew rate limit their outputs where edges
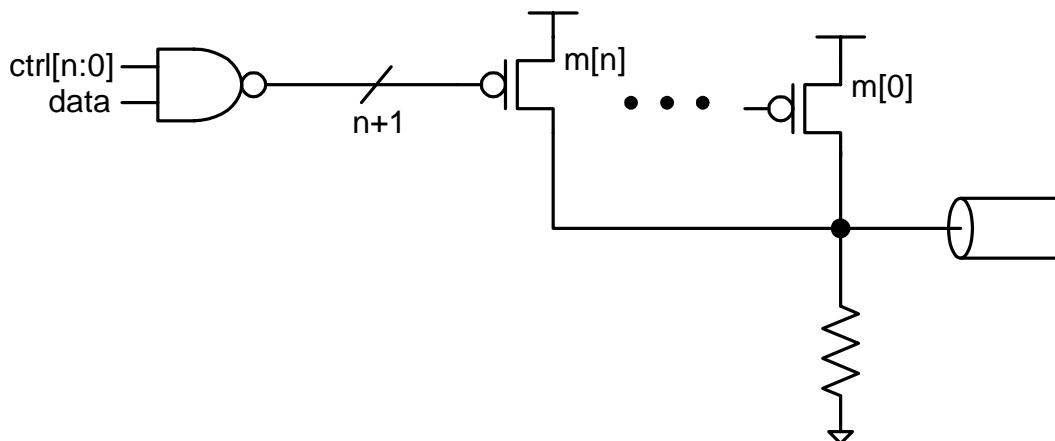
Figure 4.18. transmitter output swing control

consume a quarter to a third of the bit time.

In conventional designs, limiting the slew rate can be difficult, and several approaches have been published [19],[26],[9]. However, a dynamically regulated supply voltage environment again provides the process and environment monitoring required to automatically control the output slew rate without any additional hardware. The core DLL locks the delay of inverters in the delay-line to half a clock period. This means that the delay of each inverter is a fixed percentage of the clock period. This also hold true for the edge rates of the internal signals in the delay-line and for other digital circuits operating off the same regulated voltage. Therefore, setting the transition times of the predriver to a fixed percentage of the bit time through sizing ensures this percentage to remain fixed across a wide range of process, temperature, and clock frequencies. A potential concern of using this approach comes from the short-circuit current that may arise due to slow edge rates at the output of the predrivers. Given a clock frequency that corresponds to 8 FO4 inverter delays, transition times that consume a third of the bit time nominally correspond to the output transition time of a FO4 inverter. This fanout is typically found in general digital CMOS circuits and therefore short circuit currents are not especially significant.

However, operating both the output driver and predriver off the same regulated supply voltage with controlled slew rates creates a different problem. Due to the finite threshold voltage of the current source devices, current does not flow until the gate is below a threshold voltage. This means that a fifty percent duty-cycle input to the output driver generates a narrower pulse at the output. Duty-cycle distortion directly affects timing margins and is critical to link performance. To address this distortion, the predrivers pre-shape its output to generate the desired 50-% duty-cycle pulse width at the output of the high-impedance driver. The shaping is achieved by properly sizing the PN ratios of the two inverting buffers shown in Figure 4.19. A digital control word selectively enables parallel legs to change its effective pull-up and pull-down drive strengths. A pair of these buffers are used to make it immune to p-to-n skews. Unfortunately, with this solution, the PN ratio configuration does not track with voltage and only works for limited voltage ranges. A simple control loop can be used to adjust these buffers to accommodate a wider
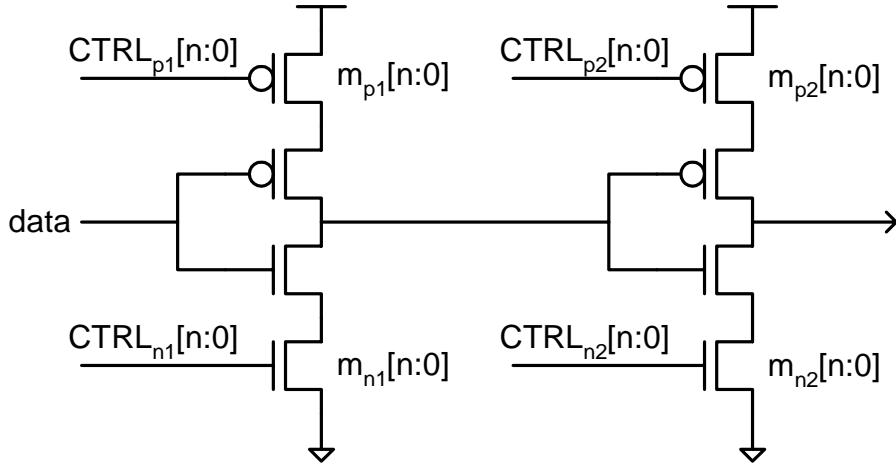
Figure 4.19. Transmitter predriver

range of regulated voltages.

4.3.3 Transmitter Summary

This section described a simple transmitter design that uses a pMOS current source to implement a high-impedance driver that generates signals swinging relative to ground. The test chip offers both single-ended and differential modes of signalling to compare their relative merits. The process and temperature tracking nature of the system enables a robust design that doesn't require explicit schemes to tune the transmitter output signal swing. Furthermore, accurate control of signal magnitudes and slew rates that are fixed relative to process and operating environment are possible. Some configurability has been built into the fabricated transmitter design to explore minimum power operation and compensate for low-voltage effects.

4.4 Receiver Design

One of the few parts of this I/O interface that is not entirely comprised of digital gates is the receiver. However, the design can again leverage a dynamically regulated supply environment to build a simple and yet robust receiver that filters high frequency noise. As described in Section 1.2, conventional receivers are clocked with a quadrature shifted clock to sample the incoming data in the middle of the eye to maximize timing margins. Several incarnations of a receiver design have been implemented and presented in the

literature [11],[51],[12] to maximize performance. Sidiropoulos shows that proper sampling of the data alone may not guarantee the receiver recovers the correct data value due to noise that may couple in at the moment of sampling [44]. Therefore, two-stage receiver designs are commonly used, where the first stage acts to condition the input noise in the incoming signal and the second stage amplifies the signal to full-swing digital data. An integrating receiver fully described and analyzed in [40] offers good filtering capability since its bandwidth is set by the integration time, which is equivalent to the bit time. However, it requires accurate phase alignment between the clock and data.

The test-chip receiver also relies on a two stage receiver, comprised of a bandwidth limiting amplifier followed by a regenerative latch, illustrated in Figure 4.20. It offers flexible operation by accommodating both single-ended and differential transmitted signals with configurable nMOS switches at the input to the preamplifier. In order to minimize potential filtering effects due to the pass gates, the gates are switched using the high supply voltage. Supply noise that couples in from this high supply voltage through the switches is common mode to the receiver and therefore has a negligible effect on receiver performance. A reference voltage (V_{REF}) that is set to half the swing magnitude and sent along with the transmitted signals is shared by all the receivers for receiving single-ended signals. 2-1 demultiplexing for the double data-rate signal require two
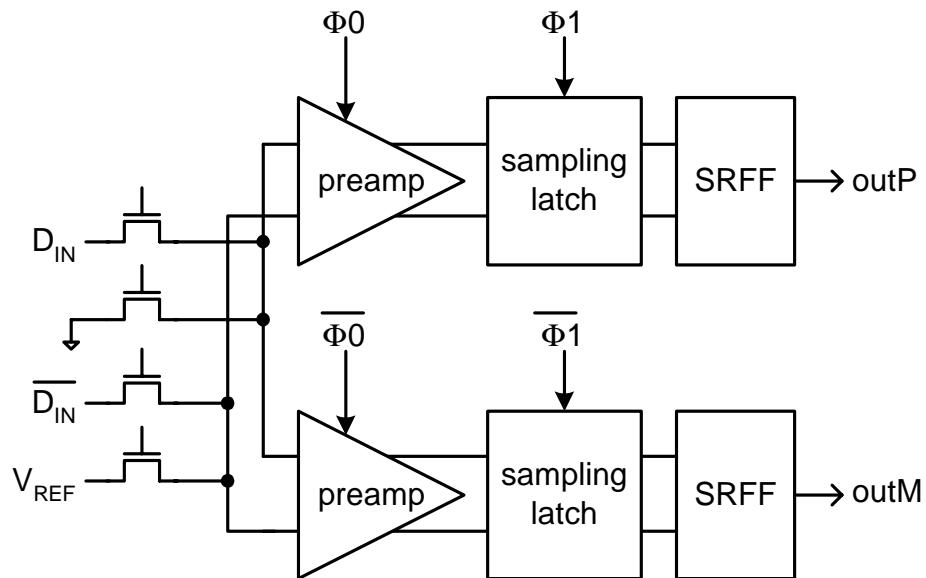
Figure 4.20. Receiver block diagram
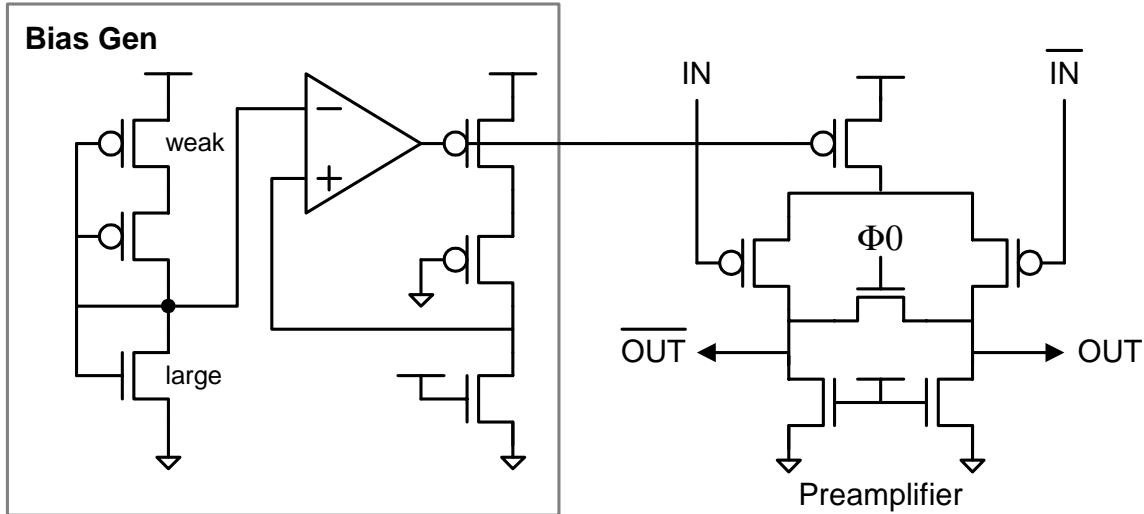
Figure 4.21. Preamplifier schematic

parallel receiver paths that operate on complementary clock phases, where one preamplifer evaluates during half a clock cycle while the other resets. A pair of regenerative latches sample the output of the preamplifier on the falling edge of a delayed clock $\Phi 1$ and $\overline{\Phi 1}$. Precise positioning of this clock is discussed in Section 4.4.2. Subsequent set-reset flip flops (SRFF) hold the outputs for an entire clock cycle and ultimately drive into retiming circuitry in order to synchronize the data to the system clock of the digital system that consumes the data. In the test chip, the received data is driven off chip and to internal decode logic to verify proper operation.

4.4.1 Bandwidth-Tracking Preamplifier

The first stage of the receiver is a preamplifier consisting of a pMOS differential pair with nMOS linear loads, as shown in Figure 4.21. pMOS inputs are chosen due to the low common mode of the transmitted signals. The preamplifier resets while $\Phi 0$ is high and its outputs are equalized through a shorting nMOS device. While $\Phi 0$ is low, the stage amplifies the signal for a full bit period. The preamplifier operates off of the regulated supply and the current source to the pMOS differential pair is biased through a replica self-biasing scheme [23]. A half-replica of the differential preamplifier is used in the bias generator and its output drives the positive input of an amplifier, while the negative input is biased to around V_{THn}. The output of the amplifier drives the current source of the
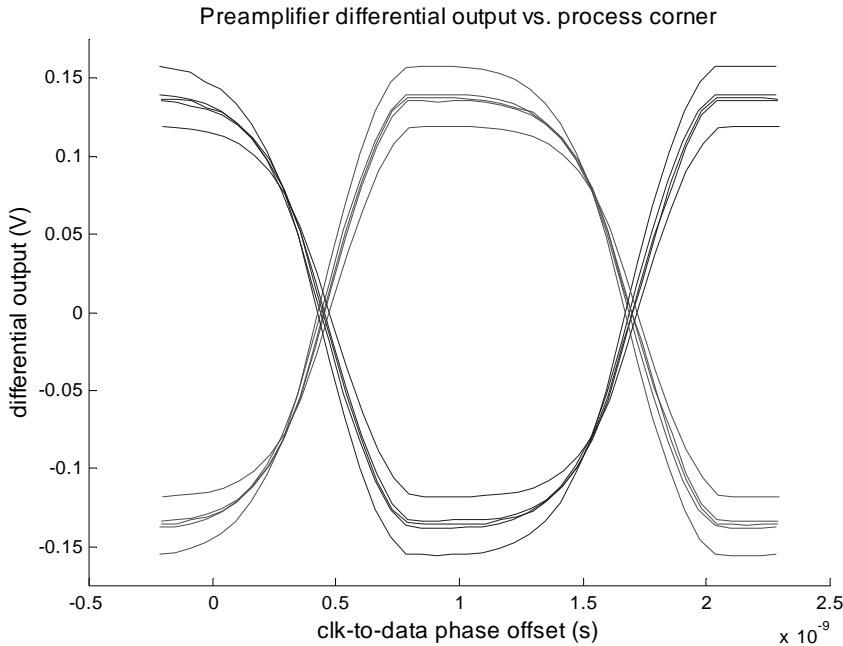
Figure 4.22. Preamplifier differential output versus process corner

half-replica and preamplifiers, and with feedback, the preamplifier's output swing magnitude is clamped to a swing of V_{THn}.

The bandwidth of the preamplifier is set by the RC product between the capacitive loading on the output of the preamplifier and its output resistance. This resistance is dominated by the nMOS load device throughout its swing. Since the supply to the gates of these nMOS loads is again the regulated voltage, their output resistance is effectively also regulated. To first order, the small signal output resistance of a non-minimum channel MOS device is inversely proportional to I_{dsat}, and tracks the saturation current that sets the delay of inverters in the delay-line of the core DLL. So feedback in the DLL that sets the regulated voltage magnitude also enables the bandwidth of the input receiver to track the bit rate of the link. This is advantageous because the bandwidth can be set to only allow in frequency components up to the bit rate and filter out unwanted high-frequency noise.

This tracking filter property of the receiver's preamplifier can be verified across process corners by observing the output swing of the preamplifier versus a phase offset swept between the input data and clock ($\Phi 0$) waveforms. Figure 4.22 plots the differential output swing of the preamplifier while sweeping 200mV single-ended input data
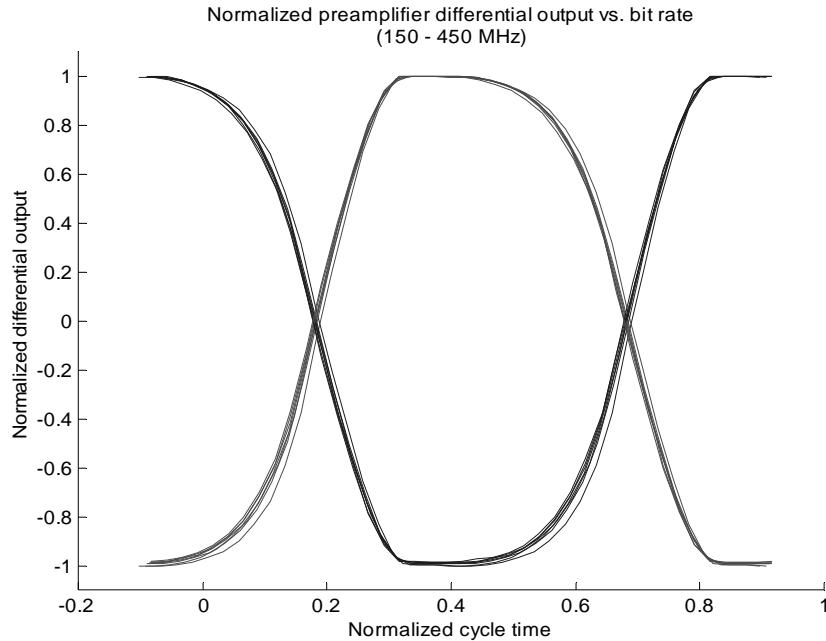
Figure 4.23. Preamplifier differential output versus bit rate

transitions relative to a 400MHz clock. Since the supply voltage of the preamplifier dynamically adjusts to the process corner, the time constants of the waveforms are similar for five process corners (TT, FF, SS, FS, and SF). Hence, it shows that the preamplifier's filtering property is independent of the operating conditions. Figure 4.23 shows that the RC filter also tracks relative to frequency, and plots normalized differential output voltage waveforms versus normalized phase offsets between clock and data at seven different bit rates ranging from 150 to 450 MHz.

Low-Voltage Limitations

One of the limitations that this preamplifier imposes on the receiver design stems from its minimum voltage headroom requirements. The current source and differential pair must be in saturation and requires at least $2V_{dsat}$'s across the pMOS devices and a V_{TP} from the gate to source of the differential pair. Therefore, the total voltage headroom required is:

$$V_{HEADROOM} = V_{TP} + 2V_{dsat} \tag{4-11}$$

which corresponds to 1.3-V in a HP0.35μm process. Digital CMOS logic gates that dominate the rest of the I/O subsystem do not suffer from this limitation and can operate
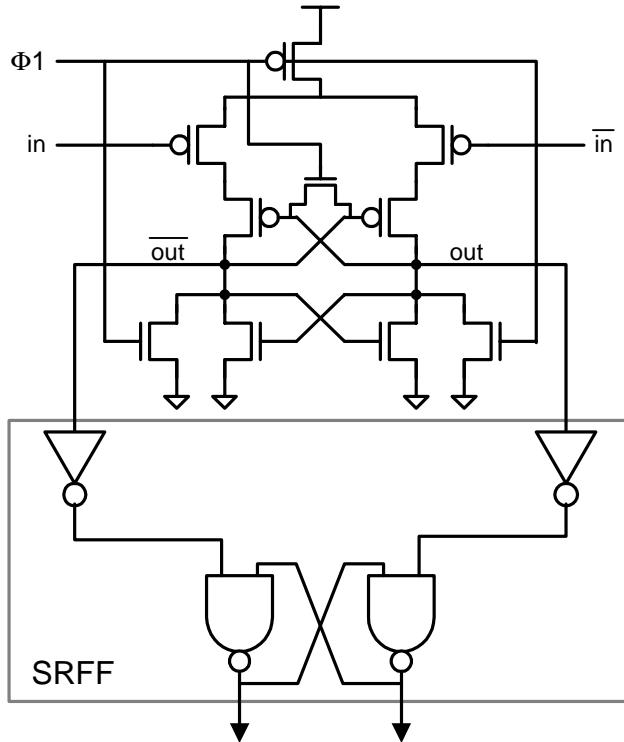
Figure 4.24. Regenerative latch and SRFF

well below this minimum headroom voltage level at the expense of slower operation. Since this preamplifier, along with the rest of the digital logic, operates off of the lower regulated voltage, the minimum operating range of the I/O interface is set by this voltage headroom limitation.

4.4.2 Regenerative Latch and Timing

The requisite high-gain second stage consists of a clocked regenerative latch that converts the limited swing output of the preamplifier to a full-swing digital signal and is shown in Figure 4.24. Its structure is that of a commonly used high-speed latch found in the strongARM processor [10] and its operation is straight forward. While Φ1 clock is high, the latch resets by disabling the PMOS evaluation transistor and equalizing the two sides of the differential pair to low. On the falling edge of Φ1, the latch begins evaluation and samples the differential voltage across its inputs. Regeneration through the cross coupled nMOS and pMOS devices quickly resolve full swing signals at the outputs. This type of regenerative latch offers the best speed, power, and area trade-off, and given its digital
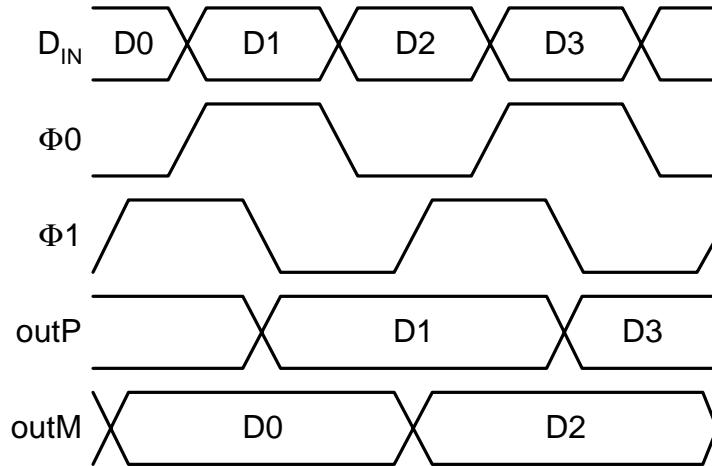
Figure 4.25. Receiver timing

nature, it can operate off of the regulated voltage and its delay tracks relative to the delay of an inverter. The regenerative latch is followed by a standard SRFF, implemented with cross-coupled NAND gates, to hold the data received on each phase of the clock for an entire clock period.

The timing for the two clock signals required by the receiver are presented in Figure 4.25. $\Phi 0$ must be aligned with the incoming data signal to evaluate during a single clock phase. A pair of receivers operating on complementary clock phases are therefore required to receive data on both phases of the clock. Once the preamplifier begins evaluation, it amplifies the incoming signal and holds the value until the subsequent regenerative latch samples the preamplifier output. Ideally, the regenerative latch ought to sample after the preamplifier has amplified the incoming signal over nearly the entire bit time, which makes this receiver behave like an integrating receiver. Although 135 degrees or more offset between $\Phi 0$ and $\Phi 1$ offers better receiver margins, the test chip offsets the sampling edge by only 90 degrees. This is due to the configuration of the phase detecting receiver in the peripheral loop used for aligning the internal clocks to the incoming I/O clock which is discussed thoroughly in Section 4.5.

4.4.3 Receiver Summary

This section described the design of the receiver that consists of two stages: one to filter out high frequency noise, and the other to convert the incoming low swing signal into

full-swing digital signals. The preamplifier operates off of the regulated not only so that its power consumption tracks with the bit rate, but it relies on the regulated voltage to set its input bandwidth and have it also track with the bit rate. The regenerative latch is a digital circuit block that translates the low-swing output of the preamplifier into full-swing digital signals and also operates off of the regulated supply. One drawback of this approach to receiver design stems from the analog nature of the preamplifier which requires a minimum overhead voltage and limits the lower frequency range of operation. Therefore, other techniques that can reduce or circumvent this minimum voltage headroom limitation is required for future technologies where V_{TH} does not scale down as quickly as circuit delays and supply voltage.

While mimicking the filtering properties of an integrating amplifier, this receiver design offers a simpler solution that does not require the sample and hold stage necessary in the integrating receiver design. Although the sample and hold stage can easily be implemented with a simple pass gate network, its operation does not scale well with lower supply voltages due to the body-effected V_{TN} of the pass transistors. Therefore, extra care must be taken to design an integrating receiver design that operates off of a lower regulated supply voltage.

Operation of the receiver and performance of the link heavily rely on the alignment of the clocks that trigger the preamplifier and regenerative latch, to the incoming data signal. This is achieved with a digital peripheral loop that locks the internal clock signals relative to the incoming parallel I/O clock and is the topic of the next section.

4.5 Timing Recovery

Timing recovery is a crucial component of high-speed interfaces and can take several different forms. In the case of a source synchronous parallel interface design that transmits a dedicated clock signal along with the data, timing recovery can be achieved with a single delay-locked loop. This section first describes a digital implementation of the peripheral loop of a dual-loop DLL design [43] that aligns the internal clock signal with the incoming I/O clock. A fully digital peripheral loop is possible by again leveraging the delay

controlled nature of digital gates with an adaptively regulated supply and replace precision analog circuit elements that would otherwise be used. Even the analog-like function of interpolation that is required by the loop can be performed in a completely digital fashion. Subsection 4.5.2 then describes a duty-cycle adjusting circuit that operates on full-swing CMOS signals. Lastly, issues associated with clock distribution for this I/O interface design are discussed.

4.5.1 Dual-loop architecture

The timing recovery block relies on a dual-loop DLL architecture that uses the core DLL, described in Section 4.1, to generate 12 evenly spaced clock edges that span 360° and drive into a digital peripheral loop that generates the desired clocks. The digital peripheral loop selects an adjacent pair of edges, and interpolates between them to finely align a clock edge relative to the input I/O clock. This dual-loop configuration enables unlimited capture range and allows a wide frequency range of operation. An architectural block diagram of the dual-loop architecture is presented in Figure 4.26. In the mux-interpolator data paths, a pair of multiplexors each select one of a pair of adjacent clock edges out of twelve edges that are each spaced an inverter delay apart. These twelve evenly spaced edges can be generated by implementing a parallel set of delay lines in the core DLL, consisting of six inverters each, and driven with complementary reference clock signals. The weak feedback inverters keep the clocks propagating through the parallel paths aligned in phase. The two adjacent clocks then feed into an interpolating block that generates a clock that can be finely placed relative to the two input clocks and is controlled by changing the relative contribution of the two clock edges to the output. Interpolation allows the resolution of clock placement to be much better finer than a single inverter delay. The interpolator output then drives through a duty-cycle adjuster and clock distribution buffers before clocking a receiver that acts as a phase detector for the peripheral loop. The phase detector output generates up and down pulses to a finite-state machine (FSM) which then closes the loop by controlling mux and interpolator settings. An additional mux-interpolator datapath generates the delayed clock $\Phi1$, which is offset from $\Phi0$. Adding a digital offset to the control bits in the FSM that set the interpolated
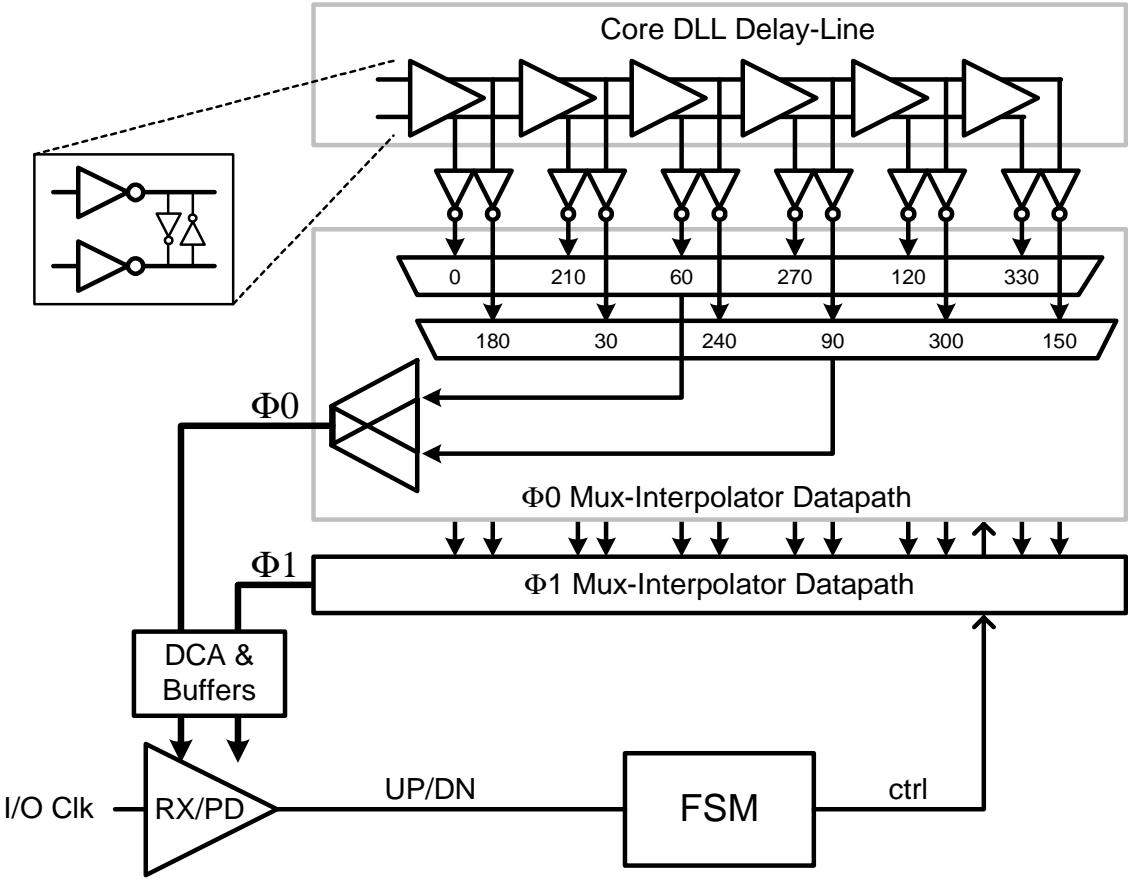
Figure 4.26. Digital peripheral loop

edge for Φ0 enables a simple mechanism for generating the control bits that drive the second Φ1 mux-interpolator datapath to create this static offset.

The original implementation of this dual-loop architecture uses analog differential delay buffers in the core delay line and interpolator with a sophisticated replica biasing scheme [43]. With an adaptively regulated supply, simple digital gates can replace the precision analog blocks in the peripheral loop since the performance of these gates track with link frequency. The multiplexors that select adjacent clock edges are implemented with transmission gates whose delays track well with the delay of an inverter across process, voltage and temperature. Therefore, the delay through these gates are always a fixed percentage of the clock period when operating off of the adaptively regulated supply.

The control signals for the multiplexors and interpolator come from a digital finite state machine (FSM) that consists of a simple binary up/down counter and decoder. Each

counter value corresponds to one of 192 possible edge positions within a clock cycle. A data receiver connected to the incoming parallel I/O clock acts as a bang-bang phase detector (RX/PD). Using the same circuitry as the data receivers means that the loop will also cancel out the data receiver set-up time. Under locked steady-state conditions, the RX/PD should generate successive up and down pulses. However, due to delay through the digital loop resulting from three metastability hardened flip-flops at the output of the phase detector, the loop cannot immediately react to the pulses from the phase detector and results in dither jitter greater than a single interpolation step. Therefore, a small front-end filter counts eight consecutive "up" or "down" pulses before making a phase adjustment decision. This allows for the effect of a phase adjustment to propagate through the loop and to the output of the phase detector before the next decision is made. This filter reduces the inherent peripheral loop dither jitter to one phase interpolation interval [44], but also reduces its effective bandwidth or slew rate response.

While operating off of the lower regulated supply is attractive, the performance of this peripheral loop may potentially be degraded due to the ripple induced on the regulated supply by the switching regulator. However, as long as the slew-rate of the induced supply is slower than the rate at which the peripheral loop can respond, the loop can track out this jitter. The worst case is under low I/O frequency conditions, because the response of the loop is proportional to the operating frequency while the switching frequency of the power converter is constant. Therefore, the peripheral loop must be designed to respond with a slew-rate higher than the power supply ripple at the lowest target frequency.

4.5.2 Digital interpolation

As mentioned earlier, interpolation is a key function required in the operation of the peripheral loop and it's operation is straight forward. As illustrated in Figure 4.27, interpolation simply blends two clock signals spaced apart by some time, Δt, and generates a clock signal that lies somewhere between them. The relative magnitude of contribution of each input edge determines the placement of the resulting output edge in time. This relative contribution is set by the interpolation weight given to each edge and have values of w and 15-w for each side. As w is swept linearly from 0 to 15, interpolated
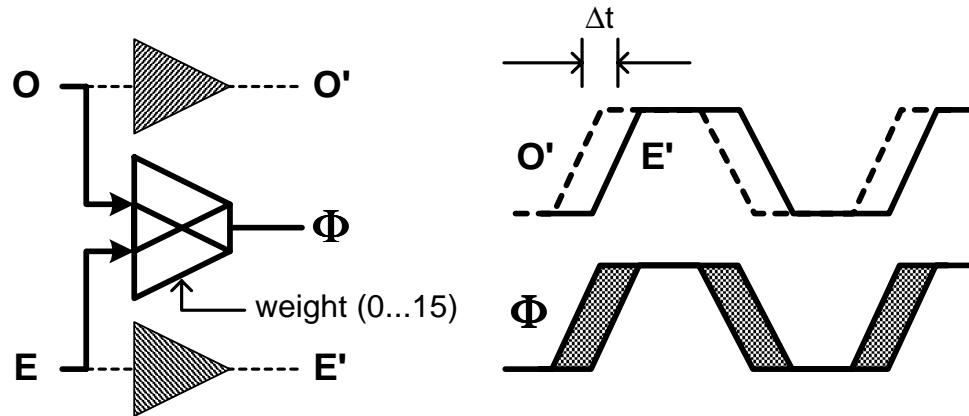
Figure 4.27. Phase interpolation

edges spaced linearly in time with respect to the weights are desirable. Even though interpolation is generally considered to be an analog operation, it can be implemented using standard digital gates. Figure 4.28 illustrates the digital interpolator consisting of two parallel sets of tri-state buffers with their outputs shorted together. Adjusting the relative drive strengths of the two sides, by digitally controlling the number of buffers enabled, varies the contribution of each input edge, O and E, to interpolate between them. The resolution of edge spacings is set by the granularity of buffer sizes that can be controlled digitally. This implementation consists of 16 interpolation weights, which
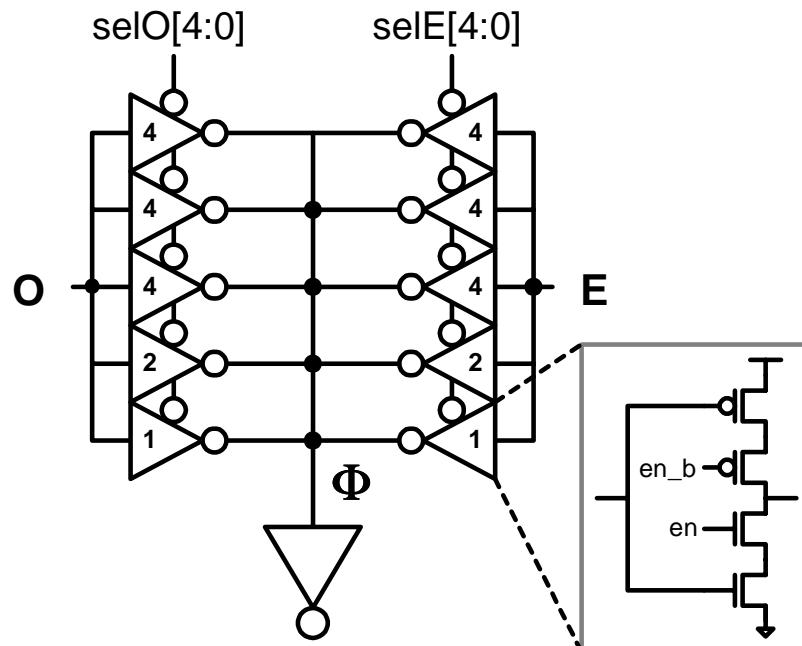
Figure 4.28. Digital interpolator
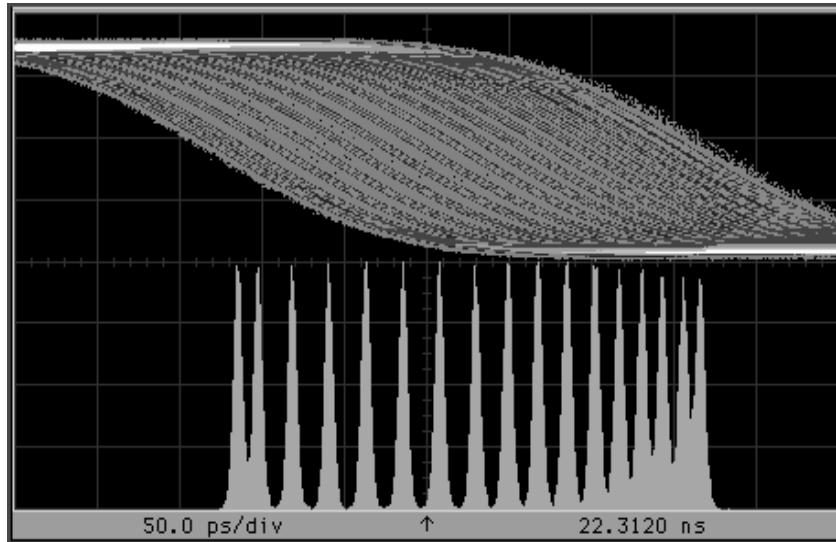
Figure 4.29. Measured interpolation histogram

results in a total of 192 edge positions possible within a clock cycle, since there are 12 evenly spaced clock edges generated by the core DLL. In order to save area for these 16 interpolation steps, the weighting is binary coded for the lowest three bits. Thermometer coding is used for the two higher order bits to avoid non-monotonic discontinuities that can arise from full binary coding due to device width variations. It is important to minimize, if not eliminate, non-monotonic discontinuities since it can directly translate into jitter, where the loop dithers about that point.

The linearity of interpolated edges strongly depends on the ratio between the edge spacing versus the output time constant of the interpolator. A measured histogram plot of 16 interpolations steps, generated by stepping though the interpolator in the test chip, is presented in Figure 4.29. A slight nonlinearity shown in the plot is due to an improper ratio of the interpolator's output time constant to the input edge spacing. The capacitive loading at the output of the interpolators is small and results in $\Delta t/RC = 2$. Δt is the delay spacing between the interpolated edges, which is the delay of a single inverter in the delay line of the core DLL. RC is the output time constant of the interpolators, set by the parallel combination of the effective pull-up and pull-down resistances of the interpolator and the capacitive load. A ratio closer to one yields better linearity, from the analysis described in [44].

In order for this interpolator to exhibit good linearity across a wide frequency range, the Δt/RC ratio must preserved. With an adaptively regulated supply, this ratio is constant since the interpolator's output time constant tracks with an inverter delay. Therefore, the same linearity can be maintained over a wide range of frequencies with a simple digital interpolator.

4.5.3 Duty-cycle adjuster

Another aspect of this timing block that requires careful design is the duty-cycle control. The transmitter took special care to ensure that the bit time for data transmitted on both phases of the clock were equal. Similarly, the duty cycle of Φ0 must be tightly controlled in order for the receiver to accurately decipher the data encoded in each clock phase. Due to skews in clock generation, an explicit duty-cycle adjusting block is necessary [28] and is described next.

Applying duty cycle correction to full-swing CMOS signals presents a challenge for implementing a duty-cycle adjustor (DCA). The basic approach, presented in Figure 4.30, relies on static current to shift the switching threshold of inverters. Two sets of current
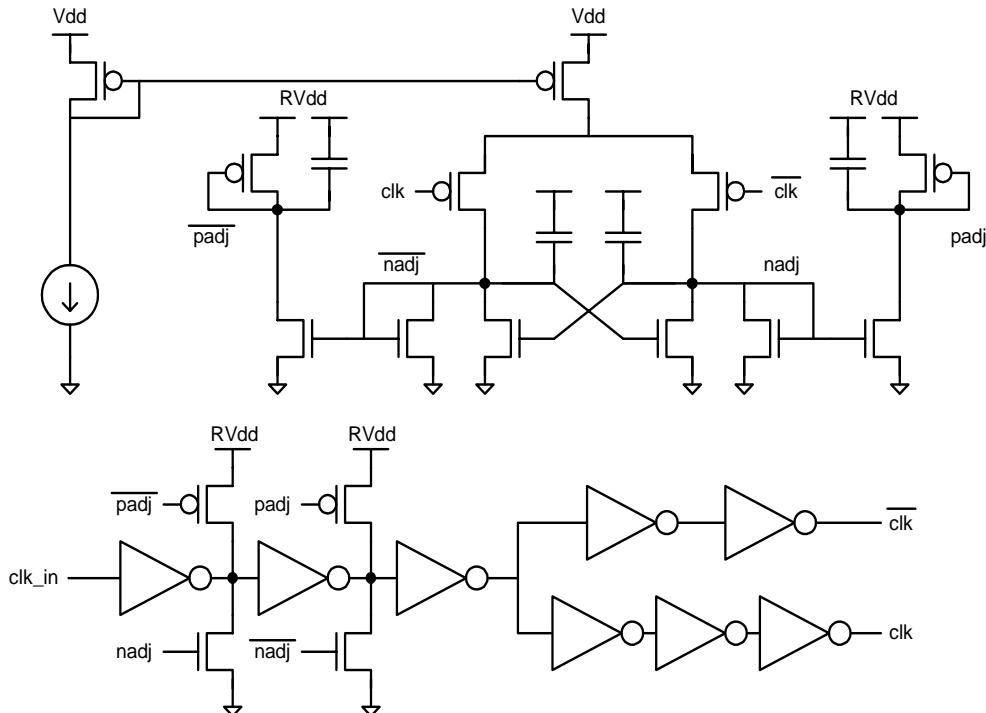
Figure 4.30. Duty-cycle adjuster schematic
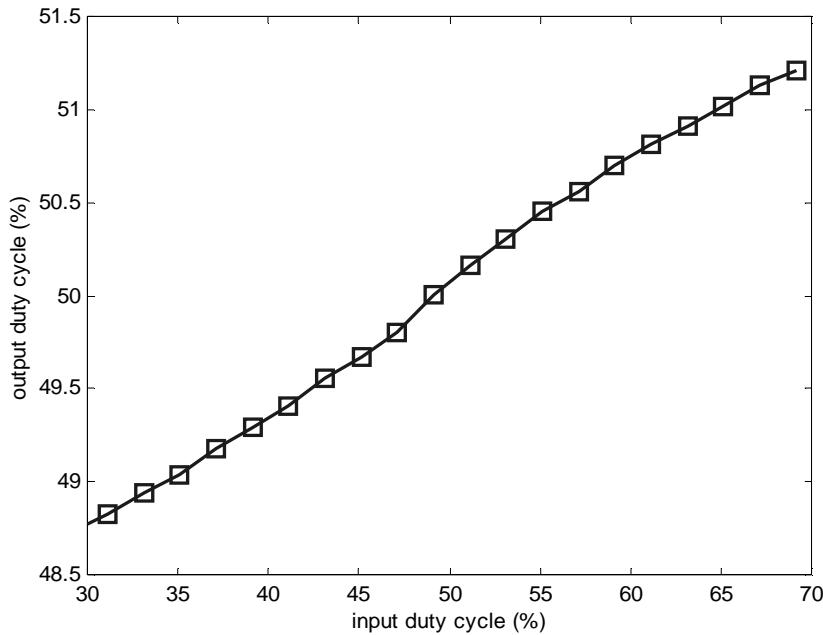
Figure 4.31. Duty-cycle adjustment

sources on two consecutive nodes within a series chain of inverters leak current to compensate for duty-cycle variations. An amplifier integrates the duty-cycle variations and sets the magnitude of the leakage currents such that the duty cycle settles to 50-% through negative feedback. The amplifier must operate off of the high supply voltage in order to generate sufficient correction swing range at the output. Simulation results show that a +/- 20% duty-cycle variation at the input to the DCA is reduced to less than +/- 2%, illustrated in Figure 4.31.

4.5.4 Clock Distribution and Relative Timing

The on-chip clock distribution in the link interface is another important component of the timing recovery block. The receiver design that was described in Section 4.4.3 requires two phase shifted clock signals, where one resets and enables the preamplifier, and the other samples the filtered data signal. Although two separate clock generator paths were implemented in the peripheral loop and distributed individually in the test chip, a simpler approach that once again leverages the delay tracking nature of digital gates with an adaptively regulated supply is possible.

The peripheral loop enables the generation of the phase-shifted clock, $\Phi 1$, by utilizing a secondary multiplexor-interpolator block whose edge selection and interpolation weight is determined by adding a binary value equivalent to the desired relative phase spacing to the output the FSM that sets $\Phi 0$. As a result, there is a fixed difference between the two edges. We opted for this approach to generating the two edges in order to arbitrarily skew the two clock edges to the receiver. However, a simpler approach is possible by locally offsetting the sampler clock through a chain of inverters from $\Phi 0$, which alone is distributed. Since the delay of each inverter is a fixed percentage of the clock period, a locally generated $\Phi 1$ will always be phase shifted relative to $\Phi 0$ by a fixed percentage of the clock period, thereby obviating the need for distributing additional clocks.

This delay tracking behavior also obviates clock retiming paths in the feedback path of peripheral loop. Since the delay through the peripheral loop consists entirely of digital gates, with a regulated supply, delay through the loop is again a fixed percentage of the clock cycle and offers another advantage over traditional designs. If the input clock edges to the interpolator happens to coincide with signals that control the mux and interpolator, it can potentially glitch the output clock signal. In traditional designs, there is no known relationship between the delay through the peripheral loop and clock frequency. Therefore, traditional loops require explicit re-timing paths to avoid potential glitches that can occur for different operating frequencies. However, with a regulated supply, delay paths are a fixed percentage of the clock cycle and such conditions can be guaranteed to never occur by construction and further simplifies the design.

4.5.5 Timing Recovery Summary

This section has described the timing recovery loop, which is an integral part of high-speed link design. It relies on a dual-loop DLL architecture, where the core loop, described in Section 4.2, not only sets the necessary regulated voltage level with respect to the bit rate, but also generates evenly spaced clock edges to the peripheral loop. The peripheral loop performs the actual clock recovery by aligning the internal clock signals with respect to the incoming source synchronous clock and data. Fine clock edge placement, down to 1/192 of the clock cycle, is possible through the multiplexor and

interpolator implementation. Furthermore, using the data receiver as a bang-bang phase detector allows the clock path to match the data. Such precise clock alignment maximizes timing margins for accurate data recovery.

As seen for the transmitter and receiver, an adaptively regulated supply offers several advantages for implementing the peripheral loop. Previous implementations relied on precision analog circuits to implement the multiplexor and interpolator in order to interface to the analog delay elements in the core loop and to control the time constants of devices in the interpolator with respect to operating frequency. By operating off of an adaptively regulated supply, the supply voltage provides process, temperature, and timing information. Therefore, a loop comprised almost entirely out of digital CMOS gates is possible, simplifying its design. The interface between the core and peripheral loop is trivial, because both sides consist of full-swing digital gates that operate at the same voltage level. And even interpolation, normally considered an analog function, is achievable with a parallel set of tri-state buffers. In addition, the delay tracking nature of the digital gates obviates clock re-timing paths and offers further simplifications to clock distribution by allowing the designer to accurately generate different clock phases locally.

4.6 Experimental Results

All of the components described so far have been implemented together and this section describes the experimental results obtained from the test-chip prototype, which was fabricated in a HP0.35µm CMOS10B NWELL process [50]. The section starts by describing additional details of the test chip, mainly, the supporting test circuitry incorporated to enable testing and to measure performance. Then, it presents the performance characteristics and analysis of the dual-loop DLL and I/O transceiver. Measured results of the power supply regulator were presented in Chapter 3 and is therefore only summarized along with the rest of the chip's overall performance. Lastly, this section investigates the implications of this adaptive supply regulation technique on power consumption.
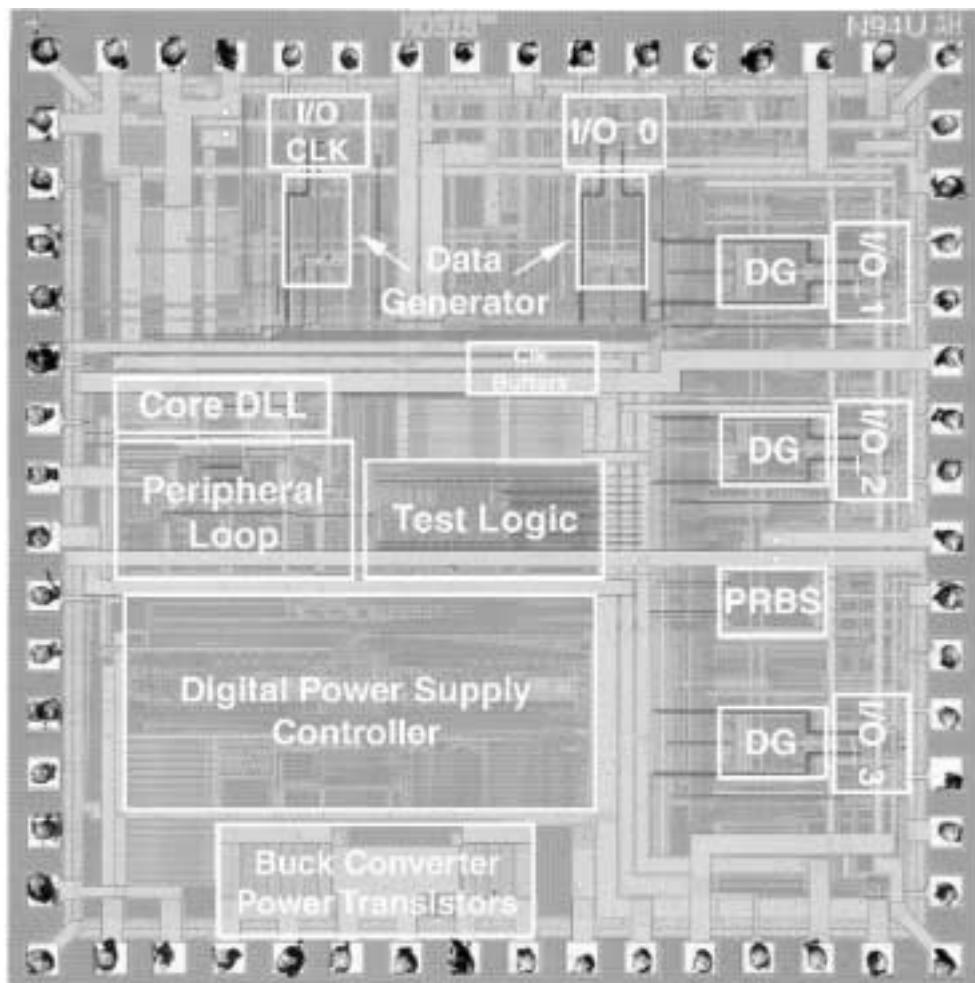
Figure 4.32. Test-chip micrograph

4.6.1 Test-chip Components and Testing Circuitry

As seen in the photo-micrograph of the test-chip prototype presented in Figure 4.32, the test chip consists of four data I/O transceivers and a parallel clock I/O that sends a parallel clock signal with the data for source synchronous operation. It relies on the parallel clock I/O receiver to act as a phase detector for the digital peripheral loop. The on-chip dual-loop DLL sets the supply voltage level for the chip, as well as providing the required clock signals. A digitally controlled adaptive power supply regulator also resides on chip with on-chip power transistors required for regulation through a buck converter, whose inductor and capacitor are off chip.

Different test configurations for the chip is managed through a control block found in the center of the test chip. There are 20 16-bit registers that are used to control the different units. Configuration data is loaded in the chip by serially scanning in 16 bits of data along with a 5-bit address. In addition, each transmitter has an 8-bit data pattern generator that can be set through this interface to enable a variety of data sequences to test proper functionality of the links. A 20-bit pseudo-random bit-sequence generator and verifier also reside on the chip and is used to measure the bit-error rate (BER) of the link. The use of 20 bits enables the links to be tested with wide spectral content, which is important since there are no requirements for DC balancing or scrambling that would normally be required in interface designs that do not have an explicit clock and therefore require clock recovery from the incoming bit stream.

4.6.2 Dual-Loop DLL

The dual-loop DLL, on the left side of the chip micrograph, consists of the core and peripheral blocks. The core DLL is supplied off of the high Vdd supply and operates from 33-500 MHz with corresponding regulated voltage settings ranging from 1.3-3.2 V as plotted in Figure 4.33. The digital peripheral loop operates off of RVdd, set by the core loop, and operates from 100-500 MHz. The receiver used as a phase detector for the
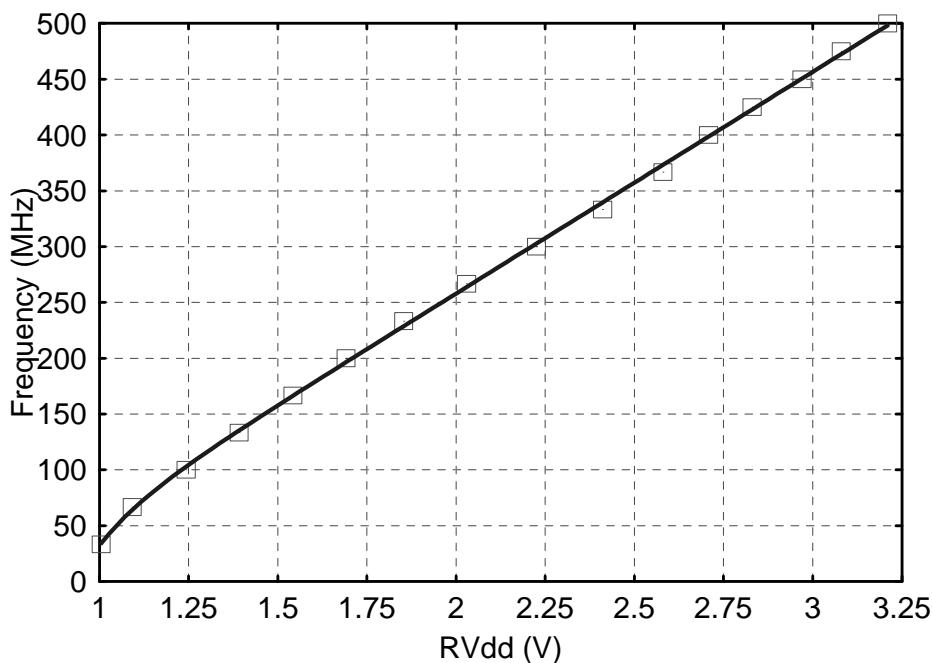

Figure 4.33. Regulated voltage vs. frequency

<div align="center">(a)   (b)</div>
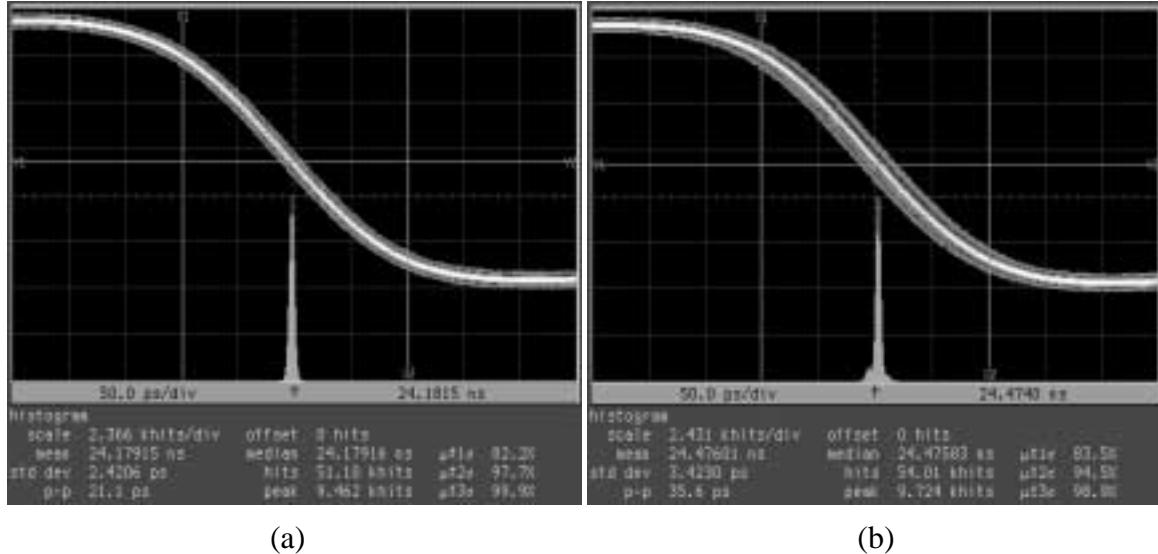
Figure 4.34. DLL jitter histogram -- (a) core, (b) dual

peripheral loop resides in the link above the DLL block and limits the lower frequency range of operation due to a minimum 1.3-V supply headroom required by the analog preamplifier. Figure 4.34 shows the core and dual loop jitter histogram plots while running at 400-MHz under quiet supply conditions. The larger jitter in the dual loop can be attributed to the peripheral loop occasionally dithering between interpolation steps. Due to a lack of on-chip supply noise generators, jitter measurements for the core loop under noisy conditions could not be accurately measured. However, a PLL design that also implements supply-controlled inverters as delay elements and a similar regulating amplifier design, presented in [42], exhibits a measured power supply rejection ratio of 15, and closely matches simulated results. Although the regulating amplifier actively rejects and filters out power supply noise to reduce jitter in the core loop, the digital circuitry in the peripheral loop has no such mechanism besides the peripheral loop. The peripheral loop can compensate for delay variations due to low frequency supply variations below its effective loop bandwidth and responds to supply steps with a time constant set by the loop's slew rate.

While operating at 400-MHz, the core loop dissipates 37-mW operating off the 3.3-V supply and the digital logic for the peripheral loop, supplied with a 2.7-V regulated

voltage, dissipates 19-mW. Table 4.1 summarizes the measured dual-loop DLL

Table 4.1. Dual-loop DLL performance summary

Operating Range		
	core	33 - 500 MHz
	peripheral	100 - 500 MHz
Jitter		
	core loop	21-ps pk-pk
	dual loop	36-ps pk-pk
Power		
	core (Vdd)	51-mW (3.3-V)
	peripheral (RVdd)	28-mW (2.7-V)
Active Area		0.035-mm^2

characteristics. Figure 4.35 plots the power consumed by the core and peripheral DLL blocks versus frequency. Given that the peripheral loop is dominated by digital logic, its power consumption exhibits an almost cubed relation to frequency, whereas the core loop's power is super-linear with frequency Due to an unidentified static current path
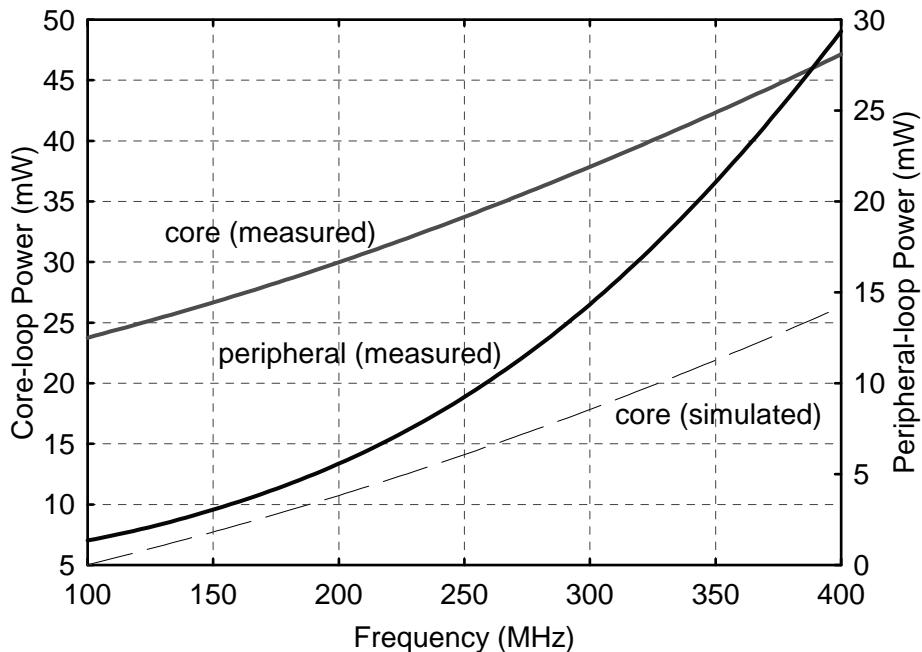

Figure 4.35. Dual-loop DLL power consumption vs. frequency

between Vdd and Gnd, the core DLL's measured power consumption is much larger than simulated results, shown by the dotted line. Therefore, the actual magnitude of power is inaccurate, but both measured and simulated power numbers exhibit the same relationship with respect to frequency.

4.6.3 I/O Transceiver

The I/O interface operating range is set by the peripheral loop and therefore successfully operates from 100-MHz to 500-MHz, which translates to a 0.2-1 Gb/s range in bit rates across a 1.3-3.2 V range in regulated voltage levels. The fabrication run for the test chip turned out slower than expected from simulations, and therefore required a high Vdd boosted to 3.7-V to comfortably meet the headroom requirements of the linear regulator in the core DLL in order to operate at the high frequency target of 500-MHz. Transmitting and receiving a 20-bit PRBS at a transfer rate of 0.8-Gb/s verifies a bit-error rate less than 10^{-14} (which corresponds to three days of operation without a single error). This test was performed by transmitting and receiving signals between two chips through 8-inches of 50-Ω traces on FR4 printed circuit boards and 36-inch coax cables.

Figure 4.36 plots the total regulated power consumed per link operating across a range of bit rates for single-ended and differential modes of operation to demonstrate the power saving potential of dynamically scaling the supply to the I/O subsystem. Although a true demonstration of the power savings possible requires a comparison between the same link design operating off of a fixed supply versus a regulated supply, since the chip was designed to only operate with a dynamically adjusted supply, experimental measurements of the chip's power consumption for a fixed supply voltage configuration was not possible. However, the estimated power consumption of the overhead power operating off of a fixed high supply voltage (3.3-V) was generated by calculating the effective switched capacitance of the digital circuitry and applying it to the dynamic power equation with a fixed supply voltage. It is presented by the dashed line in Figure 4.36 and emphasizes the power saving potential of adaptively regulating the supply. Since the regulated voltage varies with frequency, power consumption while operating off of a dynamically adjusted supply reduces dramatically for lower bit rates. It is important to note that this estimated

power is for the same process corner as the chip that was tested and does not offer insight into the potential power savings which can be achieved for different process corners and operating conditions.

To compare single-ended signalling versus differential signalling, the overhead power common to both configurations is identified by the dashed line and represents the power consumed by the receiver and a portion of the power dissipated in the bias generator, peripheral loop, clock distribution network, and testing circuitry amortized across all the links. The difference between the total power and the overhead represents the power dissipated in the transmitter at the minimum transmission swings achieved for different transmission bit rates. The minimum transmission swings achieved versus bit rate are plotted in Figure 4.37. Although differential signalling requires two parallel channels to transmit data, they require less than half the swing magnitude compared to single-ended signalling and hence consume less power. Noise on the reference voltage that is shared by all the receivers is common-mode and adversely affects the voltage margins for the receiver, thus requiring the larger swing magnitudes for single-ended signalling. Therefore, from a system perspective, since there is little difference in power
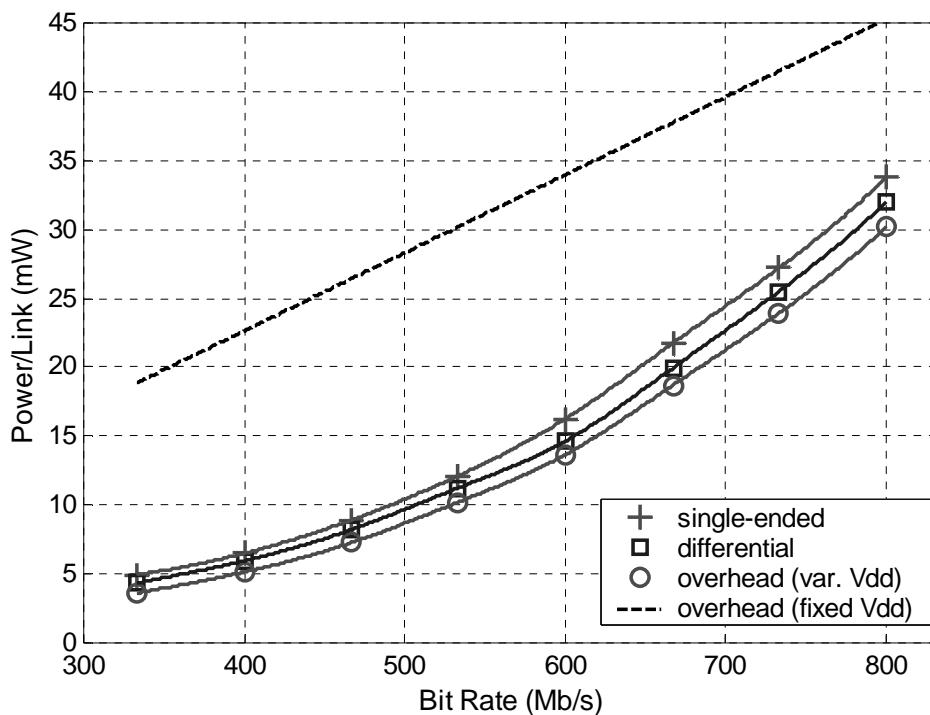
Figure 4.36. Single-ended and differential link power vs. bit rate
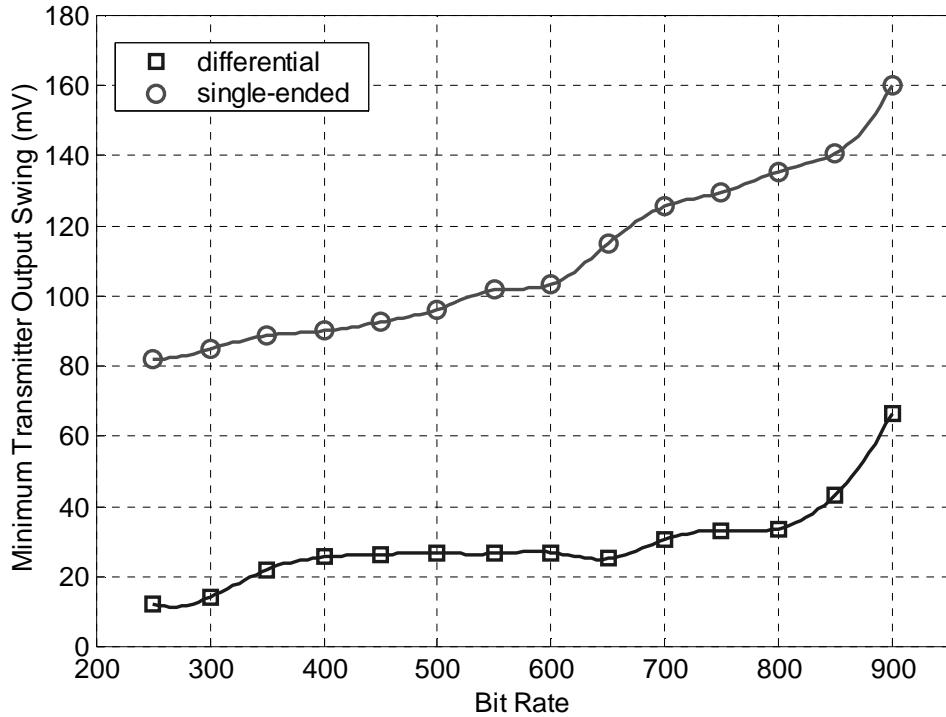
Figure 4.37. Minimum transmission swing vs. bit rate

consumption, the choice between single-ended and differential signalling would be dictated by other factors such as pin resources available for the I/O interface or communication distances which may require differential signalling.

An additional advantage of adaptively scaling the supply comes from the automatic slew-rate control of the transmitter output. Figure 4.38 presents the measured data-eye diagram for a PRBS data stream transmitted at 0.8-Gb/s. It verifies the 50-% duty-cycle signals achieved by pre-distorting the predrivers to the output driver and shows the output slews for a third of the bit time. This slew-rate control also extends to different frequencies, demonstrated by the relatively constant rise and fall transition times as a percentage of bit time, presented over a range of bit rates in Table 4.2.
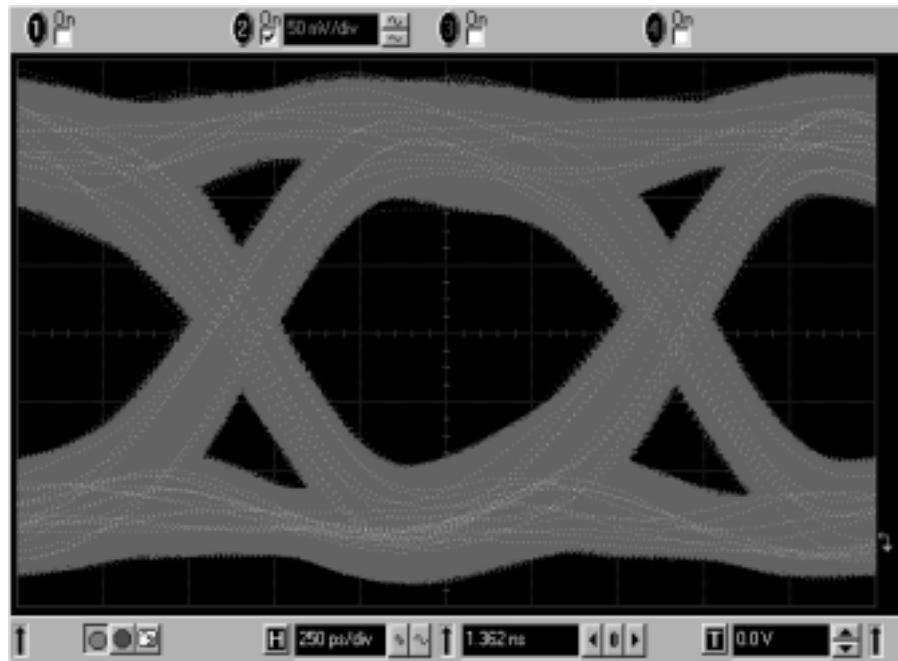
Figure 4.38. Transmitted eye at 0.8-Gb/s

Table 4.2. Transmitter output slew-rate vs. bit rate

Bit Rate (Mb/s)	Rise Time (% of bit time)	Fall Time (% of bit time)
400	32	33
467	24	25
533	26	25
600	24	24
667	29	28
733	25	24
800	30	30

4.6.4 Power Breakdown Analysis

Given the relatively low swing magnitudes required for transmission over short distances on a board, the power consumed by the digital logic in the I/O subsystem dominates for this type of interface. A breakdown of all the components of power in the I/O transceiver is presented in Figure 4.39 while transmitting at 800Mb/s. A significant
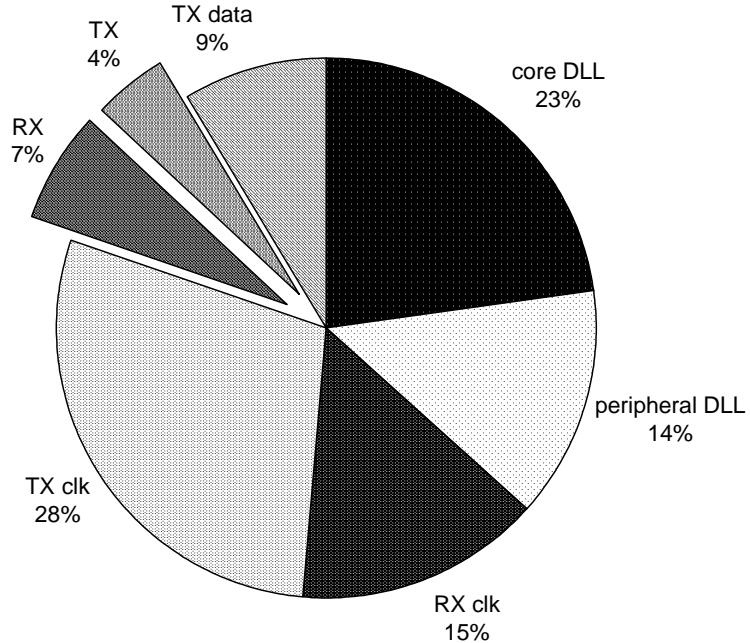
Figure 4.39. Power breakdown at 800Mb/s

portion of the power is consumed by the clock distribution, clock recovery, and data generators, while only 11-% is consumed by the transceiver itself. Therefore, this type of I/O subsystem especially benefits from the savings possible by reducing the dynamic power dissipated by digital gates with adaptive power supply regulation.

The test-chip prototype only contains 4 data links, but the measured results can be extrapolated to understand the power implications of this approach for much wider parallel I/O interfaces. The power consumption of each link grows linearly with each additional link and so does much of the clock distribution power and supporting digital circuitry that interfaces the links to the rest of the digital system. A component of power that does not scale linearly with the number of links is the timing-recovery block. Enabling more links to share a single timing recovery block reduces the overhead power consumed per link. However, due to large skews that can potentially result for links spread across a large die (both on the chip and on the board), multiple timing recovery blocks for sets of links on different parts of the chips may be necessary. Furthermore, communication with multiple chips utilizing this type of parallel interface requires multiple timing-recovery blocks for each set of links communicating to different chips.

4.7 Summary

Running a high-speed parallel I/O interface off of an adaptively regulated supply voltage provides several advantages. The process, temperature, and frequency information embedded within the regulated supply, coupled with the delay tracking nature of digital CMOS gates, leads to a simple design that minimizes precision analog circuits. A predominantly digital design enables easier integration into large digital chips. In addition, its power consumption scales not only with the environment, but also with the operating frequency. The proposed interface optimizes power consumption by reducing margins normally required in conventional, fixed-supply designs to cover all corner cases. Furthermore, the I/O can trade performance for lower power. Consequently, a digital core that can adaptively vary its I/O bit rate with respect to its communication bandwidth requirements can significantly reduce power consumption. The test chip demonstrated that cutting the bit rate down by one half reduced power consumption by a factor of 5.7. This is all possible with a digitally-controlled power-supply regulator that can also be implemented within the same die as the interface and the rest of the digital chip (except for the off-chip inductor and capacitor).

Chapter 5

Conclusions

This dissertation has shown that a power reduction technique, referred to as adaptive power supply regulation, is not only applicable to large digital cores, but can also be effectively applied to a high-speed parallel I/O interface. It enables a simple and yet robust design while facilitating efficient power consumption by tracking process variations, environmental conditions and frequency. It relies on a performance monitoring circuit, which in this case is a simple inverter, to map the relationship between circuit delay and operating conditions. Given the strong correlation between supply voltage and circuit delay, and dynamic power's quadratic dependence on voltage, significant power reduction is possible by eliminating voltage margins and operating circuits at the minimum voltage required to guarantee timing. Dynamically regulating the supply voltage requires an efficient power supply regulator to separately drive the I/O interface.

The ability to adaptively reduce supply voltage and still guarantee timing requirements requires a circuit that can track the critical delay path in the I/O interface across all process and operating conditions. In Chapter 2, an inverter was shown to be an effective delay model that accurately tracks the delay of various static and dynamic gates across process and temperature variations. Due to velocity saturation effects, tracking was not as good across voltage. Therefore, the design of the delay tracking inverter becomes more critical and in some cases may require voltage margins to guarantee timing across the entire voltage range of operation. Designing a delay tracking circuit that consists of the same types of gates that constitute the critical path minimizes these margins. While this may be difficult to do in large digital blocks where delay paths are balanced as much as possible, the critical path in the I/O interface conveniently consists of inverters that drive the clock

distribution network. Therefore, inverters worked out to be the best fit.

Finding the "right" voltage for operation with respect to process, temperature, and frequency is achievable in different ways. Chapter 2 described a digitally-controlled buck converter that regulates the output voltage with respect to an input reference frequency. And an inverter-based ring oscillator was used to model the critical path. For the I/O interface, the core loop of a dual-loop DLL used a small linear regulator to determine the "right" voltage required to match the delay through a chain of inverters to the input clock period. An efficient regulator was then used to replicate this voltage and drive the rest of the I/O interface.

Adaptively regulating the supply voltage not only offers power savings, but it can also enable a simple I/O design that replaces many precision analog circuits with digital gates. The regulated voltage contains information about the process and operating conditions for the chip, so that the delay of gates tracks the frequency of operation. This has enabled automatic slew-rate and output swing magnitude control for the transmitters and a bandwidth tracking input receiver. The clock distribution network may also take advantage of this property to locally generate necessary clock phases that are a delayed a fixed percentage of the clock period.

Chapter 4 demonstrated a parallel I/O interface, fabricated in an HP0.35μm CMOS process, that can achieve high speeds while consuming less power by adaptively regulating its supply voltage. The lower supply doesn't necessarily limit its performance since the I/O interface normally is not the performance bottleneck in a large digital chip. Instead, the interface trades its excess performance capabilities for lower power consumption. This interface achieves a BER less than 10^{-14} while running at 800-Mb/s and consuming less than 35-mW per link. Given a system that can throttle its communication bandwidth with respect to performance needs, reducing the bit rate to 400-Mb/s lowered power consumption to less than 7-mW per link. The chip's performance is summarized in Table 5.1.

Table 5.1: I/O test chip performance summary

Nominal Vdd	3.3-V
I/O Frequency Range (bit rate)	100-500 MHz (0.2-1 Gb/s)
Regulated Supply Range	1.3-3.2 V
BER @0.8-Gb/s	$< 10^{-14}$
Power - Total 0.8-Gb/s	210-mW (RVdd = 2.7-V)
Power Supply Ripple	< 25-mV
Converter Efficiency @200-mW	94-% (RVdd=2.7-V, Vdd=3.3-V)
Die Size	6.5-mm^2
Technology	0.35-μm HP/CMOS10B

The pursuit of more communication bandwidth between chips continues to be a highly sought after goal. Aggressive technology scaling has enabled higher levels of integration and performance at the expense of higher power dissipation and pin count. The nominal power supply voltage has also been scaling with feature size, which helps to reduce power consumption. Unfortunately, V_{TH} has not experienced the same scaling This asymmetric scaling adversely affects analog circuits as they run out of voltage headroom. Adaptive power supply regulation demonstrated ways to replace several precision analog circuits with digital gates. However, in order to port to future technologies, this technique must be extended to replace existing analog components in the I/O interface design with digital ones. One approach is to replace the core DLL the digital power-supply regulator to eliminate all of its analog circuits [25]. So, all that is left is to find solutions to deal with the V_{TH} and voltage headroom limitations in the transmitter and receiver.

References

[1]   B.S. Amrutur, "Design and analysis of fast low power SRAMs," *Ph.D. dissertation*, Stanford Univerisy, Stanford, CA, August 1999.

[2]   G. Besten, "Embedded low-cost 1.2Gb/s inter-IC serial data link in 0.35mm CMOS," *IEEE Int'l Solid-State Circuits Conf. Dig. Tech. Papers*, Feb. 2000, pp. 250-251.

[3]   T. Burd, et. al., "A dynamic voltage scaled microprocessor system," *IEEE Int'l Solid-State Circuits Conf. Dig. Tech. Papers*, Feb. 2000, pp. 294-295.

[4]   T. Burd, et. al., "Processor design for portable systems," *Journal of VLSI Signal Processing*., vol. 13, no. 2-3, Aug.-Sept. 1996, pp. 203-221.

[5]   A. P. Chandrakasan, et. al., "Data driven signal processing: An approach for energy efficient computing," *IEEE Int'l Symposium on Low Power Electronics and Design Dig. Tech. Papers,* Aug. 1996, pp. 347-352.

[6]   A.P. Chandrakasan, et. al., *Low Power Digital CMOS Design*. Norwell, MA: Kluwer Academic, 1995.

[7]   W.J. Dally, et. al,. "Transmitter equalization for 4-Gbps signalling" *IEEE Micro,* Jan.-Feb. 1997. vol.17, no.1, p. 48-56

[8]   A. Dancy, et. al, "Techniques for aggressive supply voltage scaling and efficient regulation," *Proceedings of the IEEE Custom Integrated Circuits Conf.*, May 1997, pp. 579-586.

[9]   A. DeHon, et. al., "Automatic impedance control," *1993 IEEE Int'l Solid-State Circuits Conf. Dig. Tech. Papers,* p. 164-5, Feb. 1993.

[10] D. Dobberpuhl, "The design of a high performance low power microprocessor," *IEEE Int'l Symposium on Low Power Electronics and Design Dig. Tech. Papers*, Aug. 1996, pp. 11-16.

[11] K. Donnelly, et. al., "A 660 MB/s interface megacell portable circuit in 0.3um-0.7mm CMOS ASIC," *IEEE Int'l Solid-State Circuits Conf. Dig. Tech. Papers*, pp. 290-291, Feb 1996.

[12] R. Farjad-Rad, et. al., "A 0.3-μm CMOS 8-GS/s 4-PAM Serial Link Transceiver", *IEEE Symposium on VLSI Circuits Dig. Tech. Papers,* p. 41-44

[13] M. Fukaishi, et. al., "A 20Gb/s CMOS multi-channel transmitter and receiver chip set for ultra-high resolution digital display," *IEEE Int'l Solid-State Circuits Conf. Dig. Tech. Papers*, Feb 2000, pp. 260-261.

[14] R. Gu, et. al., " 0.5-3.5Gb/s low-power low-jitter serial data CMOS transceiver," *IEEE Int'l Solid-State Circuits Conf. Dig. Tech. Papers*, Feb 1999, pp. 352-353.

[15] V. Gutnik, et. al., An efficient controller for variable supply voltage low power processing," *IEEE Symposium on VLSI Circuits Dig. Tech. Papers*, June 1996, pp. 158-159.

[16] R. Ho, et. al., "Interconnect scaling implications for CAD," *IEEE/ACM Int'l Conf. Computer Aided Design Dig. Tech. Papers*, Nov. 1999, pp. 425-429.

[17] P. Hofstee, et. al., "A 1GHz single-issue 64b PowerPC processor," *IEEE Int'l Solid-State Circuits Conf. Dig. Tech. Papers*, Feb. 2000, pp. 92-93.S.

[18] M. Horowitz, "Low power processor design using self-clocking," *Workshop on Low-Power Electronics*, 1993.

[19] M. Horowitz, et. al., "High-speed electrical signalling: Overview and limitations," *IEEE Micro*, vol. 18, no. 1, Jan.-Feb. 1998, pp.12-24.

[20] C. Hu, "Future CMOS scaling and reliability," *Proceedings of IEEE*, Vol. 81, no.5, May 1993, invited paper.

[21] A. Jain, et. al., "A 1.2GHz Alpha microprocessor with 44.8GB/s chip pin bandwidth," *IEEE Int'l Solid-State Circuits Conf. Dig. Tech. Papers*, Feb. 2001, pp. 240-241.

[22] D. Jeong, et. al., "Design of PLL-based clock generation circuits," *IEEE Journal of Solid-State Circuits*, vol. 22, no.2, April 1987, pp. 244-261.

[23] M. Johnson, "Bias circuit and differential amplifier having stabilized output swing," *US Patent 5452898*, Sept. 1995.

[24] J.G. Kassakian, et. al. "High-frequency high-density converters for distributed power supply systems, *Proceedings of the IEEE*, vol. 76, no. 4, 1988.

[25] J. Kim, "A digital adaptive power-supply regulator using sliding control," *IEEE Symposium on VLSI Circuits Dig. Tech. Papers*, June 2001.

[26] B. Lau, et. al., "A 2.6Gb/s multi-purpose chip to chip interface," *IEEE Int'l Solid-State Circuits Conf. Dig. Tech. Papers*, Feb 1998, pp. 162-163.

[27] J. Lee, "A low-noise fast-lock phase-locked loop with adaptive bandwidth control," *IEEE Journal of Solid-State Circuits*, vol. 35, no. 8, Aug. 2000, pp. 1137-1145.

[28] T.H. Lee, et. al., "A 2.5V CMOS delay-locked loop for 18Mbit, 500megabyte/s DRAM," *IEEE Journal of Solid-State Circuits*, vol. 29, no. 12, Dec. 1994, pp. 1491-1496.

[29] P. Maken, M. Degrauwe, M. Van Paemel and H. Oguey, "A voltage reduction technique for digital systems," *IEEE Int'l Solid-State Circuits Conf. Dig. Tech. Papers*, Feb. 1990, pp238-239.

[30] J.G. Maneatis, "Low-Jitter process independent DLL and PLL based on self-biased techniques," *IEEE Journal of Solid-State Circuits*, vol. 28, no. 12, Dec. 1993.

[31] J.G. Maneatis, "Precise delay generation using coupled oscillators," *Ph.D. dissertation*, Stanford University, Stanford, CA, June 1994.

[32] D. Monticelli, "Switching power supply design," *Proceedings of IEEE Symposium on Low Power Electronics*, Oct. 1995, p. 64.

[33] R.S. Muller, et. al., *Device electronics for integrated circuits*, John Wiley and Sons, 1986.

[34] W. Namkoong, et. al., "A high-efficiency variable-voltage CMOS dynamic dc-dc switching regulator," *IEEE Int'l Solid-State Circuits Conf. Dig. Tech. Papers*, Feb. 1997.

[35] L. Nielsen, et. al., "Low-power operation using self-timed circuits and adaptive scaling of supply voltage," IEEE Trans. VLSI Syst., vol. 2, pp 391-397, Dec 1994.

[36] H. Notani, "A 622-MHz CMOS PLL with precharge-type phase frequency detector," IEEE VLSI Symp. Dig. Tech. Papers, Feb. 1994, pp. 129-130.

[37] E. Reese, et. al. "A phase-tolerant 3.8 GB/s data-communication router for muli-processor super computer backplane," *IEEE Int'l Solid-State Circuits Conf. Dig. Tech. Papers*, pp. 296-297, Feb. 1994.

[38] S. Sakayima, et. al., "A lean power management technique: The lowest power consumption for the given operating speed of LSI's," *IEEE Symposium on VLSI Circuits Dig. Tech. Papers*, June 1997, pp. 99-100.

[39] T. Sakurai, et. al., "Alpha-power law MOSFET model and its applications to CMOS inverter delay and other formulas," *IEEE Journal of Solid-State Circuits*, vol. 25, no. 2, April 1990, pp. 584-594.

[40] S. Sidiropoulos, et. al., "A 700-Mb/s/pin CMOS signalling interface using current integrating receivers," *IEEE Journal of Solid-State Circuits*, May 1997, pp. 681-690.

[41] S. Sidiropoulos, et. al., "A CMOS 500Mbps/pin synchronous point to point interface," IEEE Symposium on VLSI Circuits, June 1994.

[42] S. Sidiropoulos, et. al., "Adaptive bandwidth DLL's and PLL's using regulated-supply CMOS buffers," *IEEE Symposium on VLSI Circuits Dig. Tech. Papers*, June 2000.

[43] S. Sidiropoulos and M. Horowitz, "A semi-digital dual delay-locked loop," *IEEE Journal of Solid-State Circuits*, Nov. 1997, pp. 1683-1692.

[44] S. Sidiropoulos, "High performance inter-chip signalling," *Ph.D. Dissertation*, Stanford University, Stanford, CA, June 1998.

[45] A.J. Stratakos, "High-efficiency low-voltage DC-DC conversion for portable applications," *Ph.D. dissertation*, University of California, Berkeley, CA, Dec. 1998.

[46] K. Suzuki, et. al., "A 300 MIPS/W RISC core processor with variable supply-voltage scheme in variable threshold-voltage CMOS," *Proceedings of the IEEE Custom Integrated Cicruits Conference*, May 1997, pp. 587-590.

[47] T. Tanahashi, et. al., "A 2Bb/s 21CH low-latency transceiver circuit for inter-processor communication," *IEEE Int'l Solid-State Circuits Conference Dig. Tech. Papers*, Feb. 2001, pp. 60-61.

[48] G. Wei, et. al. "A low power switching power supply for self-clocked systems," *IEEE Symposium on Low Power Electronics*, Oct. 1996, pp. 313-317.

[49] G. Wei, et. al., "A full-digital, energy-efficient adaptive power supply regulator," *IEEE Journal of Solid-State Circuits*, vol. 34, no. 4, April 1999, pp. 520-528.

[50] G. Wei, et. al., "A variable-frequency parallel I/O interface with adaptive power-supply regulation," *IEEE Journal of Solid-State Circuits*, vol. 35, no. 11, Nov. 2000, pp. 1600-1610.

[51] C.K. Yang, "Design of high-speed serial links in CMOS," *Ph.D. dissertation*, Stanford University, Stanford, CA, Decemeber 1998.

[52] K. Yang, "A scalable 32Gb/s parallel data transceiver with on-chip timing calibration circuits," *IEEE Int'l Solid-State Circuits Conf. Dig. Tech. Papers*, Feb. 2000, pp. 258-259.

[53] E. Yeung, et. al., "A 2.4Gb/s/pin simultaneous bidirectional parallel link with per pin skew compensation," *IEEE Int'l Solid-State Circuits Conf. Dig. Tech. Papers*, Feb. 2000, pp. 256-257.

[54] P. Yue, "On-chip spiral inductors for silicon-based radio-frequency integrated circuits," *Ph.D. dissertation*, Stanford University, Stanford, CA, July 1998.

[55] J. Zerbe, et. al., "A 2Gb/s/pin 4-PAM parallel bus interface with transmit crosstalk cancellation, equalization, and integrating receivers," *IEEE Int'l Solid-State Circuits Conf. Dig. Tech. Papers*, Feb. 2001, pp. 66-67.